Exploring Ligand Structure and Thermodynamics of the Malachite Green RNA Aptamer

by

Jason Bernard Da Costa

A thesis

presented to the University of Waterloo

in fulfillment of the

thesis requirement for the degree of

Doctor of Philosophy

in

Chemistry

Waterloo, Ontario, Canada, 2012

Author's Declaration

I hereby declare that I am the sole author of this thesis. This is a true copy of the thesis, including any required final revisions, as accepted by my examiners.

I understand that my thesis may be made electronically available to the public.

Abstract

RNA aptamers are *in vitro* sequences of RNA that have a high affinity for their target ligand. They have applications in therapeutics, biosensors and molecular machines. While the practical applications of aptamers are increasing, it is important to study their structure and thermodynamics to improve the understanding of these molecular tools. The malachite green aptamer (MGA) provides a model system to study the interactions between aptamer and ligand that do not involve hydrogen bonding between ligand and receptor. While the original application of this aptamer was abandoned, study of the MGA binding pocket revealed an electronegative environment that was harnessed for catalysis. MGA binding also supported the notion that aptamers bind by adaptive binding. Adaptive binding is the ability of molecules to mold themselves around the structure of a ligand thereby incorporating it into their three-dimensional fold.

To further expand our understanding of MGA binding and to clarify conflicting reports of affinities, we conducted isothermal calorimetry binding studies. The results reveal that the entropy of complex formation plays a large role in determining binding affinity and ligand specificity. This data combined with previous structural studies show that metal ions are required to stabilize the complexes with non-native ligands, whereas, the complex with the original selection target is stable at low salt and in the absence of divalent metal ions. Next, competitive binding studies using isothermal titration calorimetry were conducted with the aim of understanding the adaptive nature of RNA. The results of these studies reveal that there are limits to the adaptability of the aptamer. Binding of one type of ligand reduces the affinity of the aptamer pocket to a differently shaped ligand, even if this second ligand has a significantly higher affinity.

The ability of MGA to change ligand preference based on buffer conditions, and the previously reported catalysis suggested that RNA may have a potential supporting multiple functions in the same molecule. To investigate this possibility we attempted to select an aptamer that supports both ligand binding and catalysis. By conducting both a DNA and RNA selection we hoped to add to the

collection of DNA and RNA aptamers selected for the same target. There are currently too few of these to determine if any correlation can be made between DNA and RNA sequences that bind the same target. The target of the selection was fluorescein diacetate (FDA), which was chosen with the aim that it would allow the exploration of the inherent potential of the selected aptamer to cleave FDA to fluorescein. The RNA selection proved to be more successful and an attempt was made to characterize the binding of the aptamer to its target fluorescein diacetate. Unfortunately there were complications with the binding assays, but future work is proposed that should address the issues.

In order to expand the MGA catalytic repertoire attempts were made to synthesize new ligands that could exploit the catalytic potential of the MGA binding pocket. Unfortunately these attempts were unsuccessful, however further attempts are recommended. The MGA used in this study was transcribed *in vitro* using T7 RNA polymerase. This process is known to add extra nucleotides to the end of the transcription product. Attempts were made to eliminate the n+1 product by introducing a ribozyme or DNAzyme. These were met with difficulties resulting in low yield, however mass spectrometry revealed that n and n+1 MGA bind to ligand. This, along with secondary structure prediction suggests that MGA n+1 behaves the same as n.

Overall, the results presented here provide insights into the capabilities of RNA aptamers with respect to ligand binding and catalysis.

Acknowledgements

I would like to thank my supervisor, Dr. Thorsten Dieckmann, for his continued support and encouragement, as well as the opportunity to work on this research project. I would like to thank my committee members; Dr. John Honek , Dr. J. Guy Guillemette, and Dr. Richard Manderville for their time, support and advice. I would like to thank Dr. Richard Smith and Jannet Venne for their assistance with mass spectrometry and NMR spectroscopy. I would also like to thank Dr. Elaine Collins for her work preparing the aptamer template plasmids. For assistance in daily lab activities I would like to thank past and present members of my lab; in particular Jenna Collier, Marie Claire Lacassin, Cveta Manassieve, Jeffrey Lai and Mike Piazza. I would also like to thank the University of Waterloo, the Chemistry department administrative staff, the chemistry graduate student community (all graduate students in biochemistry especially). Lastly but definitely not the least I would like to thank my family for their support and love, without which none of this would be possible. Thank you.

Dedication

To my family,

Victor, Bula, Gary, Carol

Table of Contents

List of Figures

Chapter 1

Chapter 2

Chapter 3

Chapter 4

Chapter 5

List of Tables

Chapter 1

Chapter 2

Chapter 3

List of Abbreviations

CV : crystal violet

DIS : dimerization initiation site

DNA : Deoxyribonucleic acid

FDA : fluorescein diacetate

HDV MGA : HDV ribozyme appended to MGA

HDV: hepatitis delta virus

HH MGA : HH ribozyme appended to MGA

HH: hammer head

HIV : human immunodeficiency virus

IgG : immunoglobulin G

ITC : isothermal titration calorimetry

Kd : dissociation constant

lncRNA : long non-coding RNA

MG : malachite green

MGA : malachite green aptamer

MGACV: MGA pre-bound to CV

MGAMG: MGA pre-bound to MG

MGApre: MGA pre-bound to either PY or CV

MGAPY: MGA pre-bound to PY

MGATMR: MGA pre-bound to TMR

MGNCS : malachite green isothiocyanate

miRNA : micro RNA

mRNA : messenger RNA

ncRNA : non coding RNA

NMR : nuclear magnetic resonance

PCR : polymerase chain reaction

PEG : polyethylene glycol

piRNA : piwi interacting RNA

PY: pyronin Y

REV : regulator of virion expression

RNA : Ribonucleic acid

rRNA : ribosomal RNA

SELEX : Systematic evolution of ligands by exponential enrichment

siRNA : small interfering RNA

snoRNA : small nucleolar RNA

TAR :trans-activation reponse element

Tat : trans activator of transcription

TMR : tetramethylrosamine

tRNA : transfer RNA

VEGF : vascular endothelial growth factor

X-Gal : bromo-chloro-indolyl-galactopyranoside

ΔG : free energy change

ΔH : enthalpy change

ΔS : entropy change

Chapter 1: Structure and Thermodynamics of Drug-RNA Aptamer Interactions

1. Introduction

Ribonucleic acid (RNA) participates in many cellular processes including protein translation, signalling, and regulation (Bartel 2007, Beringer 2008). The first function of RNA identified was the transfer of information from deoxyribonucleic acid (DNA) to proteins. The RNA was termed messenger RNA or mRNA (Brenner, Meselson and Jacob 1961). In this model DNA is responsible for information storage and proteins are responsible for catalytic function (Crick 1958, Crick et al. 1961). The discovery that RNA was capable of catalyzing RNA cleavage changed the perception of RNA's function (Guerrier-Takada et al. 1983, Cech, Zaug and Grabowski 1981). RNA sequences that are capable of catalytic activity are called ribozymes. This discovery led to the proposal of the RNA world hypothesis which suggests that early life went through a stage where RNA was responsible for information storage and catalytic function (Gilbert 1986).

RNA involved in translation

The discovery of mRNA was followed by the identification of ribosomal RNA or rRNA (Kay 1968) and transfer RNA or tRNA (Morris and Demoss 1965). rRNA interacts with specific proteins to form the ribosome (Tso 1962). The ribosome is responsible for translation of mRNA code to protein sequence, it achieves this through interactions with tRNA and mRNA (Salas et al. 1967). tRNA assists the transcription of codons by acting as a translator (Bock, Soll and Cherayil 1967). The ribosome brings together mRNA, based on complementary interaction of mRNA and tRNA codons (Harvey Lodish 2000). Then rRNA catalyzes a peptidyl transferase reaction to elongate amino acid chain forming proteins (Nissen et al. 2000). The discovery that the RNA component of the ribosome that is

responsible for this catalysis supports the idea of an RNA world. This function of RNA showed that large proteins required RNA to be synthesized and were possible after RNA developed this ability (Cech 2009).

RNA involved in regulation

In the past 50 years more classes of RNA have been identified; these include small interfering RNA or siRNA (Hamilton and Baulcombe 1999), micro RNA or miRNA (Bartel 2007), small nucleolar RNA or snoRNA (Ganot, Caizergues-Ferrer and Kiss 1997), piwi interacting RNA or piRNA (Grivna et al. 2006), long non-coding RNA or lncRNA (Ben Amor et al. 2009) and riboswitches (Winkler, Cohen-Chalamish and Breaker 2002). RNA has also been observed recently to function as an extracellular signalling molecule (Dinger, Mercer and Mattick 2008). These RNA function in conjunction with protein molecules to achieve gene regulation, each of the different RNA are described in more detail below.

siRNA and miRNA are short sequences of RNA that by Watson Crick base pairing form double stranded strands with target RNA. These double stranded RNA are targeted by cellular degradation mechanisms (Hannon and Rossi 2004). The difference between siRNA and miRNA lies in the role they play, siRNA are largely regarded as defense against exogenous RNA while miRNA is responsible for regulation of endogenous genes (Carthew and Sontheimer 2009). snoRNA identifies RNA for modification and guides protein to modification site. These modifications, including methylation and pseudouridylation, are important for proper folding in rRNA and tRNA (Balakin, Smith and Fournier 1996). piRNA are a testis specific class of RNA.

They participate in gene silencing similar to miRNA and siRNA, and have been found to target sequences that are prone to relocating themselves within the genome also known as

transposons (Wahid et al. 2009). With the exception of mRNA the above mentioned RNA are non-coding RNA (ncRNA), meaning that they have function other than providing the code for translation. Long ncRNA are ncRNA that are longer than 200 nucleotides. lncRNA can be processed to make siRNA or miRNA but are also functional as regulators in long form (Ben Amor et al. 2009). Riboswitches are sequences of RNA that bind to a specific small molecule, the binding event causes a change in structure that regulates transcription of a neighbouring gene (Winkler, Nahvi and Breaker 2002).

2. RNA in therapeutics

The roles RNA plays in cells make it an appealing target for molecular therapeutic and diagnostic applications. RNA also makes for a potential drug molecule due to the variety of molecules it can bind. Using systematic evolution of ligands by exponential enrichment (SELEX) (Ellington and Szostak 1990, Tuerk and Gold 1990) it is possible to select for an RNA that targets a specific molecule. RNA sequences identified by SELEX to have a high affinity for a target are referred to as aptamers (Ellington and Szostak 1990).

An overview of two approaches to utilizing the properties of RNA including targeting RNA with a drug and using RNA itself as a drug will be provided. This is followed by a review of RNA aptamer : protein/RNA interactions and RNA aptamer : small molecule interactions that have medical implications.

Targeting RNA with Drugs

Types of RNA that have been targeted using small molecule drugs include rRNA, tRNA and mRNA (Thomas and Hergenrother 2008). Of the mentioned RNA targets only rRNA is targeted directly, the other two involve indirect effects. Targeting tRNA involves inhibition of aminoacyl-tRNA synthetases, which are responsible for attaching amino acids to

cognate tRNA (Jarvest et al. 2002). While targeting mRNA involves using naturally occurring riboswitch regulation by providing ligand mimics to regulate mRNA (Blount and Breaker 2006).

rRNA has long been a target for antibiotic drugs (Fourmy, Recht and Puglisi 1998), however as more is learned about rRNA function more specific drugs are being developed. For example significant progress has been made in targeting rRNA to reduce the incidence of nonsense mutations that are associated with the Duchenne muscular dystrophy phenotype. There are currently multiple drugs in phase I and II clinical trials (Muntoni and Wood 2011) pertaining to this neuromuscular disorder. PTC124 is currently being tested in phase III trials. It is a small molecule which binds to the 60S ribosome and allows for selective translational bypass of nonsense mutations (Wilton 2007). These nonsense mutations are responsible for build-up of incorrectly translated protein that leads to disease conditions (Welch et al. 2007).

RNA as a drug

Currently there are several aptamers in phase I and II clinical trials (Bouchard, Hutabarat and Thompson 2010). These include aptamers for treatment of coronary artery bypass (Dyke et al. 2006), macular degeneration (Ng et al. 2006) and acute myeologenous leukemia (Bates et al. 2009). Macugen is an aptamer based drug that targets vascular endothelial growth factor (VEGF) currently available for treatment of macular degeneration (Deissler and Lang 2008). This aptamer is conjugated to a polyethylene glycol (PEG) to increase its lifetime *in vivo*. PEG increases the lifetime of biomolecules *in vivo* by changing the biomolecules hydrophobicity and electrostatic binding properties (Veronese and Mero 2008). PEGylation turns the main disadvantages of RNA drugs, the low lifetime due to

degradation, into advantage by allowing tailoring of the lifetime of the drug based on size of PEG (Bouchard et al. 2010).

3. **Large biomolecule RNA aptamer interactions**

Many efforts have been directed at developing aptamers that target the human immunodeficiency virus or HIV by specifically targeting the HIV regulator of virion expression (Rev) peptide, trans-activation response element (TAR) HIV RNA or HIV trans activator of transcription (Tat) peptide (Lebars et al. 2008, Matsugami et al. 2003, Ye et al. 1999).

HIV Rev peptide

The HIV Rev peptide binds to the envelope gene, specifically to the Rev response element. It is responsible for transporting mRNA that encodes viral proteins to the cytoplasm (Zapp et al. 1991, Tiley et al. 1992, Heaphy et al. 1991). The study of the structures of HIV rev peptide in complex with RNA aptamers demonstrates how RNA can influence the structure of its ligand. Depending on the RNA sequence, the peptide binds in either an α-helical or elongated form (Ye et al. 1999). This knowledge is important if the peptide RNA complex is to be targeted.

HIV Tat

The HIV Tat peptide binds to TAR HIV RNA and is necessary for transcription initiation, an important part of the viral life cycle (Frankel 1992). The HIV Tat aptamer complex was studied by using the simplest analog of Tat, an argininamide molecule (Matsugami et al. 2003). Argininamide was used as an analog of Tat since the peptide is an arginine rich peptide and an arginine was implicated in binding to the TAR region (Tao and Frankel 1992). This revealed the aptamer was binding two argininamide molecules suggesting

that it interacts with two arginine residues on the peptide (Matsugami et al. 2003). Inhibition of binding of Tat to TAR was observed when Tat is captured by the aptamer (Yamamoto et al. 2000).

TAR-HIV RNA

The interaction of the aptamer selected against TAR-HIV RNA reveals a kissing complex where non canonical inter RNA interactions along with stacking interactions create a stable complex (Figure 1) (Van Melckebeke et al. 2008). These types of complexes are important to the viral life cycle. For example, the HIV-1 genomic RNA dimerization initiation site (DIS) kissing complex formed by two DIS elements triggers viral RNA dimerization (Paillart et al. 2004). It has been shown that the hydrogen bonding network within the kissing complex along with intermolecular stacking interactions is responsible for molecular recognition (Lebars et al. 2008).

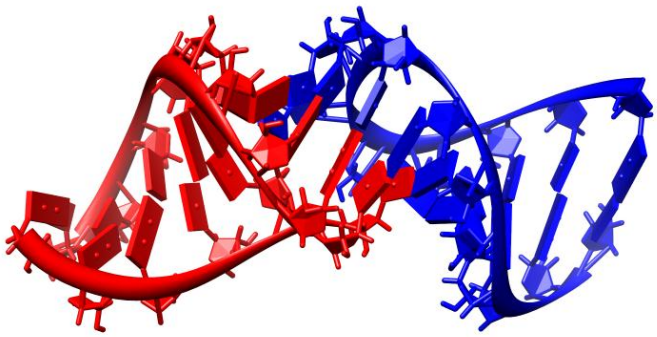

Figure 1. TAR – TAR aptamer kissing complex; in red HIV TAR and in blue HIV TAR aptamer. PDB ID 2NR1 (Van Melckebeke et al. 2008). Figure was generated using UCSF Chimera (Pettersen *et al*. 2004).

MS2 coat protein

Another virus that has been targeted for aptamer development is bacteriophage MS2. This virus has been used as a model system to study RNA-protein interactions (Stonehouse et al. 1996, Valegard et al. 1994). The MS2 coat protein is responsible for recognition of a stem loop within the genome and binding to this loop is part of a process that initiates encapsidation (Grahn et al. 1999). Structural investigations of this aptamer and MS2 coat protein revealed the aptamer binds to protein in a similar manner to other stem loop RNA's. Hydrogen bonding between protein and RNA is apparent in different stem loops as well as the aptamer (Horn et al. 2004).

RNA polymerase

Viral RNA interactions are not the only RNA interactions of interest that have been addressed by aptamer development. Other targets include RNA polymerases and initiation factors. RNA polymerases, the enzymes responsible for transcription of DNA to RNA can be inhibited by binding of RNA molecules (Espinoza, Goodrich and Kugel 2007, Trotochaud and Wassarman 2005). Structural work on the RNA aptamer bound to RNA polymerase II (Figure 2A) highlighted a possible mechanism for inhibition. The aptamer binding blocks the initiation center so template DNA cannot reach the catalytic center. B2 RNA is an ncRNA that supresses mRNA transcription by inhibiting RNA polymerase II in response to heat shock (Espinoza et al. 2004). Competitive binding of B2 RNA and RNA polymerase II RNA aptamer to RNA polymerase II was investigated. The absence of B2RNA binding revealed by these experiments suggests that B2 RNA may bind in the same way as the aptamer (Kettenberger et al. 2006). Since the RNA aptamer binds in the A-form within the RNA polymerase II cleft, it was also suggested that this maybe how 6S RNA (which also inhibits

RNA polymerase II (Trotochaud and Wassarman 2005)) binds to the RNA polymerase II, this cleft naturally accommodates B-form DNA templates (Kettenberger et al. 2006).

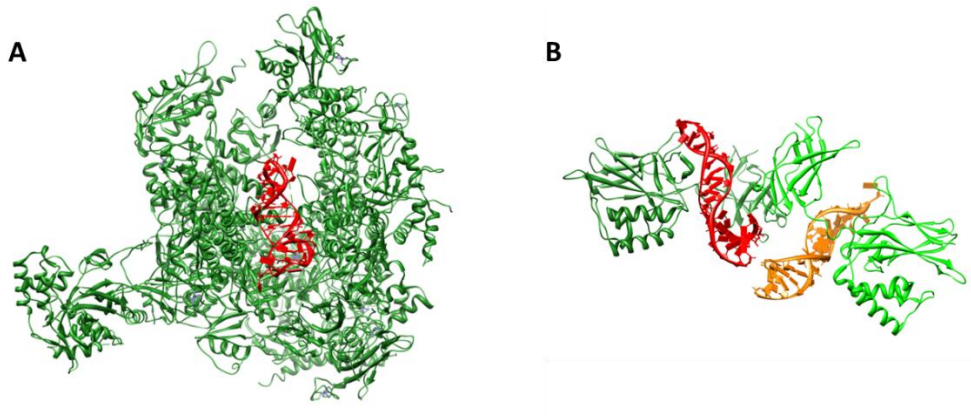

Figure 2. RNA aptamer (RED and ORANGE) bound to protein (GREEN) A) RNA polymerase II, PDB ID 2B63 (Kettenberger et al. 2006) B) Nf-kb homodimer, PDB ID 1OOA (Huang et al. 2003). Figure was generated using UCSF Chimera (Pettersen *et al*. 2004).

Initiation factors

Initiation factors are proteins that bind to the ribosome during translation. The NF-kb factor is involved in activating genes and has been the target of therapeutic inhibition of cancer cells (Darnell 2002). In the case of the mammalian transcription factor binding, the RNA aptamer mimics DNA structure (Figure 2B). The pre-bound structure of the RNA resembles B-form DNA, upon binding it adapts to the presence of the protein (Reiter, Maher and Butcher 2008). The mammalian initiation factor 4A binding interaction with its RNA aptamer were studied by obtaining structures of individual RNA aptamer loops and evaluating the interactions with the initiation factor. These studies suggest that binding involves the interaction of the aptamer's AUCGCA loop with the initiation factor (Sakamoto et al. 2005).

Future structural work may reveal how these aptamers could interfere with the factors interacting with the ribosome.

Prion protein

RNA aptamers have also been used to study protein targets whose primary function does not involve interaction with RNA, such as prion proteins and immunoglobulins. Prion proteins are infectious particles responsible for diseases like Creutzfeldt Jacob disease and spongiform encephalopathies (Huang et al. 1994). The RNA aptamer for bovine prion utilizes the electrostatic interaction between its phosphate backbone and lysine clusters, along with stacking interactions between its GGGG quadruplex and a tryptophan residue to achieve binding (Mashima et al. 2009). Prion protein has been found to bind to amyloid –β oligomers leading to synaptic dysfunction. This aptamer has been proposed for development as a therapeutic agent for Alzheimer's disease, since the prion protein plays a role in impairment of synaptic plasticity (Lauren et al. 2009). The prion aptamer has already been shown to reduce the formation of prion protein in infected cells, most likely by preventing prion protein from interacting with native proteins (Proske et al. 2002).

Human immunoglobulin G

Human immunoglobulin G (IgG) is a protein responsible for identifying pathogens (Litman et al. 1993). The structure of human IgG bound to its aptamer reveals the interactions that make it specific for this particular immunoglobulin. These involve stacking interactions with Tyr373; unlike other protein RNA interactions, the binding is not driven by the interaction of negatively charged phosphate and positively charged surface of protein (Nomura et al. 2010). This is significant because it has expanded the type of ligand that can be considered a target for aptamer development.

4. **Drug/Small molecule RNA aptamer interactions**

Neomycin

The antibiotics that target rRNA have been investigated further by the development of aptamers that bind them with high affinity and specificity. Neomycin B is an aminoglycoside antibiotic that inhibits a variety of RNA-mediated biological functions (Fourmy et al. 1998). The structure-function relationship of Neomycin B and other aminoglycosides has been studied with relation to the ribosome. Two binding sites have been identified, one on helix 44 of the small ribosomal unit and the other on helix 69 of the large ribosomal subunit. In the small ribosomal subunit, neomycin binds within a pocket formed by an A : A base pairing and an unpaired A. These residues are responsible for increasing affinity to cognate tRNA – mRNA. When antibiotic is bound the ribosome is immobilized into high affinity configuration recognizing both cognate and non-cognate tRNA-mRNA complexes leading to miscoding (Magnet and Blanchard 2005). In the large ribosomal subunit, it binds within a helix with binding stabilized by contacts including a CAAUAC loop and G1906. This helix is swung away from an interface of subunit association by the ribosome recycling factor (RRF). Binding of the antibiotic restores interactions destabilized by the RRF and inhibits ribosome recycling (Borovinskaya et al. 2007). Neomycin B in complex with HIV-1 DIS (previous mentioned) has since been crystallized and its structure determined. This binding interaction is similar to that involved in the small ribosomal unit (Bernacchi et al. 2007, Freisz et al. 2008, Ennifar et al. 2003). These structures reveal that the mode of interaction between RNA and Neomycin B can vary. The binding of Neomycin B to its aptamer has been investigated to obtain a better understanding of aminoglycosides RNA interactions, Figure 3 shows a few of the different structures of Neomycin B RNA binding pockets.

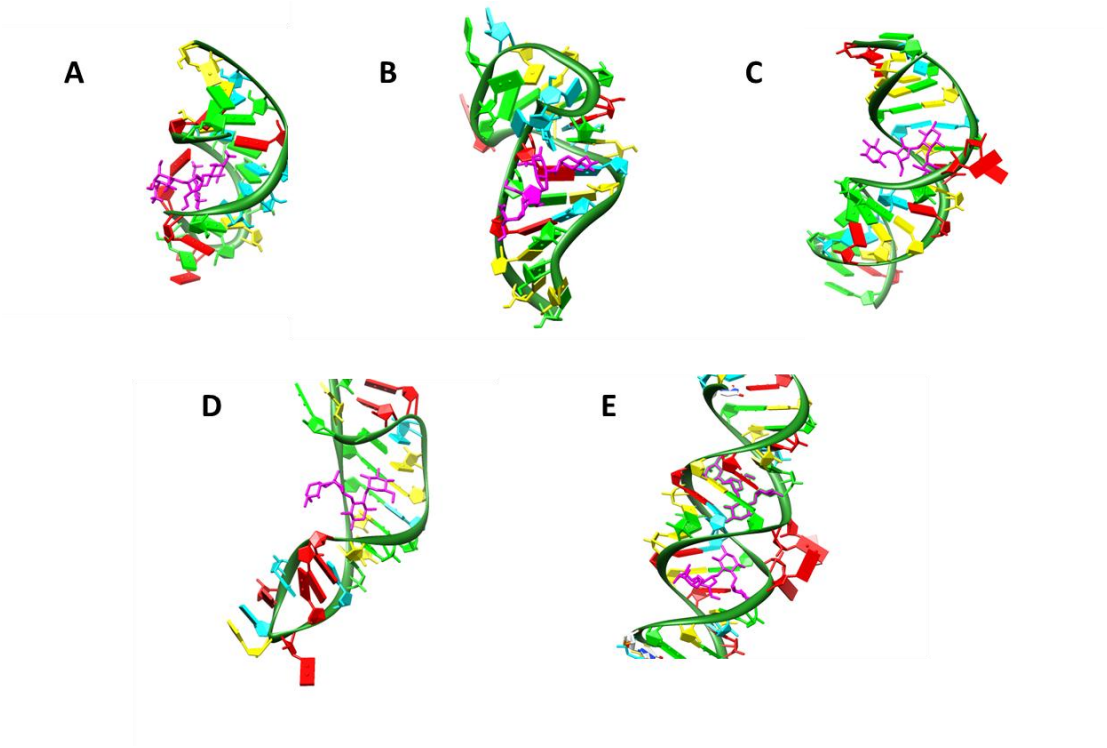

Figure 3. Neomycin B bound to RNA. A) Neomycin B aptamer, PDB ID 1NEM (Jiang et al. 1999) B) HIV Tat, PDB ID 1QD3 (Faber et al. 2000) C) 30S ribosome Neomycin binding site, PDB ID 2QAN (Borovinskaya et al. 2007) D) 50S ribosome Neomycin B binding site, PDB ID 2QAO (Borovinskaya et al. 2007) E) HIV DIS complex, PDB ID 3C7R (Freisz et al. 2008). Neomycin B is colored PURPLE. RNA is color coded A-RED, U-CYAN, G-GREEN, C-YELLOW. Figure was generated using UCSF Chimera (Pettersen *et al*. 2004).

Neomycin B binds to the aptamer within a pocket consisting of three consecutive GU base pairs and a flap formed by an adenine base (Jiang et al. 1999). This pocket is different from the aforementioned binding sites. Further investigation of this interaction determined that hydrogen bonding interactions between aptamer and ligand were the major mechanism responsible for binding (Cowan et al. 2000). A more recent study used NMR techniques to

show that protonation of Neomycin B accompanies binding its cognate aptamer, demonstrating the ability of RNA to influence its ligand (Freire et al. 2007). The thermodynamic differences in binding of these complexes and other RNA complexes will be discussed in the following section.

Other antimicrobial agents have been used as targets for development of aptamers. These include tetracycline, tobramycin and streptomycin. Characterization of these complexes has clarified different aspects of RNA small molecule interactions and most of these aptamers have also been used to develop biosensors for medical applications (Liu, Cao and Lu 2009). For example the tobramycin aptamer has been incorporated as part of an aptasensor that can detect tobramycin and other aminoglycosides in human serum (Gonzalez-Fernandez et al. 2011).

Tetracycline

Tetracycline, tobramycin and streptomycin are antibiotics that like neomycin, target the bacterial ribosome. The tetracycline aptamer boasts a more complicated aptamer structure than usually obtained by SELEX against a small molecule. The tetracycline aptamer consists of three helices, creating a binding site out of tertiary contacts between the helices. ITC studies of the tetracycline riboswitch revealed a two-step binding mechanism driven by favourable enthalpy. Tetracycline's interaction with the 30S ribosomal subunit is stabilized by hydrogen bonding interactions as opposed to the aptamer which has stacking interactions with two rings of tetracycline (Xiao, Edwards and Ferre-D'Amare 2008, Brodersen et al. 2000).

Tobramycin and Streptomycin

The structures of two aptamers selected for tobramycin have been solved. Both aptamer tobramycin complexes revealed that the antibiotic binds within a deep groove and has

multiple hydrogen bonding contacts with the RNA. While both aptamers share the binding motif, one uses a base bulge to widen RNA major groove while the other has three mismatch pairs. Since both aptamers have comparable binding affinities this example reveals that changes to the binding site can be diverse (Jiang and Patel 1998, Jiang et al. 1997). The streptomycin aptamer has also been studied by the same group that investigated the structure of tobramycin and neomycin aptamers. This aptamer consists of S turns that create a cavity to encapsulate streptomycin (Tereshko, Skripkin and Patel 2003).

Purine

Naturally occurring aptamers consist mainly of riboswitches, these sequences affect the secondary structure upon binding its ligand to allow for transcription of the following sequence. Similarity between an artificially selected aptamer and naturally occurring RNA can be seen in purine binding RNAs. The structure of the purine riboswitch has been obtained and reveals that the ligand is encapsulated by the RNA. Kinetic studies of this binding interaction suggest that the ligand first engages in Watson-Crick base pairing with Y74 followed by a loop closure that traps the ligand in the binding pocket and subsequent formation of hydrogen bonds between ligand and RNA (Gilbert et al. 2006). Furthermore mutation studies of the purine riboswitch reveal the ability of RNA to form bound-like structure through ligand mimicking. The term ligand mimicking is used to describe a receptor mimicking the presence of a ligand with a residue that has characteristics of the ligand. The mutant purine riboswitch is inactive, with one of its nucleotides (G39) occupying the active site (Delfosse et al. 2010). While the structure is not yet available, other biochemical methods suggest that an artificially selected adenine aptamer has a similar dependence on hydrogen bonding versus stacking interactions (Meli et al. 2002). The guanine aptamer has a consensus

sequence similar to tobacco ring spot virus satellite RNA hairpin ribozyme (Kiga et al. 1998). The part of purine riboswitch sequence that matches closest to the guanine aptamer is involved in binding (Figure 4).

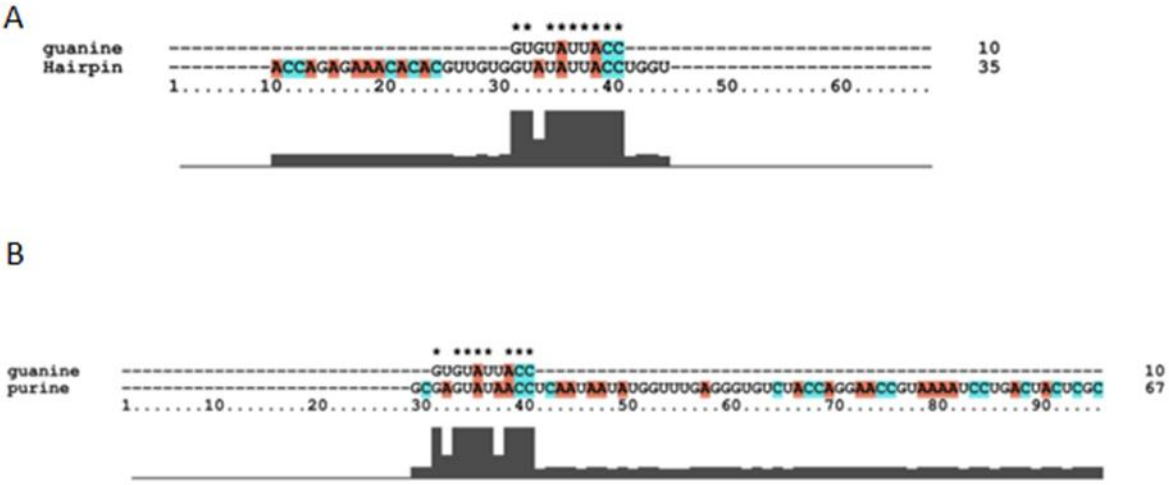

Figure 4. Comparing guanine aptamer consensus sequence to A) hairpin ribozyme B) purine riboswitch. Image generated using ClustalX 2.1.

S-Adenosyl methionine

The S-Adenosyl methionine (AdoMet) riboswitch is important in the regulation of amino acid biosynthesis (Grundy and Henkin 1998). The structural study of the AdoMet bound aptamer revealed that the interaction between RNA and AdoMet primarily involves the adenosine of AdoMet. Investigation of the interaction of other metabolites with the AdoMet riboswitch has suggested possible regulatory roles (Edwards et al. 2010). The AdoMet riboswitch is a potential target for antimicrobials due to its regulatory role in bacteria (Epshtein, Mironov and Nudler 2003).

5. Thermodynamic parameters

The binding of two molecules is generally discussed in terms of the free energy change (ΔG), the enthalpy change (ΔH), the entropy change (ΔS) and dissociation constant (K_d). The thermodynamic parameters involved in binding interactions are related to each other by the Gibbs Helmholz equation (Equation 1).

$$\Delta G = \Delta H - T\Delta S \qquad \text{(Equation 1)}$$

ΔG is related to the binding affinity by Equation 2, with (R) being the gas constant and (T) the absolute temperature.

$$\Delta G = - RT \ln(1/K_d) \qquad \text{(Equation 2)}$$

K_d is the dissociation constant defined and can be defined as the rate ligand enters binding pocket over the rate at which the ligand leaves binding pocket. It is apparent from these equations that binding is stronger, K_d lower, the more negative is the value of ΔG. From Equation 1 it can be gleaned that a negative ΔH will push the value of ΔG to a larger negative value. Likewise, a positive value for ΔS will push the value of ΔG to a larger negative value. A negative value of ΔH will be referred to as favourable ΔH and is associated with the increase of interactions between ligand and receptor, while a positive value of ΔH will be referred to as unfavourable ΔH and is associated with reducing number of interactions (Jelesarov and Bosshard 1999). A negative value of ΔS will be referred to as unfavourable ΔS and is associated with a decrease in randomness (*e.g.* restricting movement) while a positive value of ΔS will be referred to as favourable ΔS and is associated with an increase in randomness (*e.g.* release of water molecules) (Jelesarov and Bosshard 1999).

Table 1 shows a summary of thermodynamic data for binding of the above mentioned RNA targets. The general trend is that binding is driven by favourable ΔH with some

unfavourable ΔS. The two outliers to this trend are the purine riboswitch and the DIS HIV kissing loop.

Table 1: Summary of RNA binding thermodynamic data

Target	RNA	ΔH(kcal/mol)	ΔS(kcal/mol/K)	ΔG(kcal/mol)	K_d (nM)
Neomycin B(Cowan et al. 2000)	Aptamer	-21.6	-0.0440	-8.488	690
Tetracycline(Muller et al. 2006)	Aptamer	-22.9	-0.0352	-12.428	1
purine riboswitch(Gilbert et al. 2006)	Aptamer	-40.3	-0.0976	-10.730	17
AdoMet riboswitch	Aptamer	-24.0	-0.0462	-10.231	32
Tyrosinamide(Lin et al. 2008)	DNA Aptamer	-23.7	-0.0539	-7.638	2439
Malachite(Bernard Da Costa and Dieckmann 2011)	Aptamer	-25.9	-0.0569	-8.790	280
Neomycin B(Bernacchi et al. 2007)	DIS kissing-loop	-9.4	0.0027	-10.200	34
Neomycin B(Kaul and Pilch 2002)	Ribosomal A site	-16.2	-0.0279	-7.900	1550

The purine riboswitch has a higher amount of favourable enthalpy change while DIS HIV kissing loop has a lower ΔH. It is interesting to note that in both cases the variation of favourable ΔH is compensated by the inverse adjustment in unfavourable ΔS. The DIS HIV binding has a 20% greater amount of ΔG from charge related interactions than the small ribosomal binding site (Bernacchi et al. 2007). While the purine riboswitch has a significant amount of hydrogen bonding (Gilbert et al. 2006) which might explain the ΔH differences. These two examples suggest that artificially selected aptamer binding follows a different trend compared to the naturally occurring RNA small molecule interactions. However examining the AdoMet riboswitch the thermodynamic parameters are almost identical to the aptamers. This suggests that there is still too small a set of data to make generalizations about the thermodynamic trends. The similarity in energetics of binding is eclipsed by the specificity of

each binding pocket created by differences in sequence and geometry of the binding pocket (Appendix Table A1).

6. Conclusions

A common trend seen with the aptamers selected for larger biomolecules is that they mimic the type of interactions that already exist in organisms. This is seen clearly in the aptamer for TAR HIV RNA, which forms a kissing complex similar to that seen in HIV DIS (Van Melckebeke et al. 2008, Paillart et al. 2004). This phenomenon is implied by the work with RNA polymerase II aptamer and B2RNA competitive binding to RNA polymerase II (Kettenberger et al. 2006).

In the case of aptamers for antibiotics, the naturally occurring RNA that binds to the same targets has clear differences in their binding pockets. This is a reflection of the evolution of RNA, since the naturally occurring RNA did not have a selection pressure driven purely by affinity to target, but rather by their function within the system (cell/virus). As seen in the case of tobramycin with two aptamers that use different means to widen the binding pocket (Jiang and Patel 1998, Jiang et al. 1997) and multiple ATP aptamers (Huang and Szostak 2003) it is possible to have variations of sequences that have strong binding affinity and nature has had multiple variations to explore other functions.

The closer relatives to artificially selected aptamers, riboswitches, do at least in the case of adenine, share similarity. Another example of similarity in sequence between artificially selected aptamer and naturally occurring RNA is that of the ATP aptamer binding motif which was found in a bacterial virus (Shu and Guo 2003). The aptamers that select for small molecules do provide a window into the capacity for function that RNA has, and the roles it could have played in a prebiotic world.

The number of aptamers is increasing as methods to select them become more routine, even including *in silico* techniques (Chushak and Stone 2009). 2'-Locked RNA aptamers are aptamers where there is a 2'O, 4'-C methylene link which confers RNA C3' endo conformation. This change results in an entropic constraint that leads to increased affinity for target (Schmidt et al. 2004). This, along with other developments in degradation resistant nucleotides (Minakawa et al. 2008) promises many applications for aptamers to come.

RNA binding usually involves adaptive interactions and this has been seen for binding to peptides and small molecules (Patel et al. 1997, Ye et al. 1999, Flinders et al. 2004). This makes it important to probe the conformational mobility and thermodynamics of binding so that the aptamer target molecule interaction is characterized. This line of investigation can be supplemented by site-directed modification of the aptamer to change the spatial configuration or the energy of the binding interaction. For example the binding affinity of tRNAGln to glutaminyl-tRNA synthetase was improved by studying the related aptamer, the improvements did not involve the RNA protein contacts but instead were driven by tertiary structure stabilization of the RNA (Lee and McClain 2004). Another important reason for the study of structure and thermodynamics of RNA-ligand interactions is to understand the nature of RNA-induced modifications of the ligand itself. A good example of such behaviour is seen in the conformational changes induced by malachite green molecules binding to cognate aptamer, and these changes are significant enough to change the optical properties of the dye molecule (Nguyen et al. 2004). This type of binding interaction could expand modalities of drug interactions, such as aptamer-assisted pro-drug delivery.

Understanding the nature of the interactions between target and drug molecule has improved the rational design of protein targeting molecules (Noble, Endicott and Johnson

2004). The structure-function paradigm is being applied to rational design of biologically active therapeutic RNA. This effort is assisted by the use of aptamer models to understand nature of RNA-molecule interactions.

7. Research Outline

The following chapters describe our studies of RNA ligand interactions in binding and catalysis. This involves the malachite green aptamer (MGA) which was selected to bind malachite green dye (MG) (Baugh, Grate and Wilson 2000). MG or 4-[(4-dimethylaminophenyl)-phenyl-methyl]-N,N-dimethylaniline has been used in aquaculture industry to treat fish and fish eggs due to its antiseptic, antibacterial and antifungal properties (Hall and Unestam 1980, Alderman 1985). MG has been found to inhibit enzymes including acetylcholinesterase (Kucukkilinc and Ozer 2008) and multidrug-binding repressor protein QacR (Peters et al. 2011).

An introduction to MGA and the thermodynamic studies done with MGA binding, to MG and derivatives, is covered in chapter 2. This chapter was published under the title "Entropy and MG^{2+} control ligand affinity and specificity in the malachite green binding RNA aptamer" in *Molecular BioSystems* (Appendix Note A1). The introduction has been expanded and the rest of the paper has been reproduced with permission from RCS publishing (Appendix Note A2). These experiments pointed to a significant difference in the binding of the different derivatives. To further explore the nature of binding pocket, competition binding studies were conducted and are discussed in chapter 3. Chapter 3 has been submitted for publication under the title "Not so adaptive binding: Ligand competition in an RNA aptamer" and is currently under review. In addition to material submitted for publication chapter 3 contains preliminary computational work. The multiple capabilities revealed by our binding

studies and previously discovered catalytic capacity (discussed in chapter 2) stimulated the attempt to select a new aptamer and determine if this varied capacity would be replicated. This selection is discussed in chapter 4 along with a brief comparison of DNA and RNA aptamers for the same target. Finally a report of the attempts to purify MGA of uniform sequence length and attempts to expand the catalytic repertoire of MGA are covered in chapter 5.

Chapter 2: Structure and Thermodynamics in the Malachite Green RNA Aptamer

1. Introduction

Aptamers have been developed for a wide variety of targets and are excellent model systems for RNA-ligand interactions (Chapter 1). The mode of binding in different aptamers varies greatly depending on their targets and selection procedure. For example, the Neomycin B RNA aptamer binding is driven largely by hydrogen bonding (Cowan *et al*. 2000) while the malachite green RNA aptamer (MGA) binding is driven by electrostatic and stacking interactions (Flinders *et al*. 2004). MGA has been utilized as a bioprobe in combination with microtubules (Hirabayashi *et al*. 2006), as a fluorescent sensor (Xu and Lu 2010, Zhang *et al*. 2009), an assay for malachite green (MG) (Stead *et al*. 2010), as part of a diagnostic molecular automata (Hirabayashi, Ohashi and Kubo 2010) and for the validation of molecular docking software (Detering and Varani 2004).

MGA was originally engineered for binding specificity to the tri-phenyl dye malachite green (Grate and Wilson 1999) The secondary structure of MGA and chemical structure of MG are shown in Figure 1 A and B, respectively. The purpose behind selecting this aptamer was to harness MG's destructive potential. MG has been found to generate hydroxyl radical from water when irradiated with red laser light and these radicals damage surrounding biomolecules (Liao, Roider and Jay 1994). The design involved appending MGA into the non coding region of a target gene. MG is then introduced and binds to MGA. Subsequent irradiation of target region leads to formation of radicals which damage the mRNA and damaged mRNA would be degraded by the cell (Grate and Wilson 1999). The discovery of siRNA which can target mRNA sequences for degradation (Hamilton and Baulcombe 1999) without the need to introduce a carcinogenic dye made such a method obsolete. However MGA proved useful in exploring the potential

of aptamers in molecular biology, the insertion of this sequence in *S.cerevisiae* resulted in cell cycle regulation by MG. MGA was capable of doing this without the use of laser irradiation. The structural changes upon binding MG were sufficient to prevent the 40S ribosomal subunit to interact with cyclin gene transcripts (Grate and Wilson 2001).

The structure of the aptamer bound to ligand was initially solved by X-ray crystallography in complex with the MG derivative tetramethylrosamine (TMR) (Figure 2) (Baugh, Grate and Wilson 2000) and later by NMR spectroscopy in complex with the original selection target MG (Flinders *et al.* 2004) (Figure 1C). The binding pocket of the MGA (Figure 1A) consists of a base quadruple (C7:G24:A31:G29) and a Watson-Crick base pair (G8:C28) which serve as stacking platforms for malachite green (MG, Figure 1B). In addition, the nucleotides A9 and A30 are positioned in such a way that they almost completely close the pocket on one side (Figure 1C) (Flinders *et al.* 2004, Baugh *et al.* 2000). The other residues in the internal loop region of the aptamer act as linkers and anchors, for the nucleotides that are in contact with the ligand.

The major difference between the structures of the MGA-TMR and the MGA-MG complexes is that in order to accommodate the non-planar MG, the aptamer undergoes a small rearrangement that can be best described as a rotation of the upper part of the binding pocket relative to the lower part (Flinders *et al.* 2004). This provides enough space to accommodate the rings of MG in the binding pocket, but also leads to a loss of some stacking interactions. Both structures reveal a lack of hydrogen bonding between MGA and ligand, this provides an excellent model system to study the role of electrostatic and stacking interactions.

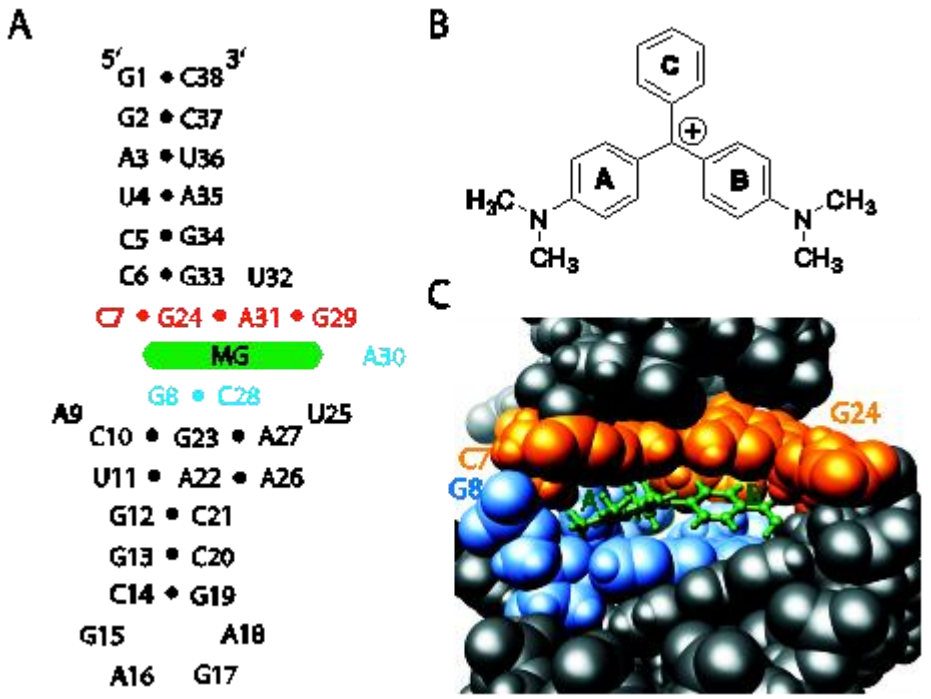

Figure 1. (A) Schematic of the MGA complex used in these studies. Nucleotides that form the top and bottom of the binding pocket are shown in orange and blue, respectively. (B) Structure of malachite green (MG). (C) Space filling model of the MGA binding pocket from the solution structure (1Q8N). The ligand is shown as ball and stick model. Same colour scheme as in (A). Graphics prepared with UCSF Chimera (Pettersen *et al*. 2004).

The study of the MGA-ligand interactions have shown that ligands can undergo significant changes in their electronic structure and charge distribution when bound inside an RNA binding pocket (Nguyen *et al*. 2002). The MG molecule responds to the unique electrostatic environment inside the RNA aptamer with a redistribution of its positive charge as well as a conformational change (Nguyen *et al.* 2004). These observations suggested that the environment inside the RNA binding pocket can have a significant effect on the chemical properties of the bound ligand. Further studies revealed that the malachite green aptamer can indeed act as a ribozyme when presented with a suitable

substrate molecule. An acetyl-ester derivative of malachite green undergoes an accelerated hydrolysis reaction when bound to the aptamer (Brackett and Dieckmann 2006), this reaction is discussed further in chapter 5.

The abovementioned studies and applications of the MGA and other aptamers indicate the need for a generalized understanding of ligand–RNA interactions as basis for further developments. Isothermal titration calorimetry (ITC) has been established as a standard method for the detailed study of the thermodynamics of RNA–small molecule and RNA–protein interactions (Chapter 1) as well as RNA folding processes (Feig 2007). Insights into the thermodynamic forces that drive ligand binding and dissociation open a way for a better understanding of these important interactions that are the basis for drug action and catalysis. We have conducted ITC studies investigating the binding of MGA to MG under a variety of solution conditions. In addition to binding of MGA to MG, MGA binding to MG derivatives was investigated. MG derivatives tested included tetramethylrosamine (TMR), pyronin Y (PY), and crystal violet (CV). Figure 2 shows the structure of these derivatives. PY has a planar structure similar to TMR, but lacks the third ring, while crystal violet (CV) has a non-planar structure similar to MG, with an extra dimethylamine group on ring C.

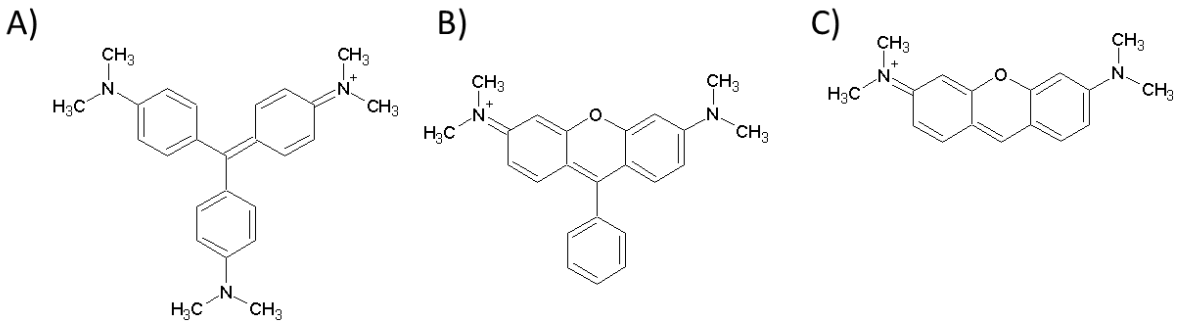

Figure 2. Chemical structure of MG derivatives used in this study: A) Crystal violet (CV) B) Tetramethylrosamine (TMR) C) Pyronin Y (PY).

2. Results

Initial binding experiments

The primary method to determine thermodynamic parameters of MGA binding to ligands was ITC studies. Initially two other methods were attempted to determine binding constants, equilibrium dialysis and fluorescence intensity titrations. These along with NMR studies provided the motivation to investigate the binding of MGA to derivatives.

In the course of NMR studies of MGA in complex with MG, TMR and PY it became apparent that the complexes with TMR and PY were not as stable as the corresponding MG complex under the NMR conditions (low salt, no divalent metal ions). This appeared to be a contradiction with the affinities reported in the original study (Baugh *et al*. 2000) where both TMR and PY formed more stable complexes with MGA than the original ligand MG. The K_d values for MG, TMR and PY were reported as 800 nM, 40 nM, and 225 nM, respectively. These values were determined at low salt but in the presence of divalent metal ions (10 mM K-cacodylate pH 5.8, 10 mM $MgCl_2$, 10 mM KCl). In our NMR studies, divalent metal ions were avoided to ensure sample stability during data acquisition and low salt was necessary to prevent the formation of RNA dimers.

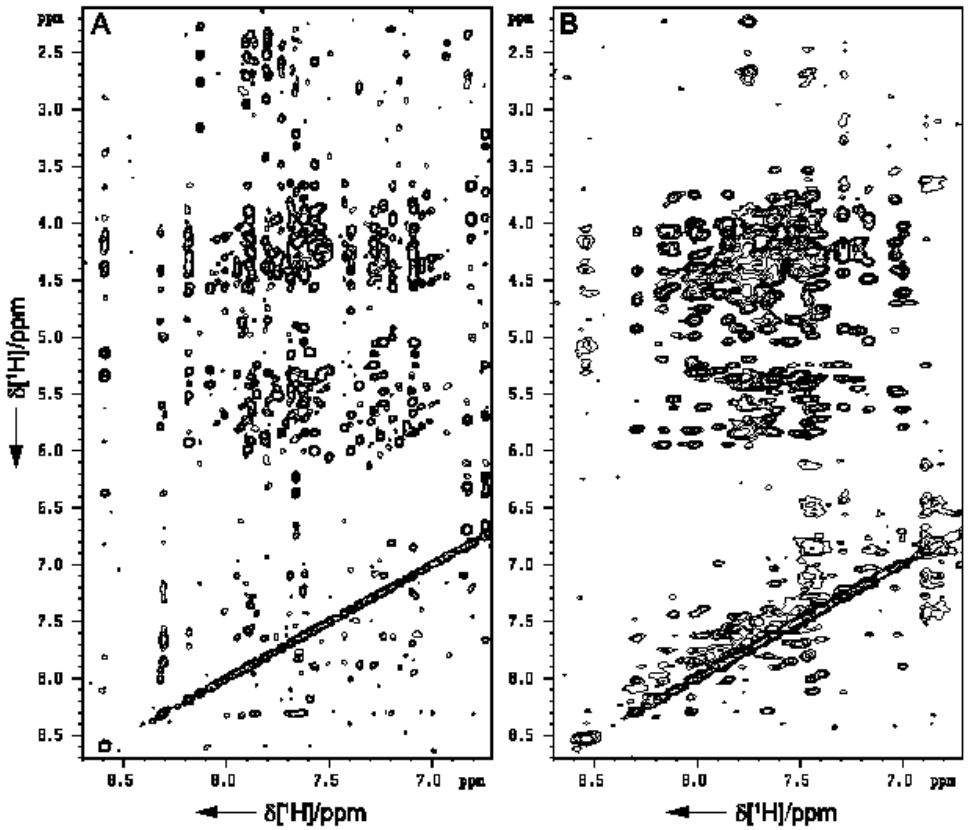

Figure 3. Comparison of 2D NOESY spectra of A) MGA-MG and B) MGA-TMR complexes in 100% D2O at 293K. The spectra were acquired on a Bruker DRX 600 MHz spectrometer in 10 mM potassium phosphate buffer, pH 6.0 and 10 mM KCl.

Figure 3 shows a comparison of 2D NOESY spectra of 1:1 mixtures of MGA:MG and MGA:TMR. It is clearly apparent that the TMR spectrum shows much broader and fewer cross-peaks than the corresponding MG spectrum, indicating a less dynamic complex (faster exchange between free and bound RNA or multiple conformations). In order to address these apparent contradictions, preliminary equilibrium dialysis experiments were conducted to determine binding affinities under conditions closer to those used in the NMR studies (100 mM phosphate buffer, 50 mM KCl, pH 6.0).

Equilibrium dialysis was conducted using DispoEquilibrium DIALYZER (Havard Apparatus, Massachusetts, USA). The DIALZYER consists of two chambers connected by a semipermeable membrane. MG and derivatives can pass through membrane, while MGA due to larger size can not. MGA is added to one chamber and due to the membrane is trapped there. MG or derivative is added to the other chamber and allowed to equilibrate. Binding of MG or derivative to MGA, shifts equilibrium of free ligand, causing more to move into MGA chamber.

These experiments showed that PY had a significantly lower affinity (8.35±3.7 µM) than MG (0.26±0.08 µM) under these conditions (Figure B1 in Appendix). These initial results prompted us to thoroughly investigate the binding behaviour of MGA in complex with its ligands using fluorescence based titration studies.

Fluorescence titration studies relied on the change in fluorescence properties of the ligands when bound to MGA (Baugh *et al.* 2000). The fluorescence binding experiments were conducted using a Nanodrop fluorometer to test all four dyes whose affinities had been previously reported. This method was chosen since it required minimal amounts of RNA and closely resembled the methodology used in the original study. The binding affinity was determined by using the change in fluorescence as concentration of MGA was increased while ligand concentration was kept constant in 50 mM phosphate buffer, 150 mM NaCl, pH 6.7.

The dissociation constants for the MGA complexes formed with MG, TMR, CV and PY were found to be 2.73±0.6 µM , 0.8±0.2 µM , 7.6±1.7 µM and 7.6±1.1 µM , respectively (see Figure B2 in Appendix). These results confirm the trend seen in the equilibrium dialysis study, but do not explain the low stability of the TMR complex seen in the NMR studies.

Surprisingly, CV, which was thought to not interact with the aptamer, seems to have a binding affinity similar to PY, but PY shows a much weaker binding than seen in the original study (Baugh *et al*. 2000). Overall these results indicated that a more comprehensive analysis of the binding behaviour of MGA with these ligands under a broad range of salt conditions was needed in order to understand binding specificity and affinity.

Isothermal titration calorimetry experiments

ITC is based on monitoring the enthalpy involved in a reaction that occurs as a ligand is gradually added to a reaction cell containing receptor. The instrument monitors the temperature and the energy required to maintain the temperature of the reaction cell. It also determines the energy required to maintain the temperature of a reference cell. This energy is subtracted from the energy required to maintain the temperature of the reaction cell, the difference corresponds to the energy involved in the reaction (Wiseman *et al.* 1989, Ladbury 2004). The analysis of this data provides ΔH, ΔS, ΔG and K_d as reported by Wiseman *et al*.

ITC studies were conducted at three different salt concentrations (1 mM, 150 mM, 1.0 M NaCl) and in the presence of the divalent metal ion (10 mM $MgCl_2$). Thermodynamic parameters for the four ligands obtained from these experiments are summarized in Table 1. Overall, the affinity of the ligands increased with salt concentration. The binding of CV at 1 mM salt was below detection threshold and the high salt value could not be determined because CV precipitated at 1 M salt. The presence of $MgCl_2$ at low salt concentrations in general increases affinity, reaching almost a third of the K_d at 150 mM NaCl for MG and TMR, and half the K_d at 150 mM for PY. The only exception is CV where the change in affinity in the presence of Mg^{2+} is not significant. MGA has comparable affinity for TMR and

MG, with TMR binding slightly tighter at higher salt concentrations and in the presence of Mg^{2+}. On the other hand, MG has a higher affinity at low salt in the absence of Mg^{2+}. Both TMR and MG bind significantly tighter than PY and CV which have similar affinities at 150 mM salt, with PY improving in the presence of magnesium. For all four ligands increasing salt concentration or the addition of Mg^{2+} leads to tighter binding. The lower K_d values are predominantly caused by more favourable entropy terms. The exception is PY for which the entropy term does not change significantly in the presence of higher salt or divalent ions.

Table 1. ITC determined thermodynamic parameters for MG, TMR, PY and CV at various salt concentrations, pH 6.7 at 25°C.

Dye	Salt Concentration	K_d(μM)[a]	ΔH(kcal/mol)[a]	ΔS(cal/mol/deg)[a]	ΔG(kcal/mol)[a]
MG	1 mM NaCl	0.80±0.06	-29.23±1.69	-70.13±5.83	-8.33±0.06
	150 mM NaCl	0.28±0.07	-25.93±2.24	-56.87±7.92	-8.98±0.14
	1 M NaCl	0.37±0.06	-25.76±2.64	-56.93±8.54	-8.79±0.10
	1 mM NaCl 10 mM $MgCl_2$	0.10±0.01	-23.10±1.35	-45.37±4.42	-9.58±0.04
TMR	1 mM NaCl	1.06±0.08	-25.23±2.94	-57.27±10.01	-8.16±0.05
	150 mM NaCl	0.28±0.04	-18.32±1.09	-31.43±3.55	-8.95±0.08
	1 M NaCl	0.14±0.05	-13.46±0.44	-13.63±1.07	-9.39±0.18
	1 mM NaCl 10 mM $MgCl_2$	0.08±0.02	-17.29±1.51	-25.50±5.26	-9.69±0.12
PY	1 mM NaCl	14.28±5.04	-13.36±2.22	-22.53±7.94	-6.64±0.20
	150 mM NaCl	4.08±0.20	-17.81±0.38	-35.03±1.20	-7.37±0.03
	1 M NaCl	2.65±0.42	-15.34±1.03	-25.93±3.71	-7.61±0.09
	1 mM NaCl 10 mM $MgCl_2$	1.65±0.67	-16.94±1.77	-30.20±6.52	-7.94±0.23
CV	150 mM NaCl	4.45±0.08	-78.27±14.60	-280.0±49.15	-7.35±0.09
	1 mM NaCl 10 mM $MgCl_2$	3.79±0.12	-54.48±9.71	-158.0±32.60	-7.40±0.01

[a] Average of three independent measurements each. Curves were fit to a single binding site model. For a typical ITC isotherm see Figure B3 in Appendix.

3. Discussion

Entropy Driven Binding

The thermodynamic characteristics of the interactions between MGA and four different derivatives of MG were measured under four different buffer conditions by isothermal titration calorimetry. The binding affinity of MGA for each dye is predominantly controlled by the entropy of binding (Figure 4). CV is the most flexible of the four ligands

and also has the most even distribution of partial charge prior to binding. Hence it suffers the largest entropy penalty upon binding when it is forced into a restricted conformation and localized charge distribution that is dictated by the RNA binding pocket. At 150 mM monovalent salt concentration TMR and PY have similar binding entropy values, whereas MG binding is accompanied by a larger entropy penalty. This can be rationalized because in TMR and PY rings A and B are planar due to the bridging oxygen atoms. On the other hand, the MG molecule is more flexible in its free form with rings A and B able to rotate independent of each other and hence it shows a larger entropy penalty upon binding.

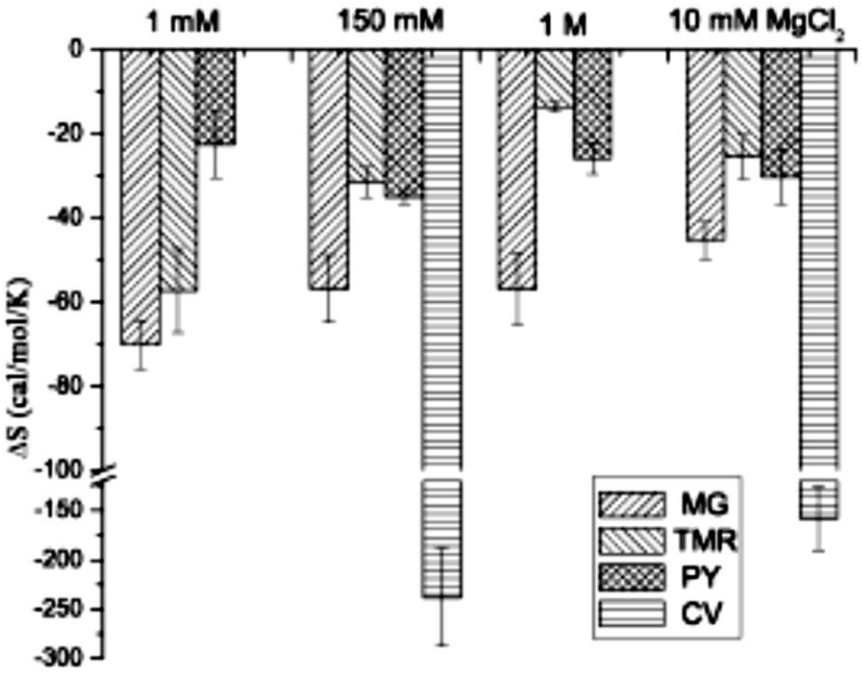

Figure 4. Relationship between entropy of complex formation and salt concentration for dye derivatives binding to MGA.

This behavior is similar to that observed for intercalation binding of small molecule ligands to DNA. Intercalators show a thermodynamic signature with a large favourable

enthalpy contribution originating predominantly from stacking interactions which is countered by a near zero or unfavourable entropy component. The latter is caused by the need to reorganize the structures of nucleic acid and ligand into more rigid or entropically less favourable conformations (Chaires 2008). The observation of this kind of thermodynamic signature makes sense for the MGA complexes because ligand binding and recognition in these molecules does not involve any hydrogen bonding interactions between RNA and ligand, relying exclusively on stacking as well as electrostatic interactions (Baugh *et al*. 2000, Flinders *et al*. 2004).

Metal ions control specificity

Interestingly, the entropy penalty for PY binding does not significantly decrease at higher salt concentrations or in the presence of Mg^{2+} as seen for the binding of MG and most clearly for TMR. PY differs from TMR and MG by the lack of the third phenyl ring (Ring C). Hence it seems that the changes in binding entropy at low and high salt can be largely attributed to interactions between the MGA and ring C of the ligand. An examination of the crystal structure of the MGA-TMR complex (Baugh *et al*. 2000) and the NMR structure of the MGA-MG complex (Flinders *et al*. 2004) shows that A30 which is stacked against ring C of the ligand is part of a bulge/loop structure consisting of A30, A31, U32 and G33. Previous mutation studies have shown that this structure element is important for binding of MG and TMR (Flinders *et al*. 2004). Interestingly, in the crystal structure a Sr^{2+} ion is positioned in such way, that it can interact with the phosphate oxygen atoms of A30, A31 and G33. This suggests that the presence of divalent ions (Mg^{2+}) or a sufficiently high concentration of monovalent ions (KCl or NaCl) is needed to stabilize this element of the binding pocket and thereby the interaction with the ligand. This becomes especially noticeable when ligands other

than the original selection target (MG) are bound. The preference for a divalent metal ion is not surprising considering the presence of Mg^{2+} during the original selection procedure (10 mM $MgCl_2$) (Grate and Wilson 1999).

The influence of magnesium on binding affinities is interesting because it shows that the ligand specificity of the MGA is controlled by the solution conditions. While the aptamer has a lower affinity for all the ligands at low salt concentrations (Figure 5), the binding affinity of MGA for MG is higher than its affinity for TMR at low salt. This is the reverse of what is seen at high salt concentrations where TMR has higher affinity.

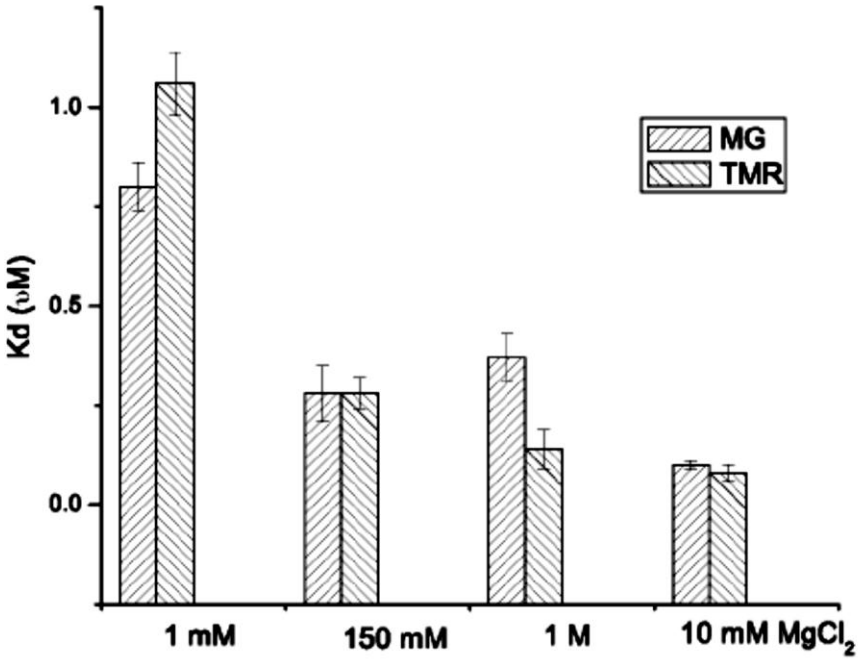

Figure 5. Relationship between salt concentration and affinity for MG and TMR binding to MGA as determined by ITC.

Even though the effect is small, this change in ligand preference is significant in an aptamer selected solely for binding to one target (MG). The ability of MGA to change its

ligand preference depending on the solution conditions demonstrates the large influence of environmental factors on RNA selection/evolution and also highlights the adaptability of RNA.

Comparison to Previously Reported Affinities

The binding affinities reported here differ from some of the values previously reported in the literature (Baugh *et al*. 2000, Babendure, Adams and Tsien 2003, Flinders *et al.* 2004, Wang *et al.* 2009). The affinity for TMR (K_d = 0.08±0.02 µM) is similar to that originally reported by Baugh *et al.* (K_d = 0.04 µM) (Baugh *et al.* 2000). These affinities were determined under comparable buffer conditions. Baugh *et al*. used fluorescence intensity or anisotropy to follow titrations of MGA with TMR and PY. They also reported the binding affinity for MG and CV. These values were determined by competitive inhibition of TMR binding. The affinity of MG reported by Baugh *et al.* (K_d = 0.80 µM) is lower than our value (K_d = 0.10 µM), which is similar to that determined by Babendure *et al*. (K_d = 0.117 µM) (Babendure et al. 2003). The latter value was determined by following the fluorescence intensity of MG during a titration. This discrepancy is likely due to the use of a pre-bound MGA-TMR complex. With a preformed binding pocket that is matched to the planar TMR molecule, the binding of MG is kinetically unfavourable and the reported K_d value might not be determined at equilibrium. It should be noted that the affinity for MG was also determined by Wang *et al.* (Wang *et al.* 2009) using fluorescence intensity. However, their studies were carried out at a higher pH and lower $MgCl_2$ concentration (K_d = 1.03±0.53 µM). The concept of a preformed binding pocket reducing affinity for other ligands is supported by the low affinity for CV (K_d > 1 mM) as reported by Baugh *et al.*. The conformation of CV deviates significantly from that of TMR and thus it would have difficulty to replace TMR in a

preformed complex. This would explain the large difference to our value (K_d = 3.79±0.12 µM) which was determined for CV binding to an unoccupied RNA pocket. One puzzling observation is that the affinity for PY reported by Baugh *et al*. (K_d = 0.225 µM) is significantly higher than the value found in our ITC (K_d = 1.65±0.67 µM) and fluorescence intensity-based studies (K_d = 7.6 µM , no Mg^{2+}) under comparable buffer concentrations. This difference could potentially be a result of intercalation/unspecific binding of PY in addition to the regular binding inside the MGA pocket. PY is known to bind to nucleic acids via intercalation in double stranded regions with a preference for RNA (Darzynkiewicz *et al.* 1986, Kapuscinski and Darzynkiewicz 1987). However, under the conditions used in our studies we do not see any evidence of significant intercalation for PY or any of the other dyes.

Electrostatic contributions

For aptamers where the binding affinity was studied as a function of salt concentration, the common trend is in general a decrease in affinity and an increase in entropy penalty as salt concentration increases (Cowan *et al.* 2000, Hossain and Kumar 2009, Islam and Kumar 2009, Stampfl *et al.* 2007). This observation is typically rationalized by the decrease in polyelectrostatic interactions or a destabilization of bound complex and can be utilized to reveal the effect of hydrogen bonds which are unaffected by the salt concentration. Since the MGA complexes lack hydrogen bonding interactions between ligand and RNA, it was expected that the affinity would decrease as salt concentration increases. However the effect we see is an increase in affinity with increasing salt concentration. As discussed above, this effect is most likely due to a structural stabilization of the binding pocket by metal ions. Wyman (Wyman 1964) and Tanford (Tanford 1969) have proposed the following equation for describing the electrostatic contribution due to ion release for DNA/protein interactions:

$$\Delta G_{elec} = Z\phi RT \ln[Na^+] \qquad \text{(Equation 1)}$$

Z is the apparent charge on the bound ligand, and ϕ is the fraction of Na^+ bound per nucleic acid phosphate. $-Z\phi$ can be obtained from the slope of a log K_a versus log $[Na^+]$ plot (Mascotti and Lohman 1990, Record, Lohman and Dehaseth 1976).

$$\partial \log K_a / \partial \log [Na^+] = -Z\phi \qquad \text{(Equation 2)}$$

These equations have previously been used to analyze the thermodynamic properties of the Neomycin (Cowan *et al.* 2000) and L-tyrosinamide aptamers (Lin *et al.* 2008). In both these cases the $Z\phi$ value was a positive one since the slope from equation (2) was negative. Using this positive value of $Z\phi$ in equation (1) results in a negative value for ΔG_{elec}, since $\log[Na^+]$ is a negative value for concentrations below 1 M. For the MGA complexes in our study, the slope of log K_a vs. log $[Na^+]$ is positive (see Figure B4 in Appendix) and thus results in a positive value for ΔG_{elec}. This suggests that the electrostatic contribution from ion release is not favourably assisting complex formation in the case of MGA. It is important to note that equations (1) and (2) were intended to account for the polyelectrostatic effect which suggests that a large part of nucleic acid binding interactions involves the entropy from the displacement of Na^+ ions. In the case of MGA this effect is probably masked by the structural stabilization outlined above.

Enthalpy-Entropy Compensation

Enthalpy-entropy compensation is seen for the binding of the different ligands to MGA as a function of salt concentration. This phenomenon has been observed for a variety of biomolecules (Cooper *et al*. 2001). The slope of a line generated by plotting entropy vs. enthalpy at different salt concentrations for the different ligands produces a linear correlation

with the equation $\Delta S = m\Delta H + b$. The compensation effect seen for MGA-MG binding (Figure 6), has a similar slope (m = 3.19) as seen in other aptamers, for example the Neomycin RNA aptamer and the L-tyrosinamide aptamer (m = 3.27 when plotting the ΔH vs. ΔS values from these studies) (Lin *et al*. 2008, Cowan *et al*. 2000). Interestingly, this slope is also similar to that reported for several proteins (m = 3.33) (Cooper *et al*. 2001). These similarities may be an effect of entropy and enthalpy reaching equilibrium.

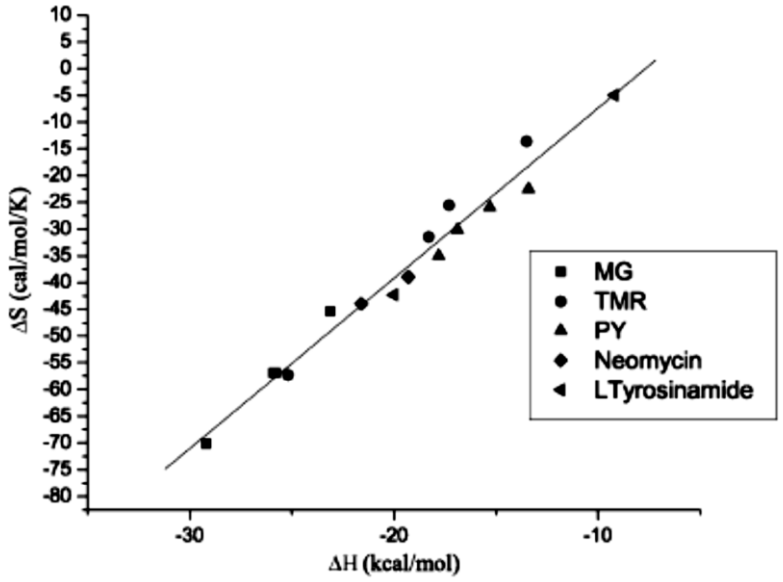

Figure. 6 Enthalpy-Entropy compensation with increasing salt concentration for several RNA aptamer–ligand complexes. MG,TMR and PY in complex with MGA . Neomycin and L-tyrosinamide in complex with their respective aptamer. The line represents a linear fit of all data points and has a slope of 3.19.

4. Conclusions

The results of the binding studies presented here illustrate the adaptability of RNA aptamers. This was seen when the aptamer was presented with derivatives or close relatives of

the original selection target. This property of small RNAs would be a significant advantage when it comes to responding to a changing environment and selection pressure in a pre-biotic setting. The functional adaptability would have allowed early RNA sequence pools to quickly diverge and expand their abilities during the establishment phase of an "RNA world" (Joyce and Orgel 1993).

The comparison of the results from our study and the previous studies discussed above also illustrates the necessity for taking solution conditions into account when comparing structures and binding properties for RNA aptamers. Even though the original *in vitro* selection utilized magnesium ions as buffer component, the NMR study of the MGA-MG complex (Flinders *et al*. 2004) did not reveal any beneficial effect of adding Mg^{2+} ions to the solution. In fact, the rapid degradation of the samples in the presence of magnesium and the difficulty of obtaining monomeric RNA hairpins at higher salt led to the use of a low salt buffer for the structure determination. On the other hand, the MGA-TMR complex yielded very poor quality NMR spectra under these conditions which were puzzling at the time because of the high affinity of TMR that was seen in binding studies. The necessity of high salt or Mg^{2+} for the formation of a stable MGA-TMR complex that is revealed by the ITC study explains these observations.

The results of the ITC binding studies illustrate the importance of the third ring for MGA binding. MG and TMR both have a high affinity with different entropy values due to the differences in planarity and rigidity. PY which is planar but lacks the third ring shows an affinity similar to CV which has the third ring but is non-planar. This suggests a crucial interaction between the third ring of the ligand and MGA. The solvent conditions affect the affinity and specificity of MGA for the different dyes. At low salt, MGA has the highest

affinity for MG, while at high salt MGA has highest affinity for TMR. This is consistent with the crystal structure of the TMR-MGA complex which shows a possible binding site for a divalent metal (Baugh *et al*. 2000). These observations suggest that the optimal structure for MGA to bind MG versus TMR might be different, with MGA bound to TMR structure requiring added stability provided by divalent ion. To investigate this phenomena further competition binding experiments were undertaken discussed in the following chapter.

5. Materials and Methods

Ligand Preparation

Malachite green was purchased from Sigma Aldrich (Sigma-Aldrich Corporation, Milwaukee, U.S.A). Tetramethylrosamine was purchased from Invitrogen (Invitrogen Corporation, California, U.S.A). Pyronin Y was purchased from Acros Organics (Acros Organics, Geel, Belgium). Crystal Violet was purchased from Fisher Scientific (Fisher Scientific Company, Ottawa, Ontario, Canada). Dyes were dissolved in water to make 20 mM stock solutions. Dilutions for different buffer conditions were prepared from these stocks.

Synthesis of RNA

The MG aptamer used for ITC was prepared enzymatically from a synthetic DNA template by using T7 RNA polymerase and unlabeled NTPs (Milligan *et al*. 1987, Milligan and Uhlenbeck 1989), as described previously (Flinders *et al*. 2004). After transcription, the pyrophosphate was removed by centrifugation and the RNA was collected by precipitation with ethanol. The RNA was then separated from NTPs and aborted products on a 12% PAGE. The resulting RNA band was then run on a HiPrep 16/10 DEAE FF anion-exchange column,

followed by desalting on a Hiprep 26/10 Desalting column and lyophilization to dryness. All columns used for RNA preparation were purchased from GE Healthcare, Uppsala, Sweden.

Isothermal titration calorimetry studies

Experiments were performed at 25 ^{o}C on a MicroCal ITC 200 microcalorimeter (MicroCal, Inc., Northampton, Massachusetts, U.S.A). The 10-15 μM RNA solution was prepared by dissolving lyophilized RNA in pH 6.7 10 mM sodium phosphate buffer at desired salt concentration. The 100-150 μM dye solutions were prepared by dissolving solid dye in pH 6.7 10 mM sodium phosphate buffer at desired salt concentration. The ITC cell was filled with RNA solution and was titrated with dye solution from the syringe. Each experiment consisted of 16 injections of 2.54 μl every 300 s, with a first injection of 0.5 μl to a final molar ratio of 2:1 dye:RNA. In order to account for heat of dilution of dye solution, a blank run with buffer in cell and dye in syringe was run and subtracted from the experimental run. All data sets were analyzed using the Origin software package provided by MicroCal and fitted to a one set of sites binding model that assumes a single set of equivalent binding sites.

NMR Spectroscopy

NMR experiments were conducted and analyzed by Dr. Thorsten Dieckmann. All spectra were collected on a Bruker DRX-600 spectrometer equipped with a HCN triple resonance, triple-axis PFG probe. Quadrature detection for the indirect dimensions in multidimensional experiments was achieved using the States-TPPI method (Marion *et al.* 1989). The two-dimensional NOESY spectra (Kumar, Ernst and Wüthrich 1980) in 100% D_2O were acquired at 293 K with a mixing time of 250 ms. All NMR samples were in standard 5 mm NMR tubes

with final RNA concentrations of 0.8 to 1.8 mM in 10 mM potassium phosphate buffer, pH 6.0 and 10 mM KCl and a 10% excess of ligand

Fluorescence Binding Studies

MGA solutions were prepared at concentrations between 0.2 and 13 µM. To each solution dye was added to get a final concentration of 1 µM. The series had a final buffer concentration of 50 mM phosphate buffer, 150 mM NaCl at pH 6.7. The sample fluorescence was measured on a NanoDrop 3300 fluorometer (Thermo Fisher Scientific Company, Ottawa, Ontario, Canada). For MG and CV, there was no detectable fluorescence in the absence of RNA. The emission maxima were 656 nm and 646 nm, respectively, when bound to the aptamer. The fluorescence increase was measured at 656 nm for MG and 646 nm for CV. For TMR and PY significant fluorescence was detected in the absence of RNA, therefore a ratio of bound fluorescence and unbound fluorescence was used. TMR bound fluorescence was measured at 584 nm and unbound was measured at 576 nm. PY bound fluorescence was measured at 576 nm and unbound was measured at 566 nm. The resulting curves were fitted to the equation $y = (B_{max}*x)/(K_d+x)$ using Origin 8.0 (OriginLab Corporation, Northampton, U.S.A).

Equilibrium dialysis experiments

Equilibrium dialysis was conducted using Dispo Equilibrium Dialyzer tubes (Harvard Apparatus, Massachusetts, U.S.A). Both dye and RNA were dissolved in a 100 mM phosphate buffer, 50 mM KCl, pH 6.7 buffer. The tubes were prepared with MGA (5 µM) in the receptor chamber and a range of dye concentration (5 µM -20 µM) were added to the ligand chamber. After 32 hours of equilibration in the dark at room temperature with gentle

agitation, a 50 µl sample was taken from each chamber and added to 450 µl acetic acid. Absorbance was measured at 546 nm on a Cary 4000 UV/Visible Spectrometer (Agilent Technologies). The binding curves were fitted to the equation $y = (B_{max}*x)/(K_d+x)$ using Origin 8.0 (OriginLab Corporation, Northampton, U.S.A).

Chapter 3: Further exploration of the malachite green RNA aptamer binding pocket

1. Introduction

Competition or displacement binding isothermal titration calorimetry (ITC) studies involve studying the interaction of a ligand "A" titrated into a receptor that is occupied by a ligand "B". This method has multiple applications including determining if both ligands have the same binding mode, characterizing a high affinity binding ligand and observing conformation flexibility.

The model used to fit competitive binding ITC data has been previously reported for multiple injections (Wang 1995, Sigurskjold 2000). The report for continuous injection was verified using simulated data and binding of cytidine monophosphate to RNaseA (Markova and Hallen 2004). The continuous injection method has several advantages over multiple injections. The chief benefit is the time involved in the experiments, continuous injections require significantly less time. The increase in speed of experiment does not decrease the amount of points collected along the isotherm curve, this method allows for more points along the isotherm curve.

The competition binding ITC has been used for studying interleukin receptor binding (Lupardus, Birnbaum and Garcia 2010), as well as other receptor ligand interactions. In these cases a low affinity ligand is first bound to lower the affinity of a high affinity ligand to a measurable affinity. The conformation flexibility and binding mode of different ligands to cytochrome p450 has been investigated using competition binding. This along with NMR studies concluded that using the same residues cytochrome p450 creates two distinct binding niches depending on the ligand (Muralidhara, Negi and Halpert 2007).

Competitive binding ITC was selected in order to further explore the changes that MGA undergoes when accommodating different ligands inside a free or occupied binding pocket. The previous chapter summarized the investigation of the binding of MG derivatives to MGA. These derivatives included pyronin Y (PY), crystal violet (CV) and tetramethylrosamine (TMR). Figure 1 shows the chemical structures of related dyes that bind to MGA. Pyronin Y (PY) has a planar structure similar to TMR, but lacks the third ring, while crystal violet (CV) has a non-planar structure similar to MG, with an extra dimethylamine group on ring C.

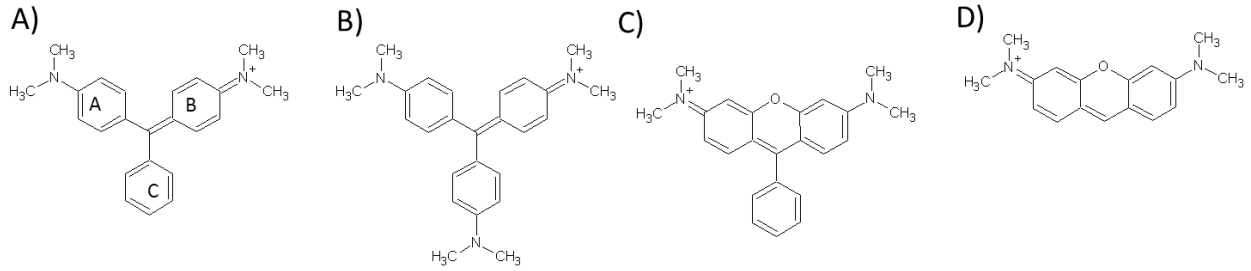

Figure 1. Chemical structures of dyes that bind to MGA A) MG (rings are labeled A,B,C) B) CV C) TMR D) PY.

Initial binding studies illustrated that the MGA binding pocket has the ability to adapt to recognize these related molecules (Baugh, Grate and Wilson 2000). This is consistent with the concept of adaptive binding. MG and TMR have higher affinities to MGA than CV and PY under all tested conditions. A comparison of our recent isothermal titration calorimetry studies (Bernard Da Costa and Dieckmann 2011) with the earlier binding studies by Baugh *et al.* that used a competition binding assay (Baugh *et al.* 2000) indicated that there might be differences in the way the free RNA and an aptamer with an already occupied binding site interact with a potential ligand. The work done in the previous chapter showed that MGA

changes its preference from the original ligand MG to TMR in the presence of Mg^{2+}. This observation emphasizes the environment dependent character of RNA-ligand interactions.

Two structures of MGA have been determined to date; a crystal structure of the aptamer bound to tetramethylrosamine (TMR) (Baugh *et al.* 2000) and a solution NMR structure of the complex with MG (Flinders *et al.* 2004). The MGA binding pocket consists of a base quadruple (C7, G24, G29, A31) and a Watson-Crick base pair (G8, C28) with two base triples (C10, G23, A27 and U11, A22, A26) and a U turn motif providing the supporting frame work. A comparison of the two MGA structures in complex with MG and TMR (Figure 2) shows that the most significant difference lies in the stacking patterns of the RNA bases at the top and bottom of the pocket. The G8:C28 base pair and the upper part of the pocket are rotated in the MG complex relative to their position the TMR complex. This leads to an un-stacking of G8 and ring A of the ligand thereby making room for the non-planar structure of MG. Another important element of the binding pockets is A30 which stacks with ring C of the ligand. A30 is part of a bulge/loop structure consisting of A30, A31, U32 and G33. In the crystal structure a Sr^{2+} ion is positioned to interact with the phosphate oxygen atoms of A30, A31 and G33, whereas no divalent ions were present in the buffer used for the NMR studies.

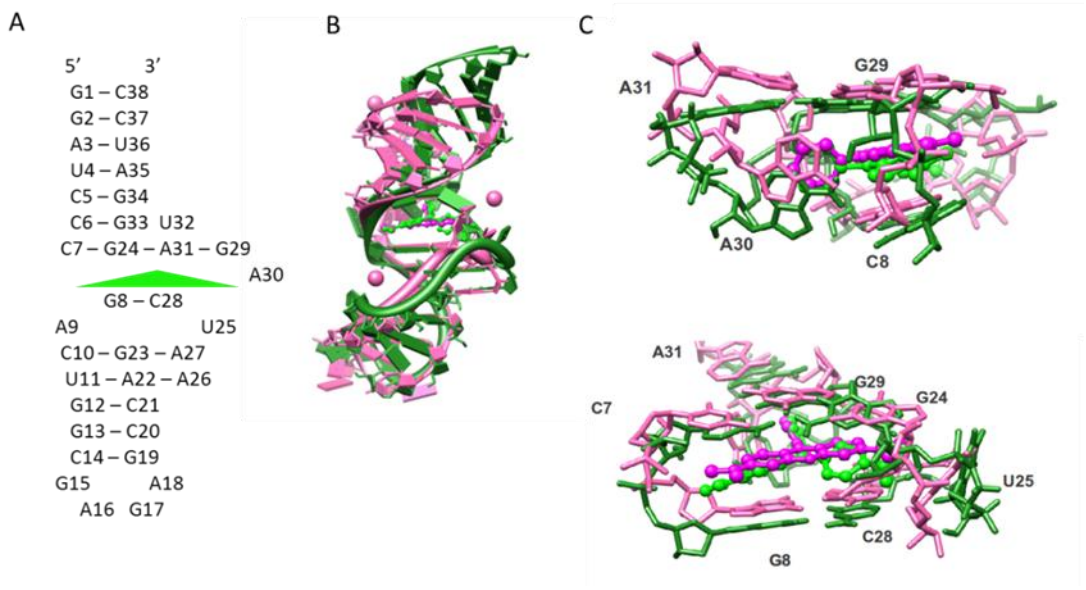

Figure 2. A) Secondary structure schematic of MGA with MG shown as green triangle. B) Superposition of the MGA NMR structure with bound MG (Green, PDB ID 1Q8N) and the MGA crystal structure with bound TMR (Purple, PDB ID 1F1T). The purple spheres indicate the position of Sr^{2+} ions in crystal structure. C) Detail view of the binding pocket of the superimposed structures; top : back view, bottom : front view. Figure was generated using UCSF Chimera (Pettersen *et al*. 2004).

We have conducted competition binding experiments where PY or CV were pre-bound to MGA (MGA_{PY} and MGA_{CV}) while MG or TMR were titrated in. These experiments illustrate how the aptamer adapts to a ligand when the binding pocket is already occupied by another small molecule

2. Results and Discussion

Characterization of free RNA by NMR spectroscopy

One of the key principles of adaptive binding in RNA aptamers is the absence of structure in the ligand- free RNA binding pocket. In order to establish if the MGA follows this

principle, we analyzed the amount of structure present in the aptamer RNA in absence of the ligand by high resolution NMR spectroscopy (Figure 3). Both the original aptamer sequence designed by Grate *et al.* and a modified version that was used for the NMR studies with an unsymmetrical stem and a UUCG tetraloop instead of the GAAA loop were prepared and analyzed by homonuclear NMR spectroscopy. Both sequences behaved identically. In the absence of ligand, the spectra acquired in H_2O indicate that the first 6 base pairs in stem 1 and the stem-loop starting at G12:C21 are formed and contain stable base pairs. This is confirmed by the observation of sequential NOE patterns typical for A-form RNA and the UUCG/GNRA hairpin loops in NOESY spectra acquired in D_2O and H_2O. The signals originating from nucleotides in the internal loop/ligand binding site are heavily overlapped and show very few NOEs. All visible NOEs between aromatic protons originate from nucleotides in the two stem regions. The signal dispersion and the amount of NOEs observed increases drastically after addition of either malachite green or tetramethylrosamine ligand (Figure 3 C and D).

The analysis of the NOE data indicates that the aptamer does not have a preferred structure for most nucleotides in the internal loop in the absence of MG or TMR. However, there is evidence for the formation of the G29:C7 base pair at the top of stem 1. Stacking NOEs between the C6:G33 base pair and a purine residue that is base paired to a cytidine nucleotide suggest that this base pair, which becomes part of the base quadruple formed by C7, G29, G24 and A31, is already preformed in the ligand free RNA. The structures of the MGA-MG and MGA-TMR complexes (Figure 2) show that the binding pocket adopts a somewhat different structure when binding MG (a non-planar ligand) versus TMR (a ligand with planar rings A + B). Since part of the base quadruple is pre-formed in the free form and

stabilized in the bound form as well as by the presence of divalent metal ions, we decided to investigate the effect of pre-binding one ligand within the pocket. The determination of the affinity of a second ligand that displaces the pre-bound one should provide insights into the effect of the structural re-arrangement that is necessary to accommodate the new ligand on the binding affinity.

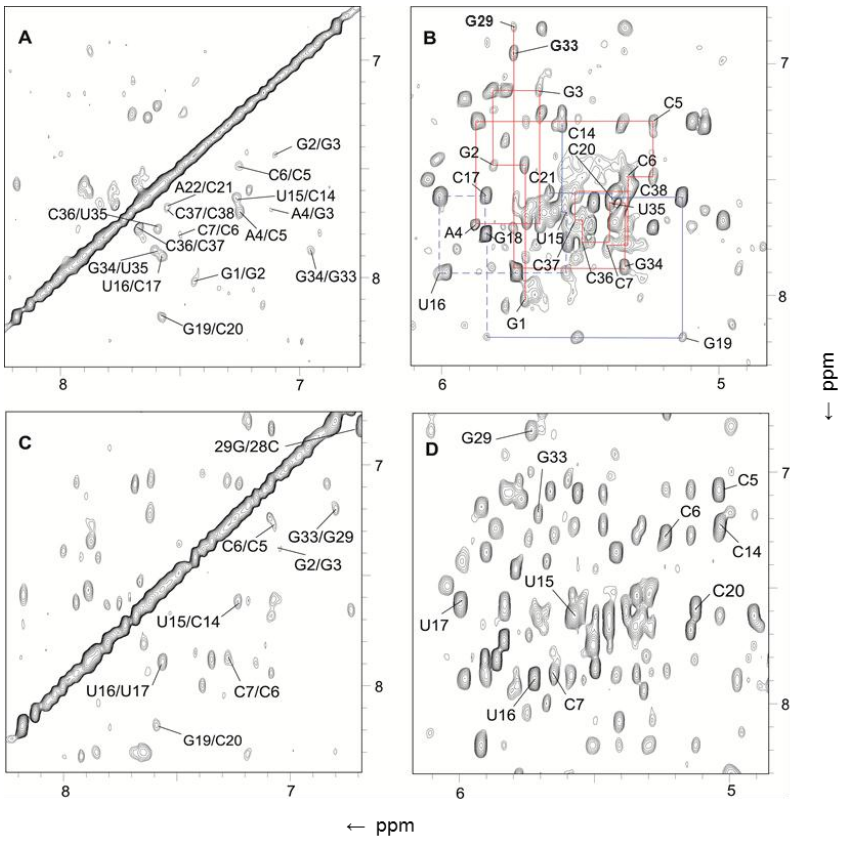

Figure 3. 2D D2O NOESY Spectra of MGA at 293K (mixing time 250 ms). A) Aromatic to aromatic region of free MGA B) Ribose region of free MGA. Red lines trace H1' to base proton NOEs in the lower stem. Blue lines trace H1' to base NOEs in the upper stem, while dashed blue lines trace the connectivity through the UUCG tetraloop C) Aromatic to aromatic region of MGA with malachite green bound. D) Ribose region of MGA with malachite green bound.

Competitive isothermal titration calorimetry experiments

ITC studies were conducted at two different buffer conditions, 150 mM NaCl and 1 mM NaCl, 10 mM $MgCl_2$. These conditions are based on our previous ITC binding studies with free MGA.[17] The competition experiments were performed with PY and CV pre-bound to the aptamer since pre-bound TMR and MG did not show any detectable signal when the competing ligand was titrated in (Figure C1 in Appendix). This is expected since MG and TMR had significantly higher binding affinities than CV and PY.

Table 1. ITC determined thermodynamic parameters for MG and TMR binding to MGA_{PY} or MGA_{CV} complexes at different salt concentrations, pH 6.7 at 25 °C.

Salt Concentration	Pre-bound	Titrant	K_d(μM)[a]	ΔH(kcal/mol)[a]	ΔS(cal/mol/K)[a]	ΔG(kcal/mol)[a]
150 mM NaCl	-	CV	4.45±0.08	-78.27±14.6	-280.0±49.1	-7.35±0.09
	-	PY	4.08±0.20	-17.81±0.38	-35.03±1.20	-7.37±0.03
	-	MG	0.28±0.06	-25.93±2.24	-56.87±8.54	-8.98±0.14
	CV	MG	0.10±0.01	-91.63±0.43	-276.04±1.53	-9.37±0.07
	PY	MG	0.50±0.16	-37.09±0.71	-95.45±1.61	-8.65±0.23
	-	TMR	0.28±0.04	-18.32±1.09	-31.43±3.55	-8.95±0.08
	CV	TMR	n/a	n/a	n/a	n/a
	PY	TMR	0.32±0.07	-21.80±0.46	-43.44±1.94	-8.86±0.12
1 mM NaCl, 10 mM $MgCl_2$	-	CV	3.79±0.12	-54.48±9.71	-158.0±32.6	-7.40±0.01
	-	PY	1.65±0.67	-16.94±1.77	-30.20±6.52	-7.94±0.23
	-	MG	0.10±0.01	-23.10±1.35	-45.37±4.42	-9.58±0.04
	CV	MG	0.13±0.02	-60.56±0.53	-171.7±1.79	-9.40±0.09
	PY	MG	0.21±0.06	-28.79±1.84	-66.02±6.72	-9.11±0.16
	-	TMR	0.08±0.02	-17.29±1.51	-25.50±5.26	-9.69±0.12
	CV	TMR	n/a	n/a	n/a	n/a
	PY	TMR	0.27±0.07	-19.55±1.66	-34.57±5.81	-9.25±0.26

[a] Average of three independent measurements each

Table 1 summarizes the data obtained from the competition experiments. Table 1 also includes results from previous chapter for convenient comparison. CV can readily be replaced in MGA_{CV} by MG with a K_d of 0.1 μM, while TMR did not show any observable binding to the MGA_{CV} complex despite the fact that its affinity for free MGA is 16 times higher than that

of CV. PY is replaced in MGA_{PY} in the by TMR easier (K_d 0.3 µM) than MG. Binding to MGA_{PY} complex is reduced compared to the free RNA and involves a smaller favourable enthalpy change compared to that involved in binding to MGA_{CV}. The smaller favourable enthalpy change when MG replaces PY vs. CV suggests that this complex does not easily rearrange the structure of the binding site to an optimal MG binding pocket. These results illustrate that the binding pocket formed by adaptive binding to the pre-bound ligand is quite stable once formed and the rearrangement to accommodate a ligand with somewhat different shape is not instantaneous. This could be compared to a beanbag chair which after adapting to the shape of one occupant will need some time to recover its ability to optimally fit itself to the shape of a new occupant. The aptamer shows a degree of structure memory once it has adapted to a particular shape of ligand and hence there is an energy penalty when a ligand with a different shape attempts to displace the pre-bound ligand. This explains why MG has a lower affinity for MGA_{PY} complex than for MGA_{CV} and TMR has a lower affinity for MGA_{CV} than for MGA_{PY}. MG binding to MGA_{CV} complex has a large favourable enthalpy due to an optimized, pre-shaped binding pocket. It should be noted that some of the enthalpy and entropy detected could be due to the solvation of CV or PY as it exits binding pocket, since both CV and PY have different solubility than MG or TMR.

Table 2. Ratio of binding values obtained directly over binding values from competition experiment

Buffer	Prebound	Titrant	$K_d/K_{d\,pre}$	$\Delta H/\Delta H_{pre}$	$\Delta S/\Delta S_{pre}$	$\Delta G/\Delta G_{pre}$
150 mM NaCl	CV	MG	2.80	0.28	0.21	0.96
	CV	TMR	n/a	n/a	n/a	n/a
	PY	MG	0.56	0.70	0.60	1.04
	PY	TMR	0.88	0.84	0.72	1.01
1 mM NaCl, 10 mM $MgCl_2$	CV	MG	0.77	0.38	0.26	1.02
	CV	TMR	n/a	n/a	n/a	n/a
	PY	MG	0.48	0.80	0.69	1.05
	PY	TMR	0.30	0.88	0.74	1.05

In order to illustrate the differences between combinations of complex formation, we have calculated the ratios of the thermodynamic parameters for MG or TMR binding to free MGA (Bernard Da Costa and Dieckmann 2011) , over the values for MG or TMR binding to MGA_{pre} (Table 2). For K_d a ratio above one means that the ligand has higher affinity for MGA_{pre} while below one indicates that the ligand has higher affinity for free MGA. For ΔH a ratio above one indicates the ligand has larger favourable enthalpy change for interactions with MGA while a value below one means that the ligand has larger favourable enthalpy change when binding to MGA_{pre}. For ΔS a ratio above one means ligand has a larger unfavourable entropy contribution when binding to MGA, while values below one indicate that the ligand has larger unfavourable entropy contributions when binding to MGA_{pre}. Interestingly, the ratio for ΔG is close to one in all cases; displaying an example of entropy-enthalpy compensation[29]. This phenomenon suggests that biomolecules work within a limited free energy window, where favourable enthalpy interactions are balanced by the necessary unfavourable entropy needed to make interactions

TMR binding to MGA_{PY} has values close to those for binding to free MGA (ratio is close to one) at 150 mM NaCl. However, in the presence of 10 mM Mg^{2+} TMR binding to MGA_{PY} is slightly reduced. This suggests that the stabilization of the pocket provided by Mg^{2+} reduces the ability of the aptamer to accommodate TMR.

MG binding to MGA_{CV} has a significantly higher affinity compared to binding to free MGA at 150 mM NaCl. This is accompanied by a large increase in favourable enthalpy change and unfavourable entropy change. However, in the presence of 10 mM Mg^{2+} the binding affinity is similar to binding affinity to free MGA with a comparable enthalpy change and a slight increase in unfavourable entropy. The increase in unfavourable entropy in this

case is consistent between the two conditions suggesting it may have more to do with the solvation of CV than the binding event. The increase in binding affinity seen at 150 mM NaCl suggests that MG can interact more efficiently with a pre-formed binding pocket if the previous ligand had a similar shape as in the case of CV. In the presence of Mg^{2+}, which stabilizes the internal loop region that includes the binding pocket, the RNA loses some of its plasticity and hence the ability of MG to replace CV is reduced. This observation agrees with our previous report that MGA changes its ligand preference from MG to TMR in the presence of 10 mM Mg^{2+}.

MG binding to MGA_{PY} shows a decrease in affinity under both buffer conditions compared to binding to MGA (0.56 and 0.48). The favourable enthalpy at both buffer conditions was comparable to MGA binding but there is an increase in unfavourable entropy (0.60 and 0.69). Taken together with the lower binding affinity this suggests that MGA_{PY} has a pocket that doesn't allow optimal interactions as seen in MG binding MGA_{CV}.

Computational Investigation

Computational methods have been used to probe conformation flexibility in biomolecules along with other methods (Muralidhara *et al.* 2007). These simulations provide insight into the subtle changes in conformation that accompany binding. An unpublished communication from Dr. Charles Wilson used molecular dynamic simulation to supplement kinetic studies revealing that the interactions that unraveled at 500K in simulation were the same interactions that were least formed in folding transition state ensemble. These residues whose interactions with ligand were least formed were identified as A30, A9 and G24. The simulation was conducted with potassium ions and using AMBER. Based on our results that

reveal the importance of the role of Mg^{2+}, we have attempted to repeat the simulations using magnesium ions.

The NMR structure of MGA was used in the simulations since it represents the solution structure of the aptamer. The derivatives were placed in MGA and the solution was heated to 500K. The complexes were then equilibrated at 500K. Equilibration was determined to be complete when the potential energy of the system plateaued (Figure C2 in Appendix). Examining the equilibrated structures shows that the distortion of the binding pocket is correlated with the binding affinity to ligand. MGA_{CV} has the most distorted binding pocket followed by MGA_{PY}, while MGA_{TMR} and MGA_{MG} have the least distortion from reported binding pocket (Figure 4). Computational experiments have to be continued to yield more insights into the unfolding process as the ligand leaves binding pocket, these experiments are discussed in the following section.

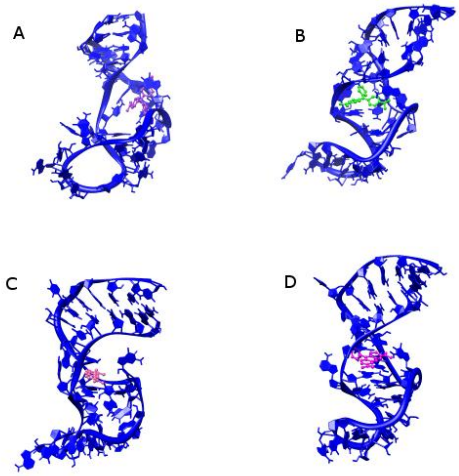

Figure 4. MGA NMR structure equilibrated at 500K complexed with A) CV B) MG C) PY D) TMR. Figure was generated using UCSF Chimera (Pettersen *et al*. 2004).

3. Conclusions and Future Work

In summary, the ITC experiments described here show that MGA maintains a certain level of structural memory of the initial target it binds, even when challenged with a competing ligand that has a higher affinity for the free RNA than the pre-bound one. The plasticity of the free RNA aptamer allows it to adapt to somewhat differently shaped ligands, planar and non-planar tri-phenyl dye derivatives in this case. However, once the RNA has adopted the optimal fold for a specific shape of ligand it maintains this fold at least partially for some time after the ligand leaves the pocket. This results in an energy penalty for binding a differently shaped ligand, because the pocket needs to be partially unfolded in order to accommodate the new binding partner.

This effect is most likely due to the ligand bound structure of the RNA representing an energy minimum in the RNA folding pathway. Hence the molecule becomes kinetically trapped in the adopted conformation and requires additional energy and time to return to an unfolded state that can readily adapt to a different ligand. Fully characterizing this behaviour is critical for understanding the way in which small molecules interact with RNA aptamers, for example in biosensors where initial binding of a lower affinity ligand can potentially prevent detection of a high affinity target or in drug development where interactions between different potential ligands can reduce the efficiency of an RNA targeting drug *in vivo*.

The results presented here also explain the apparent contradiction between the binding affinities for MG (K_d = 800 nM at 10 mM Mg^{2+}) and CV (K_d > 1mM at 10 mM Mg^{2+}) reported (Baugh *et al.* 2000) and our recent ITC studies (K_d = 100 nM for MG and 3.8 μM for CV at 10 mM Mg^{2+}) (Bernard Da Costa and Dieckmann 2011). The earlier affinities were determined indirectly by measuring changes in TMR fluorescence anisotropy in competition

experiments. The data presented here shows that a planar ligand like TMR cannot easily replace a non-planar ligand like CV during the time-frame of a typical binding experiment (approximately fifteen minutes for the ITC studies) and thus the K_d values determined from the competitive fluorescence studies significantly underestimate the affinity of MG and CV. This possibility needs to be taken into account when designing experiments that characterize RNA aptamer –ligand interactions.

Further ITC experiments will be conducted to examine the presence of a specific Mg^{2+} binding site. This will be done by having MGA in a buffer without Mg^{2+} placed in the cell and titrating Mg^{2+} into cell. This experiment will help confirm the role of Mg^{2+} suggested by our recent work. Further computational experiments will involve cooling down complexes currently at 500 K down to 300 K. This annealing process should allow for MGA to adapt to its ligand. After the complexes are equilibrated at 300K it will be used for two separate experiments. The first experiment will involve removal of the ligand and equilibration of the empty MGA to observe how the pocket adjusts after ligand is removed. The second experiment will involve the slow extraction of the ligand and determination of the energy involved in extracting the ligand. This energy can be used to determine the affinity of the ligand for the complex (Lee and Olson 2006, Villa, Wohnert and Stock 2009). The affinity determined will then be compared to the affinities we have previously determined by ITC. This approach will also allow for the examination of the unfolding process more closely as the force used to pull ligand can be adjusted and correlated with the interactions with MGA that are broken.

4. Materials and Methods

RNA preparation

The RNA used for ITC and NMR spectroscopy was prepared enzymatically from a synthetic DNA template by using T7 RNA polymerase and unlabeled NTPs (Milligan *et al*. 1987, Milligan and Uhlenbeck 1989). After transcription magnesium pyrophosphate was removed by centrifugation and the RNA was collected by precipitation with ethanol. The RNA was then separated from NTPs and aborted transcription products by PAGE using a 12% gel. The RNA product was then extracted from the gel by electro-elution and run on a HiPrep 16/10 DEAE FF anion-exchange column (GE Healthcare, Uppsala, Sweden), followed by salt removal on a Hiprep 26/10 Desalting column (GE Healthcare, Uppsala, Sweden) and lyophilization to dryness.

NMR samples for studying exchangeable protons were prepared by dissolving the lyophilized RNA in a 90% H_2O / 10% D_2O solution. Samples used for studying non-exchangeable protons were prepared by dissolving the RNA in 99.996% D_2O (Cambridge Isotopes, Andover, Massachusetts, U.S.A). All NMR samples were 500 μL in standard 5 mm NMR tubes with final RNA concentrations of 0.8 to 1.8 mM in 10 mM KCl and 10 mM potassium phosphate buffer, pH 5.8.

ITC studies

Experiments were performed at 25 °C on a MicroCal ITC 200 microcalorimeter (MicroCal, Inc., Northampton, Massachusetts, U.S.A). The 10–15 μM RNA solution was prepared by dissolving lyophilized RNA in 10 mM sodium phosphate buffer, pH 6.7 at the desired salt concentration. The 100–150 μM dye solutions were prepared by dissolving solid

dye in 10 mM sodium phosphate buffer, pH 6.7 at the desired salt concentration. RNA and dye for the preparation of pre-bound samples (MGA_{CV} or MGA_{PY}) were mixed in a 1:2 ratio. The ITC cell was filled with the pre-bound RNA solution and titrated with the second ligand (MG or TMR) solution from the syringe. Each experiment consisted of a single injection over 396 sec at a continuous flow of 0.1 μL/s to a final molar ligand /RNA ratio of 1.5. In order to account for heat of dilution of dye solution, a blank run with the pre-bound dye buffered in cell and second dye in syringe was run and subtracted from the experimental run. The validity of the data obtained by continuous injection was verified by comparing the data obtained via the standard multiple injection method with a corresponding continuous injection set (Table C1 in Appendix). No significant differences for binding constants or thermodynamic parameters were found. All data sets were analyzed using the Origin software package provided by MicroCal and fitted to a competitive binding model.

NMR experiments

NMR experiments were conducted and analyzed by Dr. Thorsten Dieckmann. All spectra were collected on a Bruker DRX-600 spectrometer equipped with a HCN triple resonance, triple-axis PFG probe. Solvent suppression for samples in 90% H_2O / 10% D_2O was achieved using 11-spin echo pulse sequences (Sklenar and Bax 1987) or WATERGATE (Piotto, Saudek and Sklenar 1992). Quadrature detection for the indirect dimensions in multidimensional experiments was 2D CITY-TOCSY (Briand and Ernst 1991) with a mixing-time of 50 ms, a DQF-COSY (Piantini, Sørensen and Ernst 1982), and NOESY spectra with mixing times of 250, 200, and 50 ms in 100% D_2O were measured at 293 K. The spectra were analyzed and assigned as previously described (Flinders *et al.* 2004).

Computational experiments

Computational experiments were conducted with the guidance of Dr. Pierre-Nicholas Roy, using a method similar to that used by Jason Tao to explore MG derivatives in MGA, these included MGOAc, MGOH and MGO. This involved inserting the derivative into the NMR structure of MGA using xleap. Mg^{2+} ions were added using xleap before solvating the complex in a 30Å rectangular water box. The system was then minimized using 1000 steps with the solute held fixed, followed by a 10 ps MD at 300 K while placing 25 kcal/mol Å restraints on all solute atoms and counter ions. Then the restraints were reduced gradually to 0 kcal/mol Å. The system was then annealed by increasing temperature gradually (10 K per 10 ps) to 500 K. The system was then equilibrated at 500 K for 30 ps. Computation were all performed using AMBER either on sharcnet.ca or roycluster.uwaterloo.ca.

Chapter 4: Selection of a Fluorescein Binding Aptamer

1. Introduction

The word aptamer is derived from the latin *aptus* meaning to fit and *mer* the unit used to measure the length of nucleotides (Ellington and Szostak 1990). Naturally occurring riboswitches have been identified as aptamers (Winkler, Cohen-Chalamish and Breaker 2002). However, many aptamers, including the first biomolecule to be identified as an aptamer (Ellington and Szostak 1990), have been artificially selected through a method known as Systematic Evolution of Ligands by Exponential Enrichment (SELEX) (Ellington and Szostak 1990, Tuerk and Gold 1990, Proske et al. 2005).

SELEX

Briefly, this involves starting with a pool of random sequences, applying a selection pressure (usually a column with a ligand bound), enriching the pool by polymerase chain reaction (PCR) of the nucleic acid sequences that survive the first round of selection pressure. This is followed by repeating the process on the new pool (Figure 1). This is repeated until the pool converges to a few unique sequences that have a high affinity for the target. This technique has been used to select aptamers for a wide variety of targets from small molecules to whole cells (Barbas et al. 2010, Shi, Hoffman and Lis 1999, Holeman et al. 1998).

The use of the SELEX method has itself evolved and may include multiple selection pressures and negative selection pressures (Stoltenburg, Reinemann and Strehlitz 2007). The selection pressure step has expanded from simple columns to include magnetic beads (Nutiu and Li 2005), capillary electrophoresis (Mendonsa and Bowser 2004), flow cytometry (Blank et al. 2001), surface plasmon resonance (Misono and Kumar 2005), and *in silico* methods

(Chushak and Stone 2009). There are currently two aptamer databases that are attempting to amalgamate all the data available to increase the understanding of the SELEX process (http://aptamer.icmb.utexas.edu/ and http://aptamer.freebase.com/).

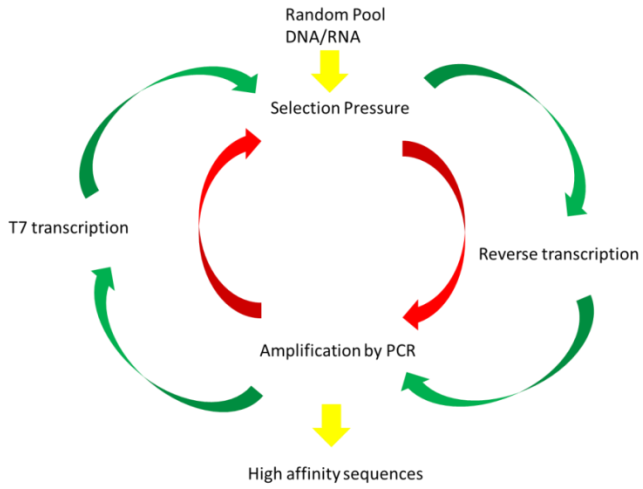

Figure 1 Schematic of SELEX procedure. Red arrows indicate DNA SELEX. Green arrows indicate RNA SELEX.

RNA versus DNA Aptamer

Both DNA and RNA aptamers show robust binding affinities for various targets (Neves et al. 2010, Baugh, Grate and Wilson 2000, Dieckmann et al. 1995). There are two key differences in the building blocks of DNA and RNA. Firstly, as the name suggests RNA has a ribose sugar moiety while DNA has a deoxyribose, in which the 2' OH is absent (Figure 2a). Secondly, DNA uses thymine as a pyrimidine base instead of uracil (Figure 2b). The lack of the 2' OH gives DNA greater stability, while in RNA this group can participate in a self cleavage reaction. The lack of the 2' OH also leads to a difference in preferred sugar

puckering which affects the overall structure DNA forms.

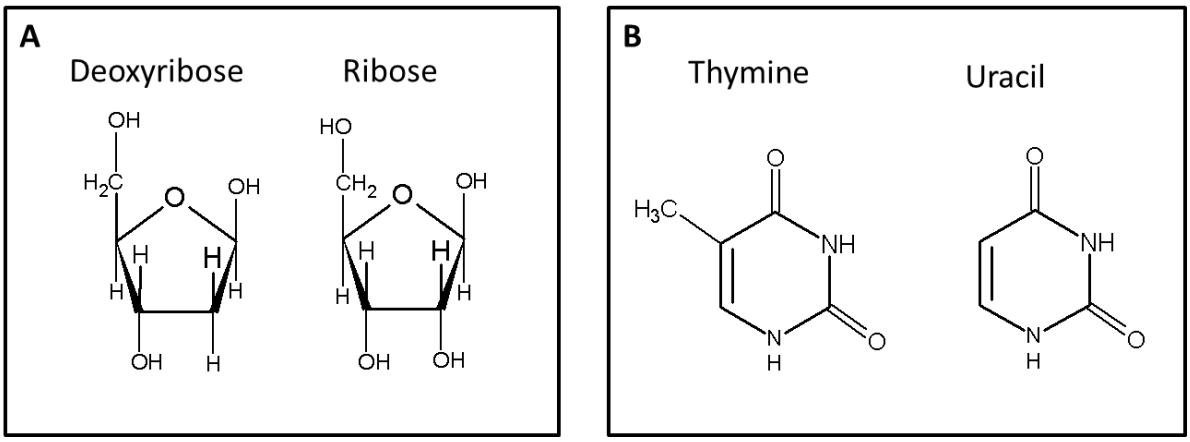

Figure 2. Chemical structure representations of A) Deoxyribose and Ribose B) Thymine and Uracil.

The effect of these differences can be seen in DNA and RNA aptamers that bind the same ligand. These ligands include lysozyme (Potty et al. 2011), thrombin (Long et al. 2008), human immunodeficiency virus trans-acting responsive element (HIV TAR) (Darfeuille et al. 2006), hemin (Liu et al. 2009a), interferon γ (Min et al. 2008), vascular endothelial growth factor (VEGF) (Ng et al. 2006), and dopamine (Walsh and DeRosa 2009). In the case of lysozyme, HIV TAR, VEGF and dopamine, the selected DNA aptamer is the analog of the RNA selected aptamer. The lysozyme DNA aptamer has a lower affinity than the RNA aptamer but is less sensitive to salt concentration. The lysozyme RNA aptamer K_d increases 270 fold when concentration of NaCl in buffer is increased by 20 mM, while the DNA aptamer K_d only increases 2 fold. This suggests that electrostatic contribution is significant in the lysozyme RNA aptamer (Potty et al. 2011). Regardless of its lower affinity, the lysozyme DNA aptamer has been used as an electrochemical sensor (Li et al. 2010) and for the

voltammetric detection (Cheng, Ge and Yu 2007) of lysozyme. The HIV TAR RNA aptamer forms a kissing complex such as the one mentioned in Chapter 1. The DNA analog has a similar affinity to the RNA aptamer and competes for binding with Tat (Darfeuille et al. 2006). The VEGF RNA aptamer has been developed into the first therapeutic aptamer with a binding affinity in the picomolar range (Ng et al. 2006). The DNA analog VEGF aptamer has a binding affinity in the nanomolar range (Potty et al. 2009). Interestingly, both the RNA and DNA dopamine binding aptamers have similar affinity and mutation studies point to the same binding site (Walsh and DeRosa 2009).

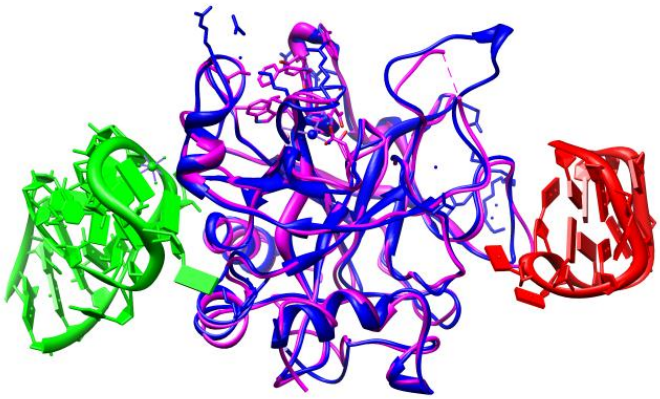

Figure 3. Overlap of thrombin bound DNA aptamer (RED aptamer; PINK thrombin; PDB ID 1HUT) and RNA aptamer (GREEN aptamer; BLUE thrombin; PDB ID 3DD2). (Long et al. 2008) (Nimjee et al. 2009). Figure was generated using UCSF Chimera (Pettersen *et al*. 2004).

The hemin, thrombin, and interferon γ, DNA and RNA aptamers were selected through two independent selections. Both hemin aptamers have similar peroxidase activity though the DNA aptamer (K_d = 27 nM) (Liu et al. 2009a) has a higher affinity than the RNA

aptamer (K_d 0.8 µM) (Liu et al. 2009b). The presence of peroxidase activity in both cases supports the idea that RNA and DNA are capable of catalysis given the right ligand. The crystal structures of both DNA and RNA aptamers bound to thrombin have been solved. These reveal that the thrombin RNA and DNA aptamers bind at different sites and have different binding interactions (Figure 3) (Long et al. 2008, Nimjee et al. 2009). While no crystal structure is available for the interferon γ aptamers, based on their sequences it is safe to conclude that they have different binding modes. The interferon γ RNA aptamer sequence (Kubik et al. 1997) is 5'GGAGGACGAUGCGGACACCGUUAAUCUGAGGCCCUGUCCUAUUCCUUCACGCCUCAGA3' while the DNA aptamer sequence (Balasubrananian et al. 1998) is 5'GGGGTTGGT TGTGTTGGGTGTTGTGT3'. An electrochemical detection of interferon-γ with these aptamers by Ban C. *et al*. showed that the RNA aptamer had an order of magnitude lower detection limit than the DNA aptamer (Min et al. 2008). Briefly, this involved attaching aptamer to a gold electrode and monitoring the charge transfer resistance. This value is correlated with the amount of ligand interaction with the electrode surface, which is related to affinity to the aptamer.

The difference in sequence and binding seen from selections of RNA and DNA aptamers compared to using analogs of a selected aptamer suggest that more data is required to fully understand the correlation between RNA and DNA sequence structure-function relationship. This was the rationale for trying both an RNA and DNA aptamer selection.

Fluorescein as target

The aptamer target was selected in order to provide the possibility for practical applications. One of the practical applications of aptamers, as mentioned in Chapter 1, is as

signalling molecules. Detection methods for monitoring signals include electrochemical (Min et al. 2008), colorimetric (Stojanovic and Landry 2002), piezoelectric (Bini et al. 2007), and fluorescence (Stojanovic and Kolpashchikov 2004). Two examples of the ways to use fluorescence as detection method include the use of the malachite green RNA (MGA) aptamer chimeric probe for the detection of adenosine and the binary MGA aptamer for the detection of target nucleotide sequences. In the chimeric probe, the MGA is appended to an adenosine aptamer. The addition of a bridge sequence complementary to a part of MGA and part of the adenosine aptamer keeps secondary structure of MGA from folding and binding MG. The presence of adenosine causes the interaction with the bridge sequence to weaken and allows MGA to fold and bind MG, produces a detectable signal (Figure 4a) (Xu and Lu 2010). In the binary probe, MGA is split in two with each half attached to part of the target sequence. Binding to the target sequence brings the two halves together which allows for the binding of MG which produces a detectable signal (Figure 4b) (Kolpashchikov 2005).

Fluorescein has a significantly higher quantum yield of fluorescence than MG. MG has very little fluorescence when free and increases when bound making it useful as sensor in conjunction with MGA. Fluorescein is fluorescent when free in solution, while fluorescence is quenched by guanosine when bound to a DNA aptamer (Unruh et al. 2005). The acetylated fluorescein molecule has virtually no fluorescence (Figure 5). We have conducted a selection for an aptamer targeted at fluorescein diacetate (FDA) to add to the repertoire of signalling molecules and further explore RNAs capacity for catalysis. The application here would be to use FDA in conjunction with a catalytic aptamer to produce detectable fluorescence signal.

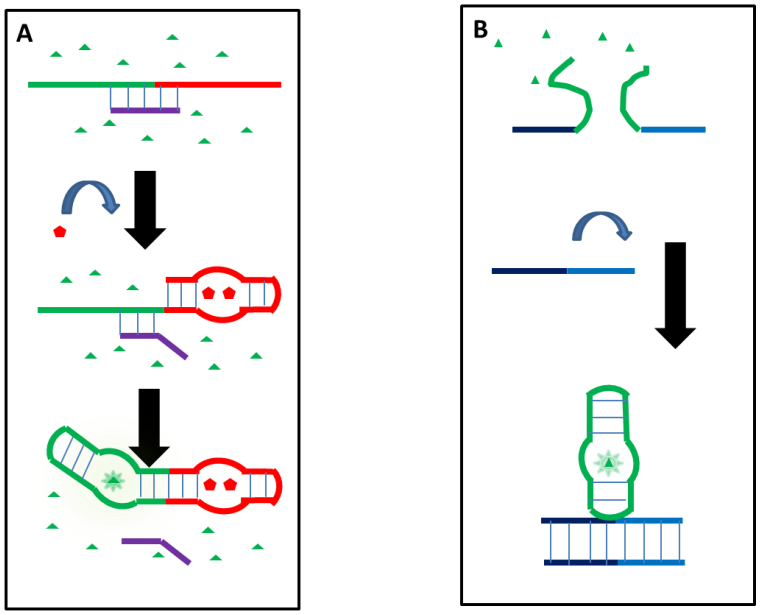

Figure 4 Schematic of different uses of the MGA. A) MGA (green line) attached to adenosine aptamer (red line) with the bridge sequence (purple line); adenosine (red pentagon) is added then MG (green triangle) is bound and fluorescence is produced. B) Part of target sequence (blue line) attached to half of MGA (green line), both target sequences binding to target brings the MGA halves together to allow for MG binding and fluorescence produced.

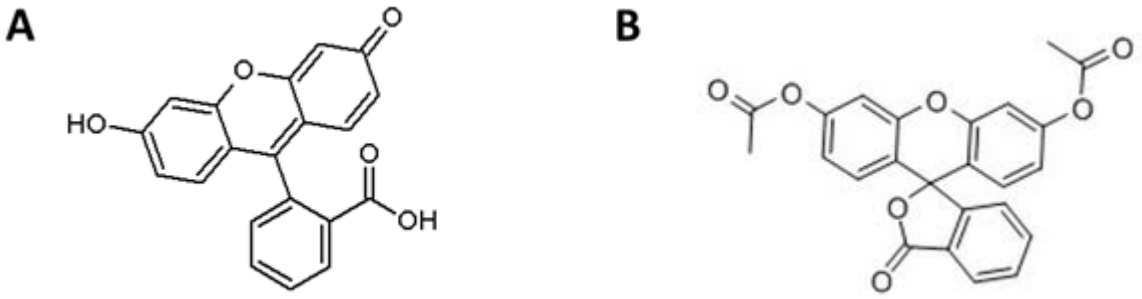

Figure 5 Chemical structure of A) Fluorescein B) Fluorescein diacetate

2. Results

Aptamer selection

The DNA selection was conducted using magnetic beads, a method developed by Li Y. *et al.* (Nutiu and Li 2005). The initial method (Method I, Figure 6a) was attempted by having the pool of DNA bind to the beads and introducing FDA. The DNA pool consisted of a bridge sequence flanked by random regions. The complement to bridge sequence was synthesized with a biotin tag (Sigma-Aldrich Corporation, Milwaukee, U.S.A) which was used to attach it to avidin coated magnetic beads (Invitrogen Corporation, California, U.S.A). The interaction of avidin and biotin has been widely used and is a high affinity interaction (Grunwald 2008). The Watson Crick base pairing between bridge sequence and complement attaches the pool to beads. These complexes were then exposed to the target. The random sequence regions that interacted with the target were expected to undergo a structural change (Nutiu and Li 2005). If the change in structure reduced the interaction between the bridge and complement sequence, the DNA was released from the beads. This DNA of interest was separated from the DNA still attached to the beads by pelleting the beads using a magnet. The supernatant contained the DNA of interest. This selection method has two selection pressures; first the DNA must bind to target and second the binding must lead to structural switch.

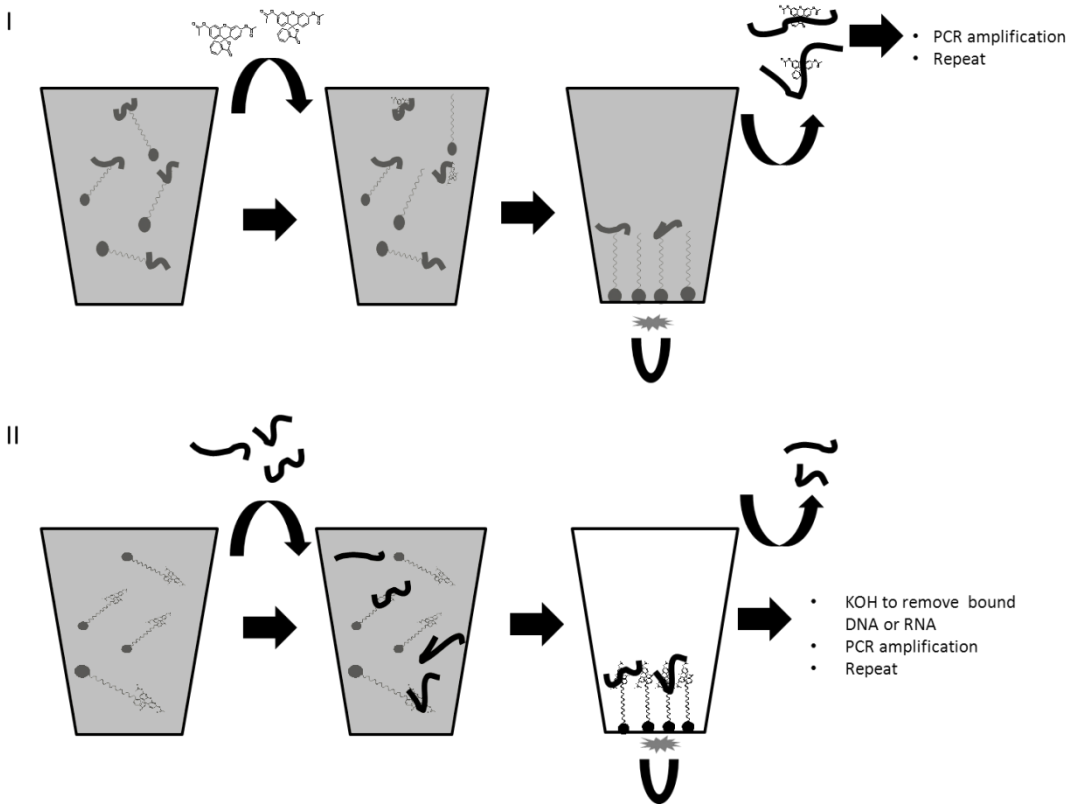

Figure 6. Methods used for SELEX I) Method I: DNA pool is attached to beads, FDA is added, magnet is applied, and supernatant contains DNA of interest II) Method II: FDA is attached to beads, DNA or RNA pool is added, magnet is applied, supernatant discarded, and pellet contains DNA or RNA of interest.

The second method (method II, Figure 6b) attempted involved having FDA bound to beads and introducing DNA pool. In this method, FDA was bound to the avidin coated beads via a biotin linker. The DNA pool in this case does not require a bridge sequence. However, the DNA pool used did contain a bridge sequence flanked by random regions. The DNA that interacts with FDA was pulled into pellet along with beads using a magnet. The supernatant containing DNA that does not interact with DNA was then removed and discarded. The pellet was then dissolved in denaturing buffer. This prevents DNA from folding and interaction with FDA. When the beads were pelleted this time, the DNA of interest was in the supernatant.

The DNA of interest was then amplified using PCR. The minimum number of PCR cycles required to produce detectable amounts of DNA was determined. This was done by taking running samples from different numbers of PCR cycles on an agarose gel with ethidum bromide stain. As selection rounds are repeated the amount of DNA in the pool that has affinity for the target should increase leading to a decrease in the number of PCR cycles required to obtain detectable amounts of DNA.

The selection using method I did not lead to any reduction in PCR cycles required to detect DNA by the eighth selection round. Using method II, the first selection round the PCR had thirty cycles and by the eighth selection round the PCR required twenty cycles (Figure D1, in Appendix).

In order to determine if sequences of DNA had converged, colony PCR was performed using the DNA pool from round eight. Colony PCR was done using a kit purchased from Invitrogen (Invitrogen Corporation, California, U.S.A). The DNA sequences were inserted into a vector containing coding sequence for β-galactosidase α peptide regulated by the lac operon (Hu, Kornacker and Hochschild 2000, Vieira and Messing 1982). The vectors were then transformed into *E. coli* cells. The cells were plated on LB plates containing bromo-chloro-indolyl-galactopyranoside (X-Gal) and isopropyl β-D-thiogalactoside (IPTG). IPTG triggers the expression of lac operon. Insertion of DNA into vector disrupts the sequence of β-galactosidase α peptide. Colonies that have a vector with a DNA insert were not able to break down X-gal, due to disrupted β-galactosidase α peptide. These colonies appear white; colonies that appear blue have a vector with no DNA insert. β-galactosidase α peptide breaks down X-gal into 5-bromo-4-chloro-3-hydroxyindole, which breaks down into 5,5'-dibromo-4,4'-dichloro-indigo, which gives cell blue color (Gabelsberger, Liebl and Schleifer 1993). Several

blue tinted colonies were observed and twelve individual white colonies were obtained. The DNA sequence insert from the white colonies were amplified using PCR. The sequences were then sent for sequencing (Operon, Alabama, U.S.A).

Figure 7A shows the alignment of twelve sequences obtained from colony PCR of the eighth selection round. While the sequences did not appear to converge, some of the sequences are G rich. G rich sequences have a propensity to form G quadruplexes which have been shown to bind to a variety of targets (Haider, Neidle and Parkinson 2011). The twelve sequences were analyzed using an online G quadruplex predictor (QGRS Mapper). The prediction is based on an algorithm that examines the distance between G's in a sequence (Kikin, D'Antonio and Bagga 2006). Three sequences (DNA_FDA_3, DNA_FDA_6, DNA_FDA_8) were identified that might have the propensity to form a G quadruplex (Figure D2 in Appendix).

The lack of convergence of sequences was in contrast to the sequences obtained from round seven of the RNA selection, using method II, conducted by Dr. Thorsten Dieckmann (see Figure 7B). Since the RNA selection looked more promising nine more rounds of selection were conducted by Jenna Collier, then attempts were made to characterize its binding to FDA.

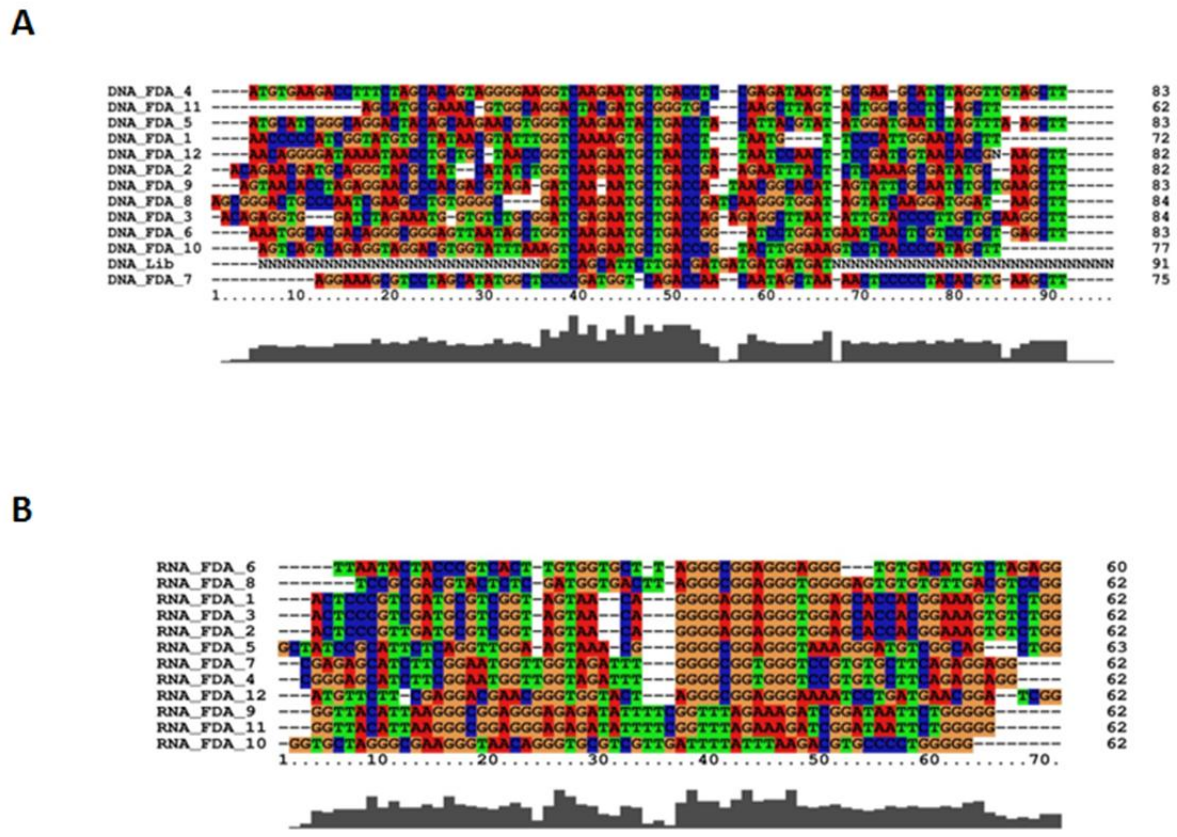

Figure 7 Multiple sequence alignment using Clustal 2.1 A) Round 8 from DNA SELEX B) Round 7 from RNA SELEX. Color coded A:RED; C:BLUE; G:ORANGE; T:GREEN. Below the sequences is a graph of homology versus sequence position.

RNA binding experiments

These experiments were performed with the assistance of Jenna Collier and Marie Claire Lacassin. The procedure is similar to method II used for selection seen in Figure 6b. The difference being that the supernatant that is discarded in the selection is collected and mixed with an indicator. The indicator in this context is a dye molecule that fluoresces upon binding RNA. The amount of fluorescence was detected and corresponds to the amount of RNA that does not bind to FDA.

The first indicator used was SyberGreen II (Invitrogen Corporation, California, U.S.A). This indicator is commonly used in RNA gels in place of ethidium bromide. Results obtained using SyberGreen II were inconsistent leading to the use of RiboGreen (Invitrogen Corporation, California, U.S.A). RiboGreen is advertised for optimal determination of RNA concentration in solution versus SyberGreen which is optimized for gel use. However these results were inconsistent as well. The initial control used was RNA exposed to beads which had no FDA bound. A control with FDA bound to beads and no RNA revealed the source of inconsistency. It appeared that some of the FDA hydrolyzed to fluorescein and was in solution. Since both SyberGreen II and RiboGreen share emission maxima with fluorescein, the fluorescence measurement did not accurately represent binding. The next indicator tested, Cy5 (Invitrogen Corporation, California, U.S.A), was obtained since it has a different emission maxima (Figure 8). Unfortunately experiments with Cy5 showed interaction of Cy5 with beads. Fluorescence measurements are summarized in Table D1 in Appendix.

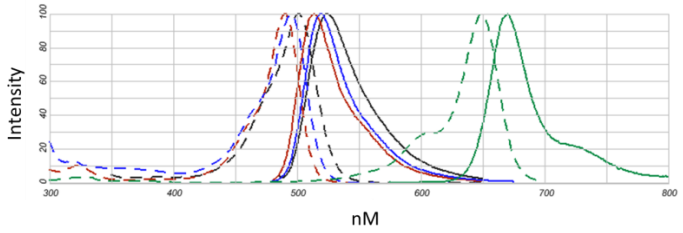

Figure 8. Emission (solid line) and Excitation spectra (dash lines) for fluorescein (red), SyberGreen II (blue), RiboGreen (black) and Cy5 (green). Created using Invitrogen SpectraViewer (Invitrogen Corporation, California, U.S.A).

3. Discussion

Aptamer selection

Method I was identical to previous reported selection for a structure switching DNA aptamer targeted at adenosine triphosphate (Nutiu and Li 2005). This method places two selection pressures; first the DNA must bind to target and second the binding of the target must trigger a structural change. The combination of both of these selection pressures may have been excessive to allow for selection for binding to FDA.

Method II had one selection pressure, which was binding to target. The removal of the selection pressure for structure switching improved the ability of DNA to survive selection rounds. The presence of possible G quadruples is interesting as these motifs are implicated in a variety of functions including translation initiation and mRNA stability. However, the presence of the bridge region could have limited the variety of structures that DNA could fold into. This explains why the RNA selection was able to converge in seven selection rounds. The RNA starting library did not contain a bridge sequence, which allowed for more sequences to be explored.

RNA binding experiments

The observation that fluorescein was interfering with indicator dye signal emphasized the need for appropriate controls. A literature search revealed that Cy5 can under some circumstances interact with avidin (Gruber et al. 2000), which could explain the observed interaction with the beads. The beads are avidin coated and FDA is attached to avidin via a biotin linker. To avoid any complications that may arise from this potential interaction, an alternate method is suggested. This method for detection of binding is outlined and discussed below.

4. Conclusions and Future work

Our attempt to obtain a DNA aptamer for FDA will be repeated with a starting library similar to the one used for the RNA aptamer selection. The bridging region is ideal for selection of an aptamer with structure switching capability; however since structure switching isn't the chief goal, this setup would not be necessary for our purposes. Removing selection pressure for structure switching should expand the number of sequences explored.

The binding properties of the RNA aptamer sequences will be further studied using radioactively labelled RNA. This method has been previously used for determining binding affinity of aptamers (Gopinath S. et al. 2006) and by Dr. Dieckmann in the RNA selection process to monitor increase in binding to beads. Briefly described, the process involves dephosphorylation of 5' of RNA using calf intestinal alkaline phosphatase followed attachment of adenosine triphosphate [γ^{32}P] to RNA using T4 polynucleotide kinase. This RNA is introduced to FDA bound beads, followed by ten washes to remove RNA that doesn't bind; the RNA that stays bound is then measured using a scintillation counter.

RNA sequences with the highest affinity will then be shortened to determine the minimal binding sequence. At this point the DNA analog of the minimal sequence will be investigated for FDA binding based on the occurrence of DNA analog binding as mentioned previously. The sequences will then be tested for the presence of FDA hydrolysis by monitoring fluorescein fluorescence.

If no catalytic activity is detected a new selection will be conducted using a pool containing FDA binding sequences and selection pressure for hydrolysis will be applied. The application of selection pressure for activity utilizes a substrate that is linked to both column

and RNA pool sequences. RNA that modifies the substrate through cleavage is separated from the sequences that stay attached to the column and thus can be isolated for enrichment (Wilson and Szostak 1999). A similar approach can be used in the search for FDA hydrolyzing RNA.

5. Materials and Methods

DNA selection

The random DNA library (approximately 10^{15} molecules) was obtained courtesy of Dr. Juewen Liu with the following sequence: 5'ACGATGCGGGTGCCAAGCTTN^{30}GGTCAGCATTCTTGACG ATGATGATGATGAT N^{30}GCGGAGCGTGGCAGG 3', along with the primer 1: 5'ACGATGCGGGTGCCA AGCTT**A**3'(**A** is ribo-terminated A in primer 3), primer 2: 5'CCTGCCACGCTCGCAAG3' and BiotinDNA: **B**GGTCAGCATTCTTGACGATGATGATGATGAT3' (**B** biotin attached) which is used in method II. As mentioned the DNA selection was preformed based on a previously described method (Nutiu and Li 2005).

For method I, 2 nmol of the DNA library, 10 nmol of BDNA and 2.5 nmol each of primer 1 and primer 2 were incubated in wash and binding (WB) buffer (100 mM NaCl, 500 mM KCl, 10 mM MgCl2, 100 mM phosphate buffer pH 7) at 277 K overnight. This mixture was then incubated with 200 µL of washed avidin-coated magnetic beads (Invitrogen Corporation, California, U.S.A) for 30 min at room temperature. The beads were washed with ten volumes of WB buffer. The beads were then pulled to bottom using a magnet and the supernatant was then removed. The beads were then washed ten more times with 200 µl of WB buffer. Then 0.1 mM FDA was added to beads and allowed to equilibrate for 30 min. The

beads were then pulled to bottom using a magnet and the supernatant containing DNA of interest was collected.

For method II, 2 nmol of the DNA library and 2.5 nmol each of primer 1 and primer 2 were incubated in wash and binding (WB) buffer (100 mM NaCl, 500 mM KCl, 10 mM MgCl2, 100 mM phosphate buffer pH 7) at 277 K overnight. This mixture was then incubated with 200 µL of washed avidin-coated magnetic beads (Invitrogen Corporation, California, U.S.A) for 30 min at room temperature. The beads were washed with ten volumes of WB buffer. The beads were then pulled to bottom using a magnet and the supernatant was then removed. The beads were then washed ten more times with 200 µl of WB buffer. Then 200 µl of 10 mM KOH was added to beads. This solution was allowed to incubate for 10 mins at room temperature. The beads were then pulled to bottom using a magnet and the supernatant containing DNA of interest was removed.

The solution containing DNA of interest was amplified using ribo-terminated primer 3 and primer 2. The number of cycles required was determined by running 30 cycles and collecting samples at 10, 15, 20 and 30 cycles. These were run on an agarose gel with ethidium bromide stain. After determining the number of cycles required a 300 µl PCR was run. After phenol chloroform extraction and ethanol precipitation the DNA was treated with 90 µl of 0.25 M NaOH at 363 K for 10 min. Followed by neutralization by addition of 10 µl of 3 M sodium acetate pH 5.5. The DNA was then ethanol precipitated and run on a PAGE gel. For the next rounds, the purified DNA from the previous round was mixed with primer 1, primer 2 and BDNA. This mixture was denatured at 363 K for 5 mins and annealed at room temperature for 30 minutes in WB buffer before addition of 200 µL washed avidin-coated magnetic beads for 15 min. Protocols for PCR are located in Table D2 in Appendix.

Colony PCR

Colony PCR was done using a kit from Invitrogen (Invitrogen Corporation, California, U.S.A) and following their procedure. Briefly descirbed, DNA from the round to be sequenced was amplified using PCR with an addition elongation step. This step adds adenosine runs to the 3' end of the sequence. Then the DNA was cloned into a vector and vector was transformed into cells. The cells were then plated on lysogeny broth (LB) plates with ampicillin and X-gal. In 12 hours white colonies were visible and some with a blue tint (Figure D3, Appendix). Blue colonies indicated a lack of insertion of vector and were not picked. White colonies are picked with pipette tip and mixed with PCR solution. This PCR includes an extra heating step to denature the cells and release DNA. After PCR the DNA is extracted using the phenol chloroform method and ethanol precipitated and then sent for sequencing. Our sequences were sent to Operon (Operon, Alabama, U.S.A). PCR protocols for elongation and colony preparation are in Table D2 in Appendix.

Binding test

RNA concentration was determined using a NanoDrop 2000 (Thermo Fisher Scientific Company, Ontario, Canada) by measuring absorbance at 260 nm. The RNA was then diluted to a 1 uM solution in WB buffer. 40 µl of RNA 1 uM solution was then added to 50 µl of washed avidin-coated magnetic beads. The solution was allowed to incubate for 10 min at room temperature. The beads were then pulled to bottom using a magnet and the supernatant was collected. This solution was mixed with an equal volume of indicator solution and fluorescence was measured using NanoDrop 3300 (Thermo Fisher Scientific Company, Ontario, Canada). SyberGreen II indicator solution was made by adding 1 ul from concentrated stock (Invitrogen Corporation, California, U.S.A) to 199 µl WB buffer.

RiboGreen indicator solution was made by adding 1 ul from concentrated stock (Invitrogen Corporation, California, U.S.A) to 199 µl WB buffer. Cy5 indicator solution was made by adding 5 ul from concentrated stock (Invitrogen Corporation, California, U.S.A) to 195 µl WB buffer.

Chapter 5: Reconstructing MGA template and ligand to improve catalytic activity

1. Introduction

This chapter covers two projects that have not fully achieved their end goal. The first project involves the design of alternate MGA DNA templates in order to maximize uniform length products from T7 polymerase transcription. The motivation for this project was to ensure that the investigation of MGA was not compromised by presence of MGA with extra nucleotides appended to 3' tail. The attempt involved using enzymes, ribozymes and DNAzymes, both of which are discussed below. The second project involves the design of a new ligand for MGA. The intent was to provide MGA with a substrate that it would be able to catalyze into a product faster than background. The notion that RNA aptamers can have catalytic activity based on ligand provided without the need for selection pressure for catalytic activity during SELEX is discussed below.

Ribozymes

Ribozymes are catalytic RNA sequences. The two ribozymes used in this work are the hammerhead and hepatitis delta virus ribozymes. Hammerhead (HH) ribozyme is found in plant viruses, this naturally occurring ribozyme cleaves phosphodiester bonds. This cleavage reaction is important for viroid replication (Prody et al. 1986, Pley, Flaherty and McKay 1994, Branch and Robertson 1984). The minimal catalytic sequence of the hammerhead ribozyme was determined and contains three stem regions and a catalytic core (Figure 1) (Scott, Finch and Klug 1995). Three nucleotides have been identified that play key roles in cleavage. G5 is responsible for positioning the substrate while G12 and G8 have been implicated in an acid-base catalysis reaction (Peracchi et al. 1998, Martick et al. 2008, Scott 2007). The full length ribozyme has higher activity achieved by optimization of the

positioning of these three nucleotides by tertiary interactions of stems (Martick and Scott 2006). Interestingly this ribozyme has been identified within fungi, archea and bacteria (Perreault et al. 2011).

The second ribozyme also plays an important role in viral replication and is found in the hepatitis delta virus (HDV) (Kuo et al. 1988). The HDV ribozyme contains five helices which are connected by a double psuedoknot (Figure 2) and is responsible for a cleavage reaction similar to HH ribozyme (FerreDamare, Zhou and Doudna 1998). In this case the ribozyme works with a divalent cation to achieve cleavage reaction (Shih and Been 2002). The divalent metal acts as a general acid along with C75 to achieve acid-base catalysis (Chen et al. 2010). This ribozyme has also been shown to induce conformational changes in its RNA substrate (Ke et al. 2004), a trait shared by MGA and other aptamers discussed in Chapter 1.

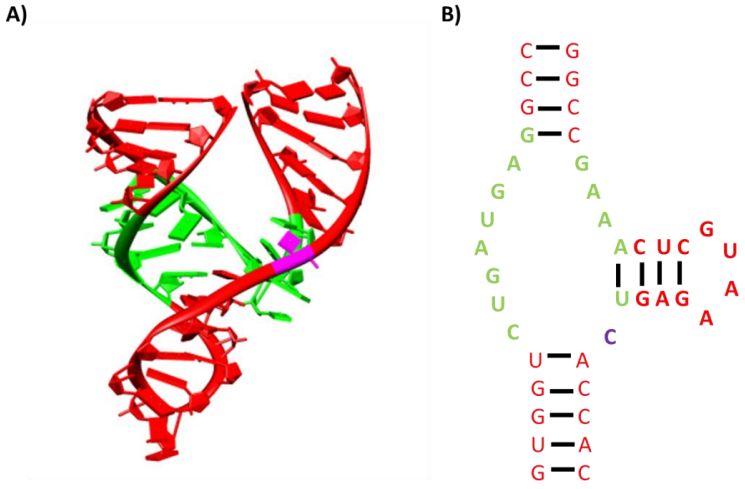

Figure 1. Structure of HH ribozyme, A) Crystal structure obtained using 2'-O-methyl cytosine to prevent cleavage (PDB 1MME). B) Secondary structure schematic. In both A) and B); Purple represents nucleotide where cleavage occurs (any nucleotide but G); Green represents the conserved sequences; Red represents other nucleotides (Scott, Finch and Klug 1995). Figure was generated using UCSF Chimera (Pettersen *et al*. 2004).

Both HH and HDV ribozymes have found application in molecular biology to ensure homogeneous *in vitro* T7 RNA polymerase transcription. Homogeneous sequences are desired since additional nucleotides could change the secondary structure of transcript. T7 RNA polymerase is prone to adding nucleotides on the 3' end of transcript. By adding a self-cleaving ribozyme at the end of the transcript, the homogeneity of the desired RNA can be obtained by removal of the ribozyme (Shields et al. 1999, Chowrira, Pavco and Mcswiggen 1994, Blight and Rice 1997).

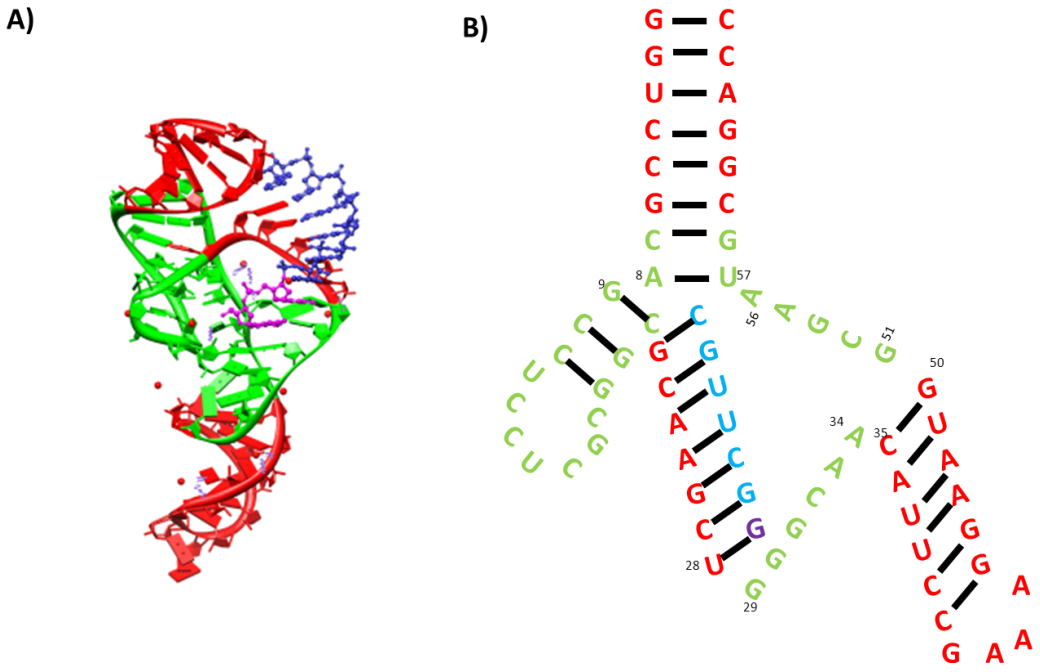

Figure 2. Structure of HDV ribozyme A) Crystal structure obtained using 2'-OH nucleophile was changed to a 2'-H. B) Secondary structure schematic. In both A) and B); Purple represents nucleotide where cleavage occurs; Green represents the conserved sequences; Red represents other nucleotides.

DNAzyme

Another method for obtaining a homogenous transcript is the use of a DNA enzyme that was selected for RNA cleavage. The enzyme consists of a 15 nucleotide core flanked by substrate complementary sequences (Figure 3) (Santoro and Joyce 1997). The activity of the DNAzyme has been shown to be dependent on the presence of Mg^{2+}. This ion is implicated in the deprotonation of the 2' OH, a role similar to the one it plays in the HDV ribozyme (Santoro and Joyce 1998). This enzyme has been used to target hepatitis C virus genomic RNA with promising results (Kumar et al. 2009).

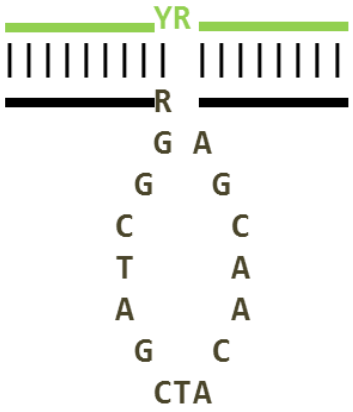

Figure 3. Secondary structure of DNAzyme catalytic motif. DNAzyme – Black; Target RNA – Green, R = A or G; Y = U or C.

Catalytic aptamers

The DNAzyme isn't the only molecule that has been selected for catalytic activity. SELEX has been modified to select catalytic RNA. Reactions that RNA sequences have been selected to catalyze include an aldol reaction (Fusz et al. 2005), aminoacylation (Illangasekare et al. 1995), amide synthesis (Wiegand, Janssen and Eaton 1997), urea synthesis (Nieuwlandt et al. 2003), Diels Alder (Agresti et al. 2005), Michael additions (Sengle et al. 2001), alkylation (Wecker, Smith and Gold 1996), peroxidase (Liu et al. 2009), metalation (Kawazoe

et al. 2001) and cofactor dependent redox reaction (Tsukiji, Pattnaik and Suga 2003). Interestingly, the RNA with peroxidase activity was selected for binding to hemin (Liu et al. 2009) and the metalation activity was seen in a RNA selected for binding to N-methylmesoporphyrin (Kawazoe et al. 2001). These aptamers were selected for binding and had inherent catalytic activity. This is also seen in MGA which was selected for binding MG. MG has a positive charge which resulted in a selection pressure for an electronegative pocket. This was harnessed by catalysis of a reaction with a positive transition state and MGA has been shown to catalyze the hydrolysis of acetoxy derivative of MG (MGOAc) (Figure 4) at 1000-fold over background of the same reaction pathway (Brackett and Dieckmann 2006).

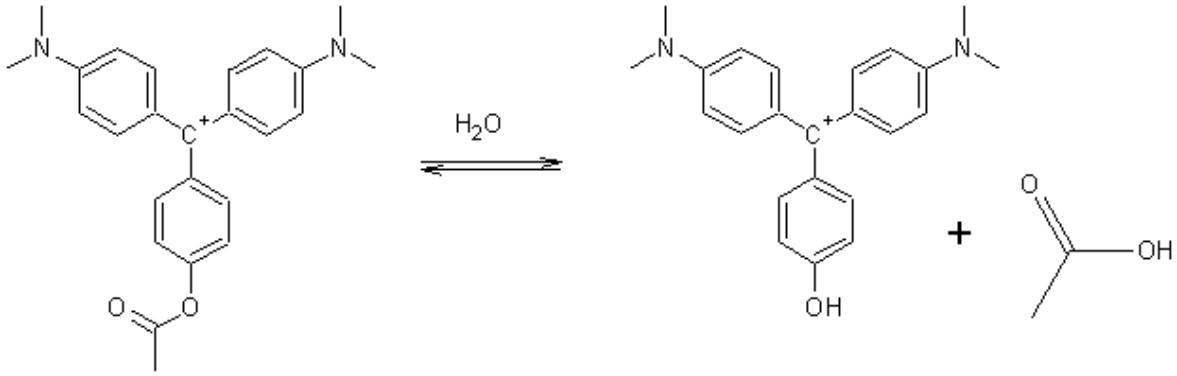

Figure 4. MGOAc hydrolysis to hydroxy MG and acetate.

2. Results and Discussion

MGA template modification

The first attempt to obtain homogenous RNA was to append HDV to the 3' end of the MGA. A second template was designed with HH to the 5’ and 3’ ends of MGA. Both template are shown in Figure 5. HDV and HH modified clones were designed and developed by Dr. Elaine Collins (San Jose State University, California, USA). The template were designed using Assembly PCR Oligo Maker (Rydzanicz, R. *et al.* 2005)

(http://startrek.ccs.yorku.ca/Epjohnson/AssemblyPCRoligomaker.html).The modified DNA templates were obtained from Sigma-Aldrich (Sigma-Aldrich, Missouri, U.S.A) and following PCR was then inserted into a vector . The vector was then transfected into cells. This allowed for large scale preparation of the templates, since large quantities of the cells could be grown. The DNA was then purified using a DNA purification kit (Qiagen). Then the DNA was excised from vector using restriction enzymes, and after purification the DNA was used in transcription reactions.

HH MGA template

CCATTATGCTGAGTGATATCCCCTCTGATCGCCCTCAGACTACTCAGGCACTCCTGCTTTGCCATGGGCCATGGCAGCTGAGG
GCTGACCGCTCTCGGTCATTGCTTACCTCAGCTGCCTCAGATCTCTGAGGCAGGACTACTCAGGCACTCCTGCTTTGAGGTTTT
ATTTGGTTCCTAGC

HDV MGA template

CCATTATGCTGAGTGATATCCCCTCGCTGACCGCTCTCGGTCCATTGCTTAGAGGGGCCAGCCGACGTCTGGGTCGGAGGAGC
GCCCGGGCTGGACCCGTAGAAGCCTACCGCTTACCCAGT

Figure 5. Ribozyme MGA templates: Highlighted in yellow is T7 promoter; in Green is MGA DNA; in Red and Purple is ribozyme; in Purple are residues important for catalysis

After the templates were purified, the RNA was transcribed as previously described. The RNA was then purified and dissolved in catalysis buffer (50 mM Tris pH 7.0, 100 mM NaCl, 10 mM $MgCl_2$). The concentration of magnesium was increased but did not result in more cleavage consistent with previous report by Chowrira *et al.* (Chowrira et al. 1994). HH ribozyme was not as active as HDV, since a large amount of uncleaved RNA was found after twelve hours. (Figure E1 in Appendix).

In an attempt to obtain cleaved homogenous RNA, without the addition of significant length, a template was designed that could be cleaved by the DNAzyme (Figure 6). The change in length of the sequence is significantly smaller than HDV or HH MGA templates. The enzyme did cleave some of the product, a significant portion was left uncleaved, and

attempts were made to vary temperature and magnesium concentration with no significant increase in catalysis (Figure E2 in Appendix).

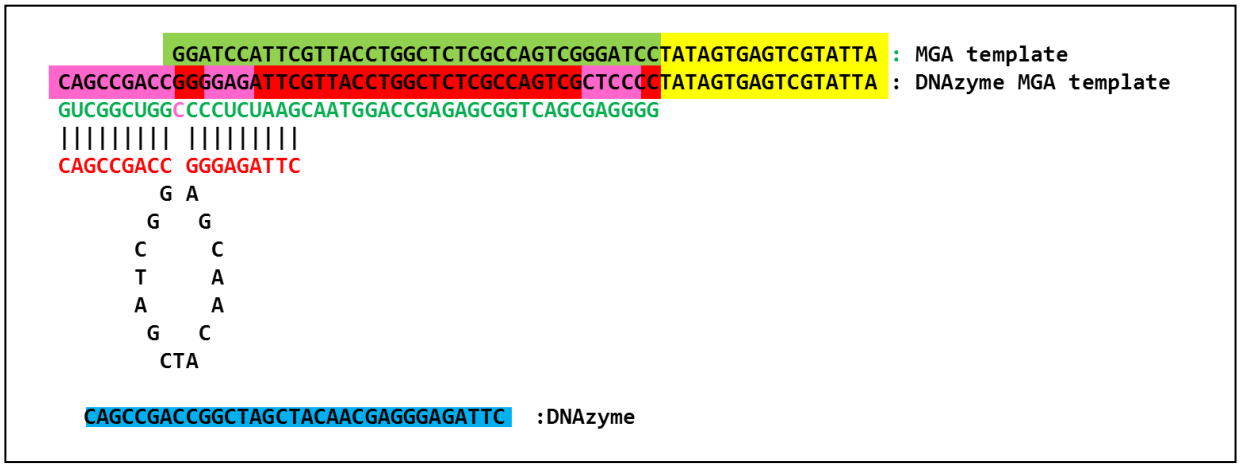

Figure 6. DNAzyme MGA template: Highlighted in yellow is T7 promoter; Green is MGA DNA, Red and Purple is DNAzyme MGA DNA; Purple is changes made to accommodate interaction with DNAzyme; Blue is DNAzyme. In Green font is MGA shown interacting with DNAzyme (Red font depicts the target identifying sequences, Black font shows the catalytic core).

The secondary structures of the three RNAs discussed are depicted in Figure 7. These structures reveal a possible explanation for the low cleavage rate. For the HDV MGA the lowest energy structure predicted does not form the required base pair interaction with nucleotides neighbouring the cleavage site. In the case of the HH MGA the trans-ribozyme is predicted to fold optimally, while the cis-ribozyme does not fold to ensure that cleavage site in the appropriate position. Also, the reduction in yield is expected because of the additional length of transcript; a significant portion of the RNA transcribed was being cleaved off to obtained homogenous samples. The DNAzyme MGA is also predicted not to fold as intended when initially designed. This is apparent because of extra base pairs formed in catalytic core with target RNA.

A)

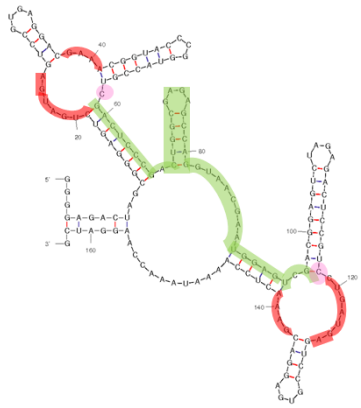

B)

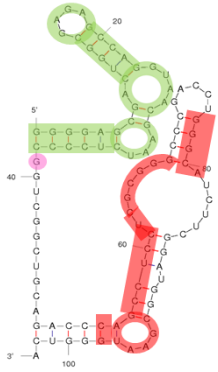

C)

GGGGAGCGACUGGCGAGAGCCAGGUAACGAAUCUCCCCGGUCGGCUG&CAGCCGACCGGCUAGCUACAACGAGGGAGAUUC

.....(((((....)))))....((((((((((((((((((&))))))))))))))))....((.....))))))))))

Figure 7. Secondary structure predictions with MGA highlighted in Green and sequences important for catalysis in Red. A) HH ribozyme MGA RNA B) HDV ribozyme MGA RNA C) DNAzyme MGA RNA and DNAzyme (separated by &). A) and B) Generated using mfold. C) Generated using Vienna RNAcofold.

Another method attempted involved addition of a 2'-O methyl group to 3' of MGA template DNA, this has previously been reported to reduce n+1 transcription products (Kao, Zheng and Rudisser 1999). Unfortunately this produced an additional band which was detected during the gel purification step (Figure E3 in Appendix). This phenomenon was not investigated further.

To determine if there was a significant presence of n+1 RNA mass spectrometry experiments were conducted. The analysis of mass spectrometry data revealed two peaks with the first peak at 12578 mass identified as n and the second peak at 12905 mass identified as n+1 (Figure 8A). Using a molecular weight calculator

(http://www.currentprotocols.com/tools/dnarnaprotein-molecular-weight-calculator), the mass of n is predicted at 12521 Da and n+1 at 12850 Da. A sample containing MGA mixed with MG was then run. This spectrum showed presence of n+1 binding dyes (Figure E4 in Appendix). Also, a secondary fold prediction of MGA with an extra nucleotide did not result in a significant change in structure (Figure E5 in Appendix), and the use of double stranded template DNA reduced the amount of n+1 significantly (Figure 8B). Based on these findings, n+1 MGA was deemed to be similar enough to MGA that further attempts to isolate homogenous MGA were deprioritized.

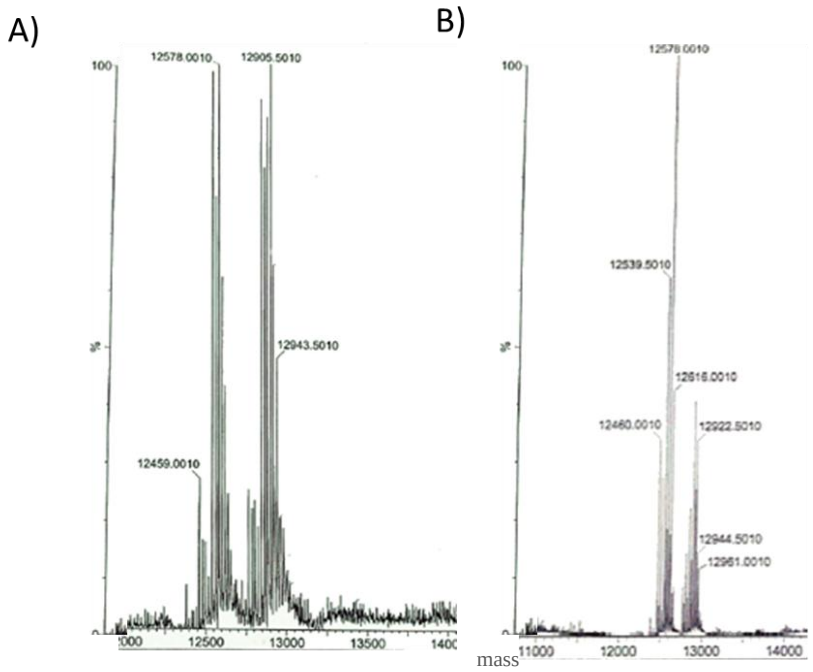

Figure 8. Mass spectra of A) MGA from transcription with a single stranded template B) MGA from transcription with double stranded template

Changes in Ligand

MGA has previously been shown to have catalytic activity (Brackett and Dieckmann 2006) when provided with an ester derivative of MG. In order to investigate the catalytic potential of MGA attempts were made to design new MG derivatives. The attempt to change

the ligand for MGA was met with limited success. MGA binds to MGNCS as seen by a shift in visible spectra (Figure 9). However no reaction was observed when this complex was exposed to lysine (Figure E7 in Appendix). This reaction was attempted since fluorescein isothiocyanate is commonly used to covalently attach fluorescein to peptides (Johnson, Yguerabide and Taylor 1984, Breier and Ziegelhoffer 2000) and MGNCS has been used for the same application (Golding et al. 1998). The covalent bond found is a thiourea bond by reaction of the side chain amine of lysine and isothiocyanate group (Breier and Ziegelhoffer 2000). While the electronegative pocket would stabilize positive transitions states it maybe that the pocket does not allow for optimal interaction of the lysine with the ligand. The hydrolysis reaction that MGA catalyzes requires that water be able to enter pocket. Lysine is a bigger molecule and the pocket does not facilitate the entry of a small molecule other than ligand.

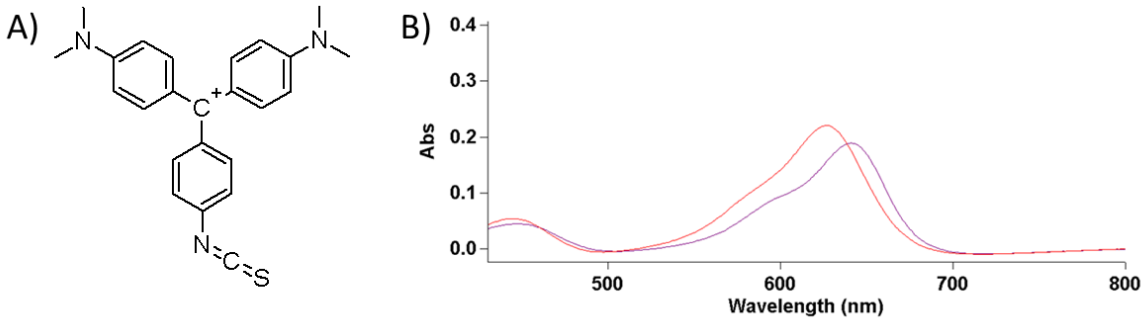

Figure 9. A) Chemical structure of MGNCS B) Visible Spectra of MGNCS (Red) and MGNCS mixed with excess of MGA (Purple).

Since formation of a bond would meet with the same difficulty as thiourea bond formation, that is the entry of the second substrate. An attempt was made to synthesize $MGCOOCF_3$ (Figure 10A), in order to observe if MGA could catalyze another hydrolysis reaction. This reaction would be similar to MGOAc hydrolysis but would result in $MGCOO^-$

which due to the negative charge would be ejected from MGA pocket. However this molecule was hydrolyzed in water at a fast rate. This was determined by mixing $MGCOOCF_3$ in both water and methanol solutions, each of the solutions were then analyzed by mass spectrometry (Figure E8 in Appendix). In water the sample spectra contained a 375 peak, which suggests MGCOO (Figure 10B). In methanol the sample spectra contained a 387 peak, which suggests $MGCOOCH_3$ (Figure 10C). In order to reduce the rate of hydrolysis an attempt was made to synthesize MGCOphenol (Figure 10D), however the product proved to be insoluble in water.

Since attempts to design a ligand that would undergo a reaction other than the previously reported ester hydrolysis that MGA could catalyze were not successful, the next approach involved placing the same ester group deeper within the pocket. Michlers ketone (Figure 10E) was purchased in order to synthesize a molecule with an ester group at central carbon, based on a report of it its reactivity with acetyl chloride (Gilman and Heck 1930). However this synthesis was unsuccessful.

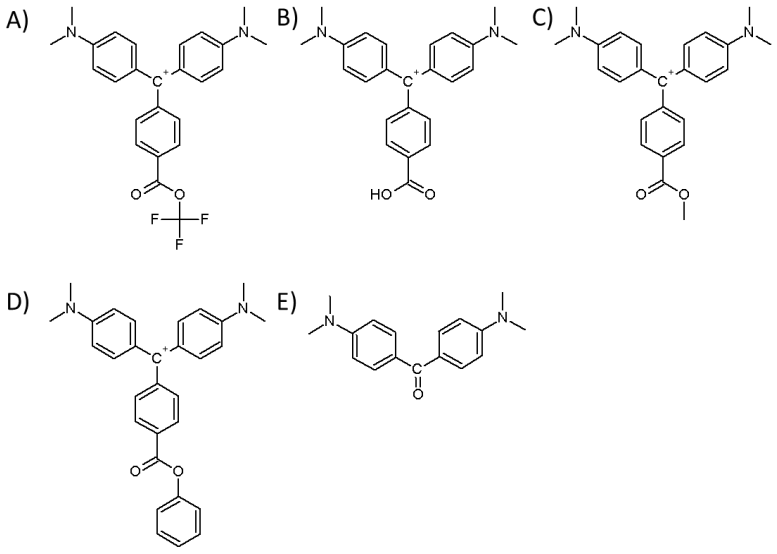

Figure 10. Chemical structures of MG derivatives A) $MGCOOCF_3$ B) MGCOO C) $MGCOOCH_3$ D) MGCOphenol E) Michlers Ketone

3. Conclusions and Future Work

While the strategy of using ribozymes to ensure homogenous transcripts is an elegant one, it may not be cost effective for a short aptamer. It appears that the gel purification method used does leave some n+1 sequence; however, in the case reported here these sequences appear to be functional. It is worthwhile to use the HDV template to generate a large amount of homogenous RNA and conduct ITC experiments to compare our current ITC data. The synthesis of new MGA derivatives should be attempted beginning with further experiments with Michlers ketone, more specifically a synthesis reaction involving Michlers ketone and benzyl chloride that was previously reported (Gilman and Heck 1930).

4. Thesis Conclusions

The goal of this work has been to show the capacity of RNA for function. Our work with MGA has shown that varying the salt concentration was able to change the preference of ligand. Secondly we have shown that binding of MGA can be influenced by a pre-bound ligand. These characteristics suggest that RNA is capable of maintaining the capacity for functions not selected for. This would have been an excellent ability in a prebiotic world, since one pool of RNA could develop multiple functions. These characteristics should be kept in mind while developing applications for MGA, since the solution conditions effects its binding ability. Our work with MGA also reaffirms the need to preform characterisations under different solution conditions. The NMR experiments were conducted in the absence of Mg^{2+} to avoid issues with degradation.

5. Materials and Methods

HH and HDV MGA DNA template preparation

In order to prepare the necessary templates Sure2 competent cells containing pUC18

plasmid, designed by Dr. Elaine Collins, were grown on lysogeny (LB) plates containing ampicillin (100 µg/mL). A single isolated colony from the plate was used to inoculate 100 mL of LB broth. Culture was incubated at 37^{o}C for 12 h. The cells were then spun down at 4000 *g* for 30 min. The plasmid from the pellet was purified using Qiagen Plasmid Plus Purification Kit (Qiagen, Toronto, Canada). The protocol provided by Qiagen (Qiagen, Toronto, Canada) was followed to obtain the plasmid in water. The plasmid was then linearized with Bam H1 (Fermentas, Burlington, Canada). Completion of digestion was observed by running a 1% agarose gel containing ethidium bromide. The reaction mixture was then purified using Qiagen PCR purification kit (Qiagen, Toronto, Canada) and concentration of purified DNA was determined using absorbance at 260 nm. Transcription reaction was performed using the protocol described in Chapter 2, the same protocol was used for double stranded and single stranded MGA templates.

Ribozyme Cleavage Reaction

RNA from transcription was dissolved in cleavage buffer I (50 mM Tris HCl, pH 7.5, 100 mM NaCl and 10 mM $MgCl_2$). This mixture incubated at 90^{o}C for 5 min then at 4^{o}C for 5 min, this hot and cold cycle was repeated three times. The solution was then allowed to react at 37^{o}C for 4 hrs. The resulting solution was then run of a 12% polyacrylamide gel and purified on columns according to the protocol described in Chapter 2.

DNAzyme Cleavage Reaction

RNA from transcription using DNAzyme MGA template was dissolved in cleavage buffer II (50 mM Tris HCl, pH 7.5, 150 mM NaCl, and 10 mM $MgCl_2$. The concentration of RNA was determined using absorbance at 260 nm. DNAzyme was added to RNA for a final molar ratio of 1:1. This mixture incubated at 90^{o}C for 5 min then at 4^{o}C for 5 min. The

solution was then allowed to react at 37^{o}C for 4 hrs. The resulting solution was then run of a 12% polyacrylamide gel and purified on columns according to protocol described in Chapter 2.

RNA Mass Spectrometry Procedure

RNA samples for MS were ethanol precipitated using two times the volume of ethanol and one tenth the volume of 3 M ammonium acetate. The procedure used for mass spectrometry analysis was adapted from a procedure reported by Gooding K.B, *et al.* (Gooding et al. 2004, Greig and Robinson 2000). Samples were dissolved in 50% isopropanol, 25% water and 25% acetonitrile. Then they were run on a Micromass Q-TOF Ultima Global (Waters Cooperation, Masssachusetts, U.S.A) with negative electrospray ionization. The resulting spectra were processed using software provided by Waters Cooperation, Masssachusetts, U.S.A.

Dye reactions

MGNCS lysine

MGNCS was purchased from Invitrogen, Ontario, Canada. The dye was weighed and dissolved in acetonitrile for storage as a 100 µM stock solution. A solution with final concentration of 5 µM MGNCS and 32 µM MGA was prepared in 50 mM NaCl, 25 mM phosphate buffer at pH 5, lysine was added to a final solution of 10 µM. The background reaction was observed with same concentration of MGNCS and buffer in the absence of MGA.

Lysine MG product was synthesized by mixing MGNCS with excess lysine in a pH 9 phosphate buffer for 60 min, procedure was based on a previous report (Johnson, Yguerabide and Taylor 1984). The visible spectra of lysine MG had a maximum at 590 nm (Figure E6 in

Appendix), there was no change in presence of MGA. The catalysis reaction was measured by monitoring decrease in MGNCS maximum at 630 nm (Figure E7 in Appendix).

.

$MGCOOCF_3$

First, MGCOOH was synthesized according to published report(Cho et al. 2003). The synthesis involved stirring dimethylaniline and 4-carboxy benzaldehyde in concentrated HCl for 12 hrs under nitrogen. This was followed by neutralization with NaOH and extraction into ether. The solution was then dried with sodium sulfate. The leuco-base was purified by flash chromatography using 9:1 hexane and ethyl acetate. The leuco-base was then dissolved in chloroform with an excess of 2,3-dichloro-5,6-dicyano-1,4-benzoquinone. The dye was then purified by flash chromatography using 5:1 chloroform and methanol. Positive ESI mass spectrometry was used to confirm the formation of the desired product. MGCOOH was then reacted with 2,2,2-Trifluoroethanol in dichloromethane, this was done following the protocol reported by Srinivas K., *et al*. (Srinivas, Mahender and Das 2003). MGCOphenol synthesis followed the same procedure with phenol instead of 2,2,2-trifluoroethanol.

Michlers Ketone

Michlers ketone was purchased from Sigma-Aldrich, Missouri, U.S.A. The alcohol was synthesized following procedure report by Dumur F., *et al.*(Dumur et al. 2008). Briefly, this involved boiling in THF in the presence of sodium borohydride. The alcohol was then reacted with excess acetyl chloride. Positive ESI mass spectrometry was used to confirm the formation of the desired product, which was absent, in this case (Figure E9 in Appendix).

References

1. Chapter 1

Alderman, D. (1985) Malachite green - a review. *Journal of Fish Diseases*, 289-298.

Balakin, A. G., L. Smith & M. J. Fournier (1996) The RNA World of the Nucleolus - Two Major Families of Small RNAs Defined By Different Box Elements With Related Functions. *Cell,* 86**,** 823-834.

Bartel, D. P. (2007) MicroRNAs: Genomics, biogenesis, mechanism, and function (Reprinted from Cell, vol 116, pg 281-297, 2004). *Cell,* 131**,** 11-29.

Bates, P. J., D. A. Laber, D. M. Miller, S. D. Thomas & J. O. Trent (2009) Discovery and development of the G-rich oligonucleotide AS1411 as a novel treatment for cancer. *Experimental and Molecular Pathology,* 86**,** 151-164.

Baugh, C., D. Grate & C. Wilson (2000) 2.8 angstrom crystal structure of the malachite green aptamer. *Journal of Molecular Biology,* 301**,** 117-128.

Ben Amor, B., S. Wirth, F. Merchan, P. Laporte, Y. d'Aubenton-Carafa, J. Hirsch, A. Maizel, A. Mallory, A. Lucas, J. M. Deragon, H. Vaucheret, C. Thermes & M. Crespi (2009) Novel long non-protein coding RNAs involved in Arabidopsis differentiation and stress responses. *Genome Research,* 19**,** 57-69.

Beringer, M. (2008) Modulating the activity of the peptidyl transferase center of the ribosome. *RNA,* 14**,** 795-801.

Bernacchi, S., S. Freisz, C. Maechling, B. Spiess, R. Marquet, P. Dumas & E. Ennifar (2007) Aminoglycoside binding to the HIV-1 RNA dimerization initiation site: thermodynamics and effect on the kissing-loop to duplex conversion. *Nucleic Acids Research,* 35**,** 7128-7139.

Bernard Da Costa, J. & T. Dieckmann (2011) Entropy and Mg^{2+} control ligand affinity and specificity in the malachite green binding RNA aptamer. *Molecular Biosystems,* 7**,** 2156-63.

Blount, K. F. & R. R. Breaker (2006) Riboswitches as antibacterial drug targets. *Nature Biotechnology,* 24**,** 1558-1564.

Bock, R. M., D. Soll & J. D. Cherayil (1967) Mechanism of codon recognition by tRNA. *Indian Journal of Biochemistry,* 4**,** 25-27.

Borovinskaya, M., R. Pai, W. Zhang, B. Schuwirth, J. Holton, G. Hirokawa, H. Kaji, A. Kaji & J. Cate (2007) Structural basis for aminoglycoside inhibition of bacterial ribosome recycling. *Nature Structural & Molecular Biology,* 14**,** 727-732.

Bouchard, P. R., R. M. Hutabarat & K. M. Thompson. 2010. Discovery and Development of Therapeutic Aptamers. *Annual Review of Pharmacology and Toxicology*, 237-257.

Brenner, S., M. Meselson & F. Jacob (1961) Unstable intermediate carrying information from genes to ribosomes for protein synthesis. *Nature,* 190**,** 576-581.

Brodersen, D. E., W. M. Clemons Jr, A. P. Carter, R. J. Morgan-Warren, B. T. Wimberly & V. Ramakrishnan (2000) The Structural Basis for the Action of the Antibiotics Tetracycline, Pactamycin, and Hygromycin B on the 30S Ribosomal Subunit. *Cell,* 103**,** 1143-1154.

Carthew, R. W. & E. J. Sontheimer (2009) Origins and Mechanisms of miRNAs and siRNAs. *Cell,* 136**,** 642-655.

Cech, T. R. (2009) Crawling Out of the RNA World. *Cell,* 136**,** 599-602.

Cech, T. R., A. J. Zaug & P. J. Grabowski (1981) In vitro splicing of the ribosomal RNA precursor of Tetrahymena: involvement of a guanosine nucleotide in the excision of the intervening sequence. *Cell,* 27**,** 487-96.

Chushak, Y. & M. O. Stone. 2009. In silico selection of RNA aptamers. *Nucleic Acids Research,* e87.

Cowan, J. A., T. Ohyama, D. Q. Wang & K. Natarajan (2000) Recognition of a cognate RNA aptamer by neomycin B: quantitative evaluation of hydrogen bonding and electrostatic interactions. *Nucleic Acids Research.,* 28**,** 2935-2942.

Crick, F. H. (1958) On protein synthesis. *Symposia of the Society for Experimental Biology,* 12**,** 138-63.

Crick, F. H., S. Brenner, Watstobi.Rj & L. Barnett (1961) General nature of genetic code for proteins. *Nature,* 192**,** 1227-&.

Darnell, J. E., Jr. 2002. Transcription factors as targets for cancer therapy. *Nature Reviews Cancer,* 740-9.

Deissler, H. L. & G. E. Lang (2008) Effect of VEGF(165) and the VEGF Aptamer Pegaptanib (Macugen (R)) on the Protein Composition of Tight Junctions in Microvascular Endothelial Cells of the Retina. *Klinische Monatsblatter Fur Augenheilkunde,* 225**,** 863-867.

Delfosse, V., P. Bouchard, E. Bonneau, P. Dagenais, J. Lemay, D. Lafontaine & P. Legault (2010) Riboswitch structure: an internal residue mimicking the purine ligand. *Nucleic Acids Research,* 38**,** 2057-2068.

Dinger, M., T. Mercer & J. Mattick (2008) RNAs as extracellular signaling molecules. *Journal of Molecular Endocrinology,* 40**,** 151-159.

Dyke, C. K., S. R. Steinhubl, N. S. Kleiman, R. O. Cannon, L. G. Aberle, M. Lin, S. K. Myles, C. Melloni, R. A. Harrington, J. H. Alexander, R. C. Becker & C. P. Rusconi (2006) First-in-human experience of an antidote-controlled anticoagulant using RNA aptamer technology - A phase 1a pharmacodynamic evaluation of a drug-antidote pair for the controlled regulation of factor IXa activity. *Circulation,* 114**,** 2490-2497.

Edwards, A., F. Reyes, A. Heroux & R. Batey (2010) Structural basis for recognition of S-adenosylhomocysteine by riboswitches. *RNA,* 16**,** 2144-2155.

Ellington, A. D. & J. W. Szostak (1990) *In vitro* selection of RNA molecules that bind specific ligands. *Nature,* 346**,** 818-822.

Ennifar, E., J. Paillart, R. Marquet, B. Ehresmann, C. Ehresmann, P. Dumas & P. Walter (2003) HIV-1 RNA dimerization initiation site is structurally similar to the ribosomal A site and binds aminoglycoside antibiotics. *Journal of Biological Chemistry,* 278**,** 2723-2730.

Epshtein, V., A. S. Mironov & E. Nudler (2003) The riboswitch-mediated control of sulfur metabolism in bacteria. *Proceedings of the National Academy of Sciences of the United States of America,* 100**,** 5052-5056.

Espinoza, C., T. Allen, A. Hieb, J. Kugel & J. Goodrich (2004) B2 RNA binds directly to RNA polymerase II to repress transcript synthesis. *Nature Structural & Molecular Biology,* 11**,** 822-829.

Espinoza, C. A., J. A. Goodrich & J. F. Kugel. 2007. Characterization of the structure, function, and mechanism of B2 RNA, an ncRNA repressor of RNA polymerase II transcription. In *RNA,* 583-96. United States.

Faber, C., H. Sticht, K. Schweimer & P. Rosch (2000) Structural rearrangements of HIV-1 Tat-responsive RNA upon binding of neomycin B. *Journal of Biological Chemistry,* 275**,** 20660-20666.

Flinders, J., S. C. DeFina, D. M. Brackett, C. Baugh, C. Wilson & T. Dieckmann (2004) Recognition of planar and nonplanar ligands in the malachite green-RNA aptamer complex. *Chembiochem,* 5**,** 62-72.

Fourmy, D., M. I. Recht & J. D. Puglisi (1998) Binding of neomycin-class aminoglycoside antibiotics to the A-site of 16 S rRNA. *Journal of Molecular Biology,* 277**,** 347-362.

Frankel, A. D. (1992) Activation of HIV transcription by Tat. *Curr Opin Genet Dev,* 2**,** 293-8.

Freire, F., I. Cuesta, F. Corzana, J. Revuelta, C. Gonzalez, M. Hricovini, A. Bastida, J. Jimenez-Barbero & J. L. Asensio (2007) A simple NMR analysis of the protonation equilibrium that accompanies aminoglycoside recognition: Dramatic alterations in the neomycin-B protonation state upon binding to a 23-mer RNA aptamer. *Chemical Communications***,** 174-176.

Freisz, S., K. Lang, R. Micura, P. Dumas & E. Ennifar (2008) Binding of aminoglycoside antibiotics to the duplex form of the HIV-1 genomic RNA dimerization initiation site. *Angewandte Chemie-International Edition,* 47**,** 4110-4113.

Ganot, P., M. Caizergues-Ferrer & T. Kiss (1997) The family of box ACA small nucleolar RNAs is defined by an evolutionarily conserved secondary structure and ubiquitous sequence elements essential for RNA accumulation. *Genes & Development,* 11**,** 941-56.

Gilbert, S., C. Stoddard, S. Wise & R. Batey (2006) Thermodynamic and kinetic characterization of ligand binding to the purine riboswitch aptamer domain. *Journal of Molecular Biology,* 363**,** 624-624.

Gilbert, W. (1986) Origin of life - the RNA world. *Nature,* 319**,** 618-618.

Gonzalez-Fernandez, E., N. de-los-Santos-Alvarez, M. J. Lobo-Castanon, A. J. Miranda-Ordieres & P. Tunon-Blanco. 2011. Impedimetric aptasensor for tobramycin detection in human serum. *Biosensors and Bioelectronics,* 2354-60.

Grahn, E., N. J. Stonehouse, J. B. Murray, S. van den Worm, K. Valegard, K. Fridborg, P. G. Stockley & L. Liljas (1999) Crystallographic studies of RNA hairpins in complexes with recombinant MS2 capsids: implications for binding requirements. *RNA,* 5**,** 131-8.

Grivna, S., E. Beyret, Z. Wang & H. Lin (2006) A novel class of small RNAs in mouse spermatogenic cells. *Genes & Development,* 20**,** 1709-1714.

Grundy, F. J. & T. M. Henkin (1998) The S box regulon: a new global transcription termination control system for methionine and cysteine biosynthesis genes in Gram-positive bacteria. *Molecular Microbiology,* 30**,** 737-749.

Guerrier-Takada, C., K. Gardiner, T. Marsh, N. Pace & S. Altman (1983) The RNA moiety of ribonuclease P is the catalytic subunit of the enzyme. *Cell,* 35**,** 849-57.

Hall, L. & T. Unestam (1980) The effect of fungicides on survival of the crayfish plague fungus, aphanomyces astaci, oomycetes, growing on fish scales. *Mycopathologia,* 72**,** 131-134.

Hamilton, A. & D. Baulcombe (1999) A species of small antisense RNA in posttranscriptional gene silencing in plants. *Science,* 286**,** 950-952.

Hannon, G. J. & J. J. Rossi (2004) Unlocking the potential of the human genome with RNA interference. *Nature,* 431**,** 371-378.

Harvey Lodish, A. B., S Lawrence Zipursky, Paul Matsudaira, David Baltimore, and James Darnell. 2000. *Molecular Cell Biology*. W. H. Freeman and Company.

Heaphy, S., J. T. Finch, M. J. Gait, J. Karn & M. Singh (1991) Human immunodeficiency virus type 1 regulator of virion expression, rev, forms nucleoprotein filaments after binding to a purine-rich "bubble" located within the rev-responsive region of viral mRNAs. *Proceedings of the National Academy of Sciences of the United States of America,* 88**,** 7366-7370.

Horn, W., M. Convery, N. Stonehouse, C. Adams, L. Liljas, S. Phillips & P. Stockley (2004) The crystal structure of a high affinity RNA stem-loop complexed with the bacteriophage MS2 capsid: Further challenges in the modeling of ligand-RNA interactions. *RNA,* 10**,** 1776-1782.

Huang, D. B., D. Vu, L. A. Cassiday, J. M. Zimmerman, L. J. Maher & G. Ghosh (2003) Crystal structure of NF-kappa B (p50)(2) complexed to a high-affinity RNA aptamer. *Proceedings of the National Academy of Sciences of the United States of America,* 100**,** 9268-9273.

Huang, Z., J. M. Gabriel, M. A. Baldwin, R. J. Fletterick, S. B. Prusiner & F. E. Cohen (1994) Proposed three-dimensional structure for the cellular prion protein. *Proceedings of the National Academy of Sciences of the United States of America,* 91**,** 7139-43.

Huang, Z. & J. W. Szostak (2003) Evolution of aptamers with a new specificity and new secondary structures from an ATP aptamer. *RNA,* 9**,** 1456-63.

Jarvest, R. L., J. M. Berge, V. Berry, H. F. Boyd, M. J. Brown, J. S. Elder, A. K. Forrest, A. P. Fosberry, D. R. Gentry, M. J. Hibbs, D. D. Jaworski, P. J. O'Hanlon, A. J. Pope, S. Rittenhouse, R. J. Sheppard, C. Slater-Radosti & A. Worby (2002) Nanomolar inhibitors of Staphylococcus aureus methionyl tRNA synthetase with potent antibacterial activity against gram-positive pathogens. *Journal of Medicinal Chemistry,* 45**,** 1959-1962.

Jelesarov, I. & H. R. Bosshard (1999) Isothermal titration calorimetry and differential scanning calorimetry as complementary tools to investigate the energetics of biomolecular recognition. *Journal of Molecular Recognition,* 12**,** 3-18.

Jiang, L. C., A. Majumdar, W. D. Hu, T. J. Jaishree, W. K. Xu & D. J. Patel (1999) Saccharide-RNA recognition in a complex formed between neomycin B and an RNA aptamer. *Structure,* 7**,** 817-827.

Jiang, L. C. & D. J. Patel (1998) Solution structure of the tobramycin-RNA aptamer complex. *Nature Structural and Molecular Biology,* 5**,** 769-774.

Jiang, L. C., A. K. Suri, R. Fiala & D. J. Patel (1997) Saccharide-RNA Recognition in an Aminoglycoside Antibiotic-RNA Aptamer Complex. *Chemistry & Biology,* 4**,** 35-50.

Kaul, M. & D. S. Pilch (2002) Thermodynamics of aminoglycoside-rRNA recognition: The binding of neomycin-class aminoglycosides to the A site of 16S rRNA. *Biochemistry,* 41**,** 7695-7706.

Kay, J. 1968. Role of ribosomal RNA (rRNA) synthesis in effects of phytohaemagglutinin (PHA) on lymphocytes. *Federation Proceedings,* 717-719.

Kettenberger, H., A. Eisenfuhr, F. Brueckner, M. Theis, M. Famulok & P. Cramer (2006) Structure of an RNA polymerase II-RNA inhibitor complex elucidates transcription regulation by noncoding RNAs. *Nature Structural & Molecular Biology,* 13**,** 44-48.

Kiga, D., Y. Futamura, K. Sakamoto & S. Yokoyama (1998) An RNA aptamer to the xanthine/guanine base with a distinctive mode of purine recognition. *Nucleic Acids Research,* 26**,** 1755-1760.

Kucukkilinc, T. & I. Ozer. 2008. Inhibition of electric eel acetylcholinesterase by triarylmethane dyes. *Chemico-Biological Interactions,* 309-311.

Lauren, J., D. A. Gimbel, H. B. Nygaard, J. W. Gilbert & S. M. Strittmatter (2009) Cellular prion protein mediates impairment of synaptic plasticity by amyloid-beta oligomers. *Nature,* 457**,** 1128-32.

Lebars, I., P. Legrand, A. Aime, N. Pinaud, S. Fribourg & C. Di Primo (2008) Exploring TAR-RNA aptamer loop-loop interaction by X-ray crystallography, UV spectroscopy and surface plasmon resonance. *Nucleic Acids Research,* 36**,** 7146-7156.

Lee, D. & W. H. McClain (2004) Aptamer redesigned tRNA is nonfunctional and degraded in cells. *RNA,* 10**,** 7-11.

Lin, P. H., S. L. Yen, M. S. Lin, Y. Chang, S. R. Louis, A. Higuchi & W. Y. Chen (2008) Microcalorimetrics studies of the thermodynamics and binding mechanism between L-tyrosinamide and aptamer. *Journal of Physical Chemistry B,* 112**,** 6665-6673.

Litman, G. W., J. P. Rast, M. J. Shamblott, R. N. Haire, M. Hulst, W. Roess, R. T. Litman, K. R. Hinds-Frey, A. Zilch & C. T. Amemiya (1993) Phylogenetic diversification of immunoglobulin genes and the antibody repertoire. *Molecular Biology and Evolution,* 10**,** 60-72.

Liu, J., Z. Cao & Y. Lu (2009) Functional nucleic acid sensors. *Chemical Reviews,* 109**,** 1948-98.

Magnet, S. & J. S. Blanchard (2005) Molecular insights into aminoglycoside action and resistance. *Chemical Reviews,* 105**,** 477-497.

Mashima, T., A. Matsugami, F. Nishikawa, S. Nishikawa & M. Katahira (2009) Unique quadruplex structure and interaction of an RNA aptamer against bovine prion protein. *Nucleic Acids Research,* 37**,** 6249-6258.

Matsugami, A., S. Kobayashi, K. Ouhashi, S. Uesugi, R. Yamamoto, K. Taira, S. Nishikawa, P. Kumar & M. Katahira (2003) Structural basis of the highly efficient trapping of the HIV Tat protein by an RNA aptamer. *Structure,* 11**,** 533-545.

Meli, M., J. Vergne, J. L. Decout & M. C. Maurel. 2002. Adenine-aptamer complexes: a bipartite RNA site that binds the adenine nucleic base. *Journal of Biological Chemistry,* 2104-11.

Minakawa, N., M. Sanji, Y. Kato & A. Matsuda. 2008. Investigations toward the selection of fully-modified 4'-thioRNA aptamers: optimization of in vitro transcription steps in the presence of 4'-thioNTPs. *Bioorganic & Medicinal Chemistry,* 9450-6.

Morris, D. & J. Demoss (1965) Role of aminoacyl-transfer ribonucleic acid in regulation of ribonucleic acid synthesis in Escherichia Coli. *Journal of Bacteriology,* 90**,** 1624-1630.

Muller, M., J. Weigand, O. Weichenrieder & B. Suess (2006) Thermodynamic characterization of an engineered tetracycline-binding riboswitch. *Nucleic Acids Research,* 34**,** 2607-2617.

Muntoni, F. & M. J. A. Wood (2011) Targeting RNA to treat neuromuscular disease. *Nature Reviews Drug Discovery,* 10**,** 621-637.

Ng, E. W. M., D. T. Shima, P. Calias, E. T. Cunningham, D. R. Guyer & A. P. Adamis (2006) Pegaptanib, a targeted anti-VEGF aptamer for ocular vascular disease. *Nature Reviews Drug Discovery,* 5**,** 123-132.

Nguyen, D. H., T. Dieckmann, M. E. Colvin & W. H. Fink (2004) Dynamics studies of a malachite Green-RNA complex revealing the origin of the red-shift and energetic contributions of stacking interactions. *Journal of Physical Chemistry B,* 108**,** 1279-1286.

Nissen, P., J. Hansen, N. Ban, P. B. Moore & T. A. Steitz (2000) The structural basis of ribosome activity in peptide bond synthesis. *Science,* 289**,** 920-930.

Noble, M., J. Endicott & L. Johnson (2004) Protein kinase inhibitors: Insights into drug design from structure. *Science,* 303**,** 1800-1805.

Nomura, Y., S. Sugiyama, T. Sakamoto, S. Miyakawa, H. Adachi, K. Takano, S. Murakami, T. Inoue, Y. Mori, Y. Nakamura & H. Matsumura (2010) Conformational plasticity of RNA for target recognition as revealed by the 2.15 A crystal structure of a human IgG-aptamer complex. *Nucleic Acids Research*, 7822-9.

Paillart, J. C., M. Shehu-Xhilaga, R. Marquet & J. Mak (2004) Dimerization of retroviral RNA genomes: an inseparable pair. *Nature Reviews Microbiology,* 2**,** 461-72.

Patel, D. J., A. K. Suri, F. Jiang, L. Jiang, P. Fan, R. A. Kumar & S. Nonin (1997) Structure, Recognition and Adaptive Binding in RNA Aptamer Complexes. *Journal of Molecular. Biology.,* 272**,** 645-664.

Peters, K. M., B. E. Brooks, M. A. Schumacher, R. A. Skurray, R. G. Brennan & M. H. Brown (2011) A single acidic residue can guide binding site selection but does not govern QacR cationic-drug affinity. *PLoS One,* 6**,** e15974.

Pettersen, E. F., T. D. Goddard, C. C. Huang, G. S. Couch, D. M. Greenblatt, E. C. Meng & T. E. Ferrin (2004) UCSF chimera - A visualization system for exploratory research and analysis. *Journal of Computational Chemistry,* 25**,** 1605-1612.

Proske, D., S. Gilch, F. Wopfner, H. M. Schatzl, E. L. Winnacker & M. Famulok (2002) Prion-protein-specific aptamer reduces PrPSc formation. *Chembiochem,* 3**,** 717-25.

Reiter, N., L. Maher & S. Butcher (2008) DNA mimicry by a high-affinity anti-NF-kappa B RNA aptamer. *Nucleic Acids Research,* 36**,** 1227-1236.

Sakamoto, T., A. Oguro, G. Kawai, T. Ohtsu & Y. Nakamura (2005) NMR structures of double loops of an RNA aptamer against mammalian initiation factor 4A. *Nucleic Acids Research,* 33**,** 745-754.

Salas, M., M. B. Hille, J. A. Last, A. J. Wahba & S. Ochoa (1967) Translation of genetic message: Effect of initiation factors on binding of formyl-methionyl-tRNA to ribosomes. *Proceedings of the National Academy of Sciences of the United States of America,* 57**,** 387-&.

Schmidt, K. S., S. Borkowski, J. Kurreck, A. W. Stephens, R. Bald, M. Hecht, M. Friebe, L. Dinkelborg & V. A. Erdmann (2004) Application of locked nucleic acids to improve aptamer in vivo stability and targeting function. *Nucleic Acids Research,* 5757-65. England.

Shu, D. & P. Guo (2003) A viral RNA that binds ATP and contains a motif similar to an ATP-binding aptamer from SELEX. *Journal of Biological Chemistry,* 278**,** 7119-7125.

Stonehouse, N. J., D. J. Scott, S. Fonseca, J. Murray, C. Adams, A. R. Clarke, K. Valegard, R. Golmohammadi, S. van den Worm, L. Liljas & P. G. Stockley (1996) Molecular

interactions in the RNA bacteriophage MS2. *Biochemical Society Transactions,* 24**,** 412S.
Tao, J. S. & A. D. Frankel (1992) Specific binding of argnine to TAR RNA. *Proceedings of the National Academy of Sciences of the United States of America,* 89**,** 2723-2726.
Tereshko, V., E. Skripkin & D. Patel (2003) Encapsulating streptomycin within a small 40-mer RNA. *Chemistry & Biology,* 10**,** 175-187.
Thomas, J. R. & P. J. Hergenrother (2008) Targeting RNA with small molecules. *Chemical Reviews,* 108**,** 1171-224.
Tiley, L. S., M. H. Malim, H. K. Tewary, P. G. Stockley & B. R. Cullen (1992) Identification of a high-affinity RNA-binding site for the human immunodeficiency virus type 1 Rev protein. *Proceedings of the National Academy of Sciences of the United States of America,* 89**,** 758-762.
Trotochaud, A. E. & K. M. Wassarman. 2005. A highly conserved 6S RNA structure is required for regulation of transcription. *Nature Structural & Molecular Biology,* 313-9.
Tso, P. O. P. (1962) Ribosomes - ribonucleoprotein particles. *Annual Review of Plant Physiology and Plant Molecular Biology,* 13**,** 45-&.
Tuerk, C. & L. Gold (1990) Systematic evolution of ligands by exponential enrichment: RNA ligands to bacteriophage T4 DNA polymerase. *Science,* 249**,** 505-510.
Valegard, K., J. B. Murray, P. G. Stockley, N. J. Stonehouse & L. Liljas (1994) Crystal structure of an RNA bacteriophage coat protein-operator complex. *Nature,* 371**,** 623-6.
Van Melckebeke, H., M. Devany, C. Di Primo, F. Beaurain, J. J. Toulme, D. L. Bryce & J. Boisbouvier (2008) Liquid-crystal NMR structure of HIV TAR RNA bound to its SELEX RNA aptamer reveals the origins of the high stability of the complex. *Proceedings of the National Academy of Sciences of the United States of America,* 105**,** 9210-9215.
Veronese, F. M. & A. Mero (2008) The impact of PEGylation on biological therapies. *Biodrugs,* 22**,** 315-329.
Wahid, F., T. Khan, K. H. Hwang & Y. Y. Kim (2009) Piwi-interacting RNAs (piRNAs) in animals: The story so far. *African Journal of Biotechnology,* 8**,** 4002-4006.
Welch, E. M., E. R. Barton, J. Zhuo, Y. Tomizawa, W. J. Friesen, P. Trifillis, S. Paushkin, M. Patel, C. R. Trotta, S. W. Hwang, R. G. Wilde, G. Karp, J. Takasugi, G. M. Chen, S. Jones, H. Ren, Y. C. Moon, D. Corson, A. A. Turpoff, J. A. Campbell, M. M. Conn, A. Khan, N. G. Almstead, J. Hedrick, A. Mollin, N. Risher, M. Weetall, S. Yeh, A. A. Branstrom, J. M. Colacino, J. Babiak, W. D. Ju, S. Hirawat, V. J. Northcutt, L. L. Miller, P. Spatrick, F. He, M. Kawana, H. Feng, A. Jacobson, S. W. Peltz & H. L. Sweeney (2007) PTC124 targets genetic disorders caused by nonsense mutations. *Nature,* 447**,** 87-U6.
Wilton, S. (2007) PTC124, nonsense mutations and Duchenne muscular dystrophy. *Neuromuscular Disorders,* 17**,** 719-20.
Winkler, W., A. Nahvi & R. R. Breaker (2002) Thiamine derivatives bind messenger RNAs directly to regulate bacterial gene expression. *Nature,* 419**,** 952-956.
Winkler, W. C., S. Cohen-Chalamish & R. R. Breaker (2002) An mRNA structure that controls gene expression by binding FMN. *Proceedings of the National Academy of Sciences of the United States of America,* 99**,** 15908-15913.

Xiao, H., T. Edwards & A. Ferre-D'Amare (2008) Structural Basis for Specific, High-Affinity Tetracycline Binding by an In Vitro Evolved Aptamer and Artificial Riboswitch. *Chemistry & Biology,* 15**,** 1125-1137.

Yamamoto, R., M. Katahira, S. Nishikawa, T. Baba, K. Taira & P. K. Kumar. 2000. A novel RNA motif that binds efficiently and specifically to the tat protein of HIV and inhibits the trans-activation by Tat of transcription in vitro and in vivo. *Genes Cells,* 371-88.

Ye, X., A. Gorin, R. Frederick, W. Hu, A. Majumdar, W. Xu, G. McLendon, A. Ellington & D. Patel (1999) RNA architecture dictates the conformations of a bound peptide. *Chemistry & Biology,* 6**,** 657-669.

Zapp, M. L., T. J. Hope, T. G. Parslow & M. R. Green (1991) Oligomerization and RNA binding domains of the type 1 human immunodefieciency virus Rev protein: A dual function for an arginine-rich binding motif. *Proceedings of the National Academy of Sciences of the United States of America,* 88**,** 7734-7738.

2. Chapter 2

Babendure, J. R., S. R. Adams & R. Y. Tsien (2003) Aptamers switch on fluorescence of triphenylmethane dyes. *Journal of the American Chemical Society,* 125**,** 14716-14717.

Baugh, C., D. Grate & C. Wilson (2000) 2.8 angstrom crystal structure of the malachite green aptamer. *Journal of Molecular Biology,* 301**,** 117-128.

Brackett, D. M. & T. Dieckmann (2006) Aptamer to ribozyme: the intrinsic catalytic potential of a small RNA. *Chembiochem,* 7**,** 839-43.

Chaires, J. B. (2008) Calorimetry and thermodynamics in drug design. *Annual Review of Biophysics,* 37**,** 135-151.

Cooper, A., C. M. Johnson, J. H. Lakey & M. Nollmann (2001) Heat does not come in different colours: entropy-enthalpy compensation, free energy windows, quantum confinement, pressure perturbation calorimetry, solvation and the multiple causes of heat capacity effects in biomolecular interactions. *Biophysical Chemistry,* 93**,** 215-230.

Cowan, J. A., T. Ohyama, D. Q. Wang & K. Natarajan (2000) Recognition of a cognate RNA aptamer by neomycin B: quantitative evaluation of hydrogen bonding and electrostatic interactions. *Nucleic Acids Research,* 28**,** 2935-2942.

Darzynkiewicz, Z., J. Kapuscinski, S. P. Carter, F. A. Schmid & M. R. Melamed (1986) Cytostatic and cytotoxic properties of pyronin-Y - relation to mitochondrial localization of the dye and its interaction with RNA. *Cancer Research,* 46**,** 5760-5766.

Detering, C. & G. Varani (2004) Validation of automated docking programs for docking and database screening against RNA drug targets. *Journal of Medicinal Chemistry,* 47**,** 4188-4201.

Feig, A. L. (2007) Applications of isothermal titration calorimetry in RNA biochemistry and biophysics. *Biopolymers,* 87**,** 293-301.

Flinders, J., S. C. DeFina, D. M. Brackett, C. Baugh, C. Wilson & T. Dieckmann (2004) Recognition of planar and nonplanar ligands in the malachite green-RNA aptamer complex. *Chembiochem,* 5**,** 62-72.

Grate, D. & C. Wilson (1999) Laser-mediated, site-specific inactivation of RNA transcripts. *Proceedings of the National Academy of Sciences of the United States of America,* 96**,** 6131-6136.

Grate, D. & C. Wilson (2001) Inducible regulation of the S-cerevisiae cell cycle mediated by an RNA aptamer-ligand complex. *Bioorganic & Medicinal Chemistry,* 9**,** 2565-2570.

Hamilton, A. & D. Baulcombe (1999) A species of small antisense RNA in posttranscriptional gene silencing in plants. *Science,* 286**,** 950-952.

Hirabayashi, M., H. Ohashi & T. Kubo (2010) Design of Bio-Inspired Multi-Stage Regulations for Diagnostic Molecular Automata. *Journal of Computational and Theoretical Nanoscience,* 7**,** 831-839.

Hirabayashi, M., S. Taira, S. Kobayashi, K. Konishi, K. Katoh, Y. Hiratsuka, M. Kodaka, T. Q. P. Uyeda, N. Yumoto & T. Kubo (2006) Malachite green-conjugated microtubules as mobile bioprobes selective for malachite green aptamers with capturing/releasing ability. *Biotechnology and Bioengineering,* 94**,** 473-480.

Hossain, M. & G. S. Kumar (2009) DNA binding of benzophenanthridine compounds sanguinarine versus ethidium: Comparative binding and thermodynamic profile of intercalation. *Journal of Chemical Thermodynamics,* 41**,** 764-774.

Islam, M. M. & G. S. Kumar (2009) Small molecule-RNA interaction: Spectroscopic and calorimetric studies on the binding by the cytotoxic protoberberine alkaloid coralyne to single stranded polyribonucleotides. *Biochimica Et Biophysica Acta-General Subjects,* 1790**,** 829-839.

Joyce, G. F. & L. E. Orgel. 1993. Prospect for understanding the origin of the RNA world. *The RNA World,* eds. R. E. Gesteland & J. F. Atkins. Plainview, NY: Cold Spring Harbor Laboratory Press.

Kapuscinski, J. & Z. Darzynkiewicz (1987) Interactions of pyronin-Y with nucleic-acids. *Cytometry,* 8**,** 129-137.

Kumar, A., R. R. Ernst & K. Wüthrich (1980) A two-dimensional nuclear Overhauser enhancement (2D NOE) experiment for the elucidation of complete proton-proton cross-

relaxation networks in biological macromolecules. *Biochemical and Biophysical Research Communications,* 95**,** 1-6.

Ladbury, J. E. (2004) Application of isothermal titration calorirnetry in the biological sciences: Things are heating up! *Biotechniques,* 37**,** 885-887.

Liao, J. C., J. Roider & D. G. Jay (1994) Chromophore-assisted laser inactivation of proteins is mediated by the photogeneration of free-radicals. *Proceedings of the National Academy of Sciences of the United States of America,* 91**,** 2659-2663.

Lin, P. H., S. L. Yen, M. S. Lin, Y. Chang, S. R. Louis, A. Higuchi & W. Y. Chen (2008) Microcalorimetrics studies of the thermodynamics and binding mechanism between L-tyrosinamide and aptamer. *Journal of Physical Chemistry B,* 112**,** 6665-6673.

Marion, D., M. Ikura, R. Tschudin & A. Bax (1989) Rapid recording of 2d NMR spectra without phase cycling - application to the study of hydrogen exchange in proteins. *Journal of Magnetic Resonance,* 85**,** 393-399.

Mascotti, D. P. & T. M. Lohman (1990) Thermodynamic extent of counterion release upon binding oligolysines to single-stranded nucleic-acids. *Proceedings of the National Academy of Sciences of the United States of America,* 87**,** 3142-3146.

Milligan, J. F., D. R. Groebe, G. W. Witherell & O. C. Uhlenbeck (1987) Oligoribonucleotide synthesis using T7-RNA polymerase and synthetic DNA templates. *Nucleic Acids Research,* 15**,** 8783-8798.

Milligan, J. F. & O. C. Uhlenbeck (1989) Synthesis of small RNAs using T7 RNA polymerase. *Methods in Enzymology,* eds. J. E. Dahlberg & J. Abelson, 51-62. New York: Academic Press.

Nguyen, D. H., S. C. DeFina, W. H. Fink & T. Dieckmann (2002) Binding to an RNA aptamer changes the charge distribution and conformation of malachite green. *Journal of the American Chemical Society,* 124**,** 15081-15084.

Nguyen, D. H., T. Dieckmann, M. E. Colvin & W. H. Fink (2004) Dynamics studies of a malachite Green-RNA complex revealing the origin of the red-shift and energetic contributions of stacking interactions. *Journal of Physical Chemistry B,* 108**,** 1279-1286.

Pettersen, E. F., T. D. Goddard, C. C. Huang, G. S. Couch, D. M. Greenblatt, E. C. Meng & T. E. Ferrin (2004) UCSF chimera - A visualization system for exploratory research and analysis. *Journal of Computational Chemistry,* 25**,** 1605-1612.

Record, M. T., T. M. Lohman & P. Dehaseth (1976) Ion effects on ligand-nucleic acid interactions. *Journal of Molecular Biology,* 107**,** 145-158.

Stampfl, S., A. Lempradl, G. Koehler & R. Schroeder (2007) Monovalent ion dependence of neomycin B binding to an RNA aptamer characterized by spectroscopic methods. *Chembiochem,* 8**,** 1137-45.

Stead, S. L., H. Ashwin, B. Johnston, J. A. Tarbin, M. Sharman, J. Kay & B. J. Keely (2010) An RNA-Aptamer-Based Assay for the Detection and Analysis of Malachite Green and Leucomalachite Green Residues in Fish Tissue. *Analytical Chemistry,* 82**,** 2652-2660.

Tanford, C. (1969) Extension of Theory of Linked Functions to Incorporate Effects of Protein Hydration. *Journal of Molecular Biology,* 39**,** 539-544.

Wang, T. J., J. A. Hoy, M. H. Lamm & M. Nilsen-Hamilton (2009) Computational and Experimental Analyses Converge to Reveal a Coherent Yet Malleable Aptamer Structure That Controls Chemical Reactivity. *Journal of the American Chemical Society,* 131**,** 14747-14755.

Wiseman, T., S. Williston, J. F. Brandts & L. N. Lin (1989) Rapid measurement of binding constants and heats of binding using a new titration calorimeter. *Analytical Biochemistry,* 179**,** 131-137.

Wyman, J. (1964) Linked Functions and Reciprocal Effects in Hemoglobin - a 2nd Look. *Advances in Protein Chemistry,* 19**,** 223-286.

Xu, W. C. & Y. Lu (2010) Label-Free Fluorescent Aptamer Sensor Based on Regulation of Malachite Green Fluorescence. *Analytical Chemistry,* 82**,** 574-578.

Zhang, X., A. S. R. Potty, G. W. Jackson, V. Stepanov, A. Tang, Y. Liu, K. Kourentzi, U. Strych, G. E. Fox & R. C. Willson (2009) Engineered 5S ribosomal RNAs displaying aptamers recognizing vascular endothelial growth factor and malachite green. *Journal of Molecular Recognition,* 22**,** 154-161.

3. Chapter 3

Baugh, C., D. Grate & C. Wilson (2000) 2.8 angstrom crystal structure of the malachite green aptamer. *Journal of Molecular Biology,* 301**,** 117-128.

Bernard Da Costa, J. & T. Dieckmann (2011) Entropy and Mg2+ control ligand affinity and specificity in the malachite green binding RNA aptamer. *Molecular Biosystems,* 7**,** 2156-63.

Briand, J. & R. R. Ernst (1991) Computer-optimized homonuclear TOCSY experiments with suppression of cross relaxation. *Chemical Physics Letters,* 185**,** 276-285.

Flinders, J., S. C. DeFina, D. M. Brackett, C. Baugh, C. Wilson & T. Dieckmann (2004) Recognition of planar and nonplanar ligands in the malachite green-RNA aptamer complex. *Chembiochem,* 5**,** 62-72.

Lee, M. S. & M. A. Olson (2006) Calculation of absolute protein-ligand binding affinity using path and endpoint approaches. *Biophysical Journal,* 90**,** 864-877.

Lupardus, P. J., M. E. Birnbaum & K. C. Garcia (2010) Molecular Basis for Shared Cytokine Recognition Revealed in the Structure of an Unusually High Affinity Complex between IL-13 and IL-13R alpha 2. *Structure,* 18**,** 332-342.

Markova, N. & D. Hallen (2004) The development of a continuous isothermal titration calorimetric method for equilibrium studies. *Analytical Biochemistry,* 331**,** 77-88.

Milligan, J. F., D. R. Groebe, G. W. Witherell & O. C. Uhlenbeck (1987) Oligoribonucleotide synthesis using T7-RNA polymerase and synthetic DNA templates. *Nucleic Acids Research.,* 15**,** 8783-8798.

Milligan, J. F. & O. C. Uhlenbeck (1989) Synthesis of small RNAs using T7 RNA polymerase. *Methods in Enzymology,* eds. J. E. Dahlberg & J. Abelson, 51-62. New York: Academic Press.

Muralidhara, B. K., S. S. Negi & J. R. Halpert (2007) Dissecting the thermodynamics and cooperativity of ligand binding in cytochrome P450eryF. *Journal of the American Chemical Society,* 129**,** 2015-2024.

Pettersen, E. F., T. D. Goddard, C. C. Huang, G. S. Couch, D. M. Greenblatt, E. C. Meng & T. E. Ferrin (2004) UCSF chimera - A visualization system for exploratory research and analysis. *Journal of Computational Chemistry,* 25**,** 1605-1612.

Piantini, U., O. W. Sørensen & R. R. Ernst (1982) Multiple quantum filters for elucidating NMR coupling networks. *Journal of the American Chemical Society,* 104**,** 6800-6801.

Piotto, M., V. Saudek & V. Sklenar (1992) Gradient-tailored excitation for single-quantum NMR spectroscopy of aqueous solutions. *Journal of Biomolecular NMR,* 2**,** 661-665.

Sigurskjold, B. W. (2000) Exact analysis of competition ligand binding by displacement isothermal titration calorimetry. *Analytical Biochemistry,* 277**,** 260-266.

Sklenar, V. & A. Bax (1987) Spin-echo water suppression for the generation of pure-phase two-dimensional NMR spectra. *Journal of Magnetic Resonance,* 74**,** 469-479.

Villa, A., J. Wohnert & G. Stock (2009) Molecular dynamics simulation study of the binding of purine bases to the aptamer domain of the guanine sensing riboswitch. *Nucleic Acids Research,* 37**,** 4774-4786.

Wang, Z. X. (1995) An exact mathematical expression for describing competitive binding of two different ligands to a protein molecule. *Febs Letters,* 360**,** 111-4.

4. Chapter 4

Balasubrananian, V., L. Nguyen, S. Balasubramanian & M. Ramanathan (1998) Interferon-gamma-inhibitory oligodeoxynucleotides alter the conformation of interferon-gamma. *Molecular Pharmacology,* 53**,** 926-932.

Barbas, A. S., J. Mi, B. M. Clary & R. R. White (2010) Aptamer applications for targeted cancer therapy. *Future Oncology,* 6**,** 1117-26.

Baugh, C., D. Grate & C. Wilson (2000) 2.8 angstrom crystal structure of the malachite green aptamer. *Journal of Molecular Biology,* 301**,** 117-128.

Bini, A., M. Minunni, S. Tombelli, S. Centi & M. Mascini (2007) Analytical performances of aptamer-based sensing for thrombin detection. *Analytical Chemistry*, 3016-3019.

Blank, M., T. Weinschenk, M. Priemer & H. Schluesener (2001) Systematic evolution of a DNA aptamer binding to rat brain tumor microvessels - Selective targeting of endothelial regulatory protein pigpen. *Journal of Biological Chemistry,* 276**,** 16464-16468.

Cheng, A., B. Ge & H. Yu (2007) Aptamer-based biosensors for label-free voltammetric detection of lysozyme. *Analytical Chemistry,* 79**,** 5158-5164.

Chushak, Y. & M. O. Stone (2009) In silico selection of RNA aptamers. *Nucleic Acids Research*, e87.

Darfeuille, F., S. Reigadas, J. Hansen, H. Orum, C. Di Primo & J. Toulme (2006) Aptamers targeted to an RNA hairpin show improved specificity compared to that of complementary oligonucleotides. *Biochemistry,* 45**,** 12076-12082.

Dieckmann, T., E. Fujikawa, X. Xhao, J. Szostak & J. Feigon (1995) Structural Investigations of RNA and DNA aptamers in Solution. *Journal of Cellular Biochemistry***,** 56-56.

Ellington, A. D. & J. W. Szostak (1990) *In vitro* selection of RNA molecules that bind specific ligands. *Nature,* 346**,** 818-822.

Gabelsberger, J., W. Liebl & K. H. Schleifer (1993) Cloning and characterization of Beta-Galactoside and Beta-Glucoside hydrolyzing enzymes of thermotoga-maritima. *Fems Microbiology Letters,* 109**,** 131-137.

Gopinath , S., Balasundaresan, D., Akitomi, J., & Mizuno, H. (2006) An RNA aptamer that discriminates Bovine Factor IX from Human Factor IX. *Journal of Biochemistry,* 140, 667-676.

Gruber, H. J., C. D. Hahn, G. Kada, C. K. Riener, G. S. Harms, W. Ahrer, T. G. Dax & H. G. Knaus (2000) Anomalous fluorescence enhancement of Cy3 and Cy3.5 versus anomalous

fluorescence loss of Cy5 and Cy7 upon covalent linking to IgG and noncovalent binding to avidin. *Bioconjugate Chemistry,* 11**,** 696-704.

Grunwald, C. (2008) A brief introduction to the streptavidin-biotin system and its usage in modern surface based assays. *Zeitschrift Fur Physikalische Chemie-International Journal of Research in Physical Chemistry & Chemical Physics,* 222**,** 789-821.

Haider, S. M., S. Neidle & G. N. Parkinson (2011) A structural analysis of G-quadruplex/ligand interactions. *Biochimie,* 93**,** 1239-1251.

Holeman, L. A., S. L. Robinson, J. W. Szostak & C. Wilson (1998) Isolation and characterization of fluorophore-binding RNA aptamers. *Folding & Design,* 3**,** 423-431.

Hu, J. C., M. G. Kornacker & A. Hochschild (2000) Escherichia coli one- and two-hybrid systems for the analysis and identification of protein-protein interactions. *Methods-a Companion to Methods in Enzymology,* 20**,** 80-94.

Kikin, O., L. D'Antonio & P. S. Bagga (2006) QGRS Mapper: a web-based server for predicting G-quadruplexes in nucleotide sequences. *Nucleic Acids Research,* 34**,** W676-W682.

Kolpashchikov, D. M. (2005) Binary malachite green aptamer for fluorescent detection of nucleic acids. *Journal of the American Chemical Society,* 127**,** 12442-3.

Kubik, M., C. Bell, T. Fitzwater, S. Watson & D. Tasset (1997) Isolation and characterization of 2'-fluoro-, 2'-amino-, and 2'-fluoro/amino-modified RNA ligands to human IFN-gamma that inhibit receptor binding. *Journal of Immunology,* 159**,** 259-267.

Li, L., Z. Chen, H. Zhao, L. Guo & X. Mu (2010) An aptamer-based biosensor for the detection of lysozyme with gold nanoparticles amplification. *Sensors and actuators B-chemical,* 149**,** 110-115.

Liu, M., T. Kagahara, H. Abe & Y. Ito (2009a) Direct In Vitro Selection of Hemin-Binding DNA Aptamer with Peroxidase Activity. *Bulletin of the Chemical Society of Japan,* 82**,** 99-104.

Liu, M., T. Kagahara, H. Abe & Y. Ito (2009b) In vitro selection of hemin-binding catalytic RNA. *Bioorganic & Medicinal Chemistry Letters,* 19**,** 1484-1487.

Long, S., M. Long, R. White & B. Sullenger (2008) Crystal structure of an RNA aptamer bound to thrombin. *RNA,* 14**,** 2504-2512.

Mendonsa, S. & M. Bowser (2004) In vitro selection of high-affinity DNA ligands for human IgE using capillary electrophoresis. *Analytical Chemistry,* 76**,** 5387-5392.

Min, K., M. Cho, S. Han, Y. Shim, J. Ku & C. Ban (2008) A simple and direct electrochemical detection of interferon-gamma using its RNA and DNA aptamers. *Biosensors & Bioelectronics,* 23**,** 1819-1824.

Misono, T. & P. Kumar (2005) Selection of RNA aptamers against human influenza virus hemagglutinin using surface plasmon resonance. *Analytical Biochemistry,* 342**,** 312-317.

Neves, M. A. D., O. Reinstein, M. Saad & P. E. Johnson (2010) Defining the secondary structural requirements of a cocaine-binding aptamer by a thermodynamic and mutation study. *Biophysical Chemistry,* 153**,** 9-16.

Ng, E. W. M., D. T. Shima, P. Calias, E. T. Cunningham, D. R. Guyer & A. P. Adamis (2006) Pegaptanib, a targeted anti-VEGF aptamer for ocular vascular disease. *Nature Reviews Drug Discovery,* 5**,** 123-132.

Nimjee, S., S. Oney, Z. Volovyk, K. Bompiani, S. Long, M. Hoffman & B. Sullenger (2009) Synergistic effect of aptamers that inhibit exosites 1 and 2 on thrombin. *RNA,* 15**,** 2105-2111.

Nutiu, R. & Y. Li (2005) In vitro selection of structure-switching signaling aptamers. *Angewandte Chemie-International Edition,* 44**,** 1061-1065.

Pettersen, E. F., T. D. Goddard, C. C. Huang, G. S. Couch, D. M. Greenblatt, E. C. Meng & T. E. Ferrin (2004) UCSF chimera - A visualization system for exploratory research and analysis. *Journal of Computational Chemistry,* 25**,** 1605-1612.

Potty, A., K. Kourentzi, H. Fang, G. Jackson, X. Zhang, G. Legge & R. Willson (2009) Biophysical Characterization of DNA Aptamer Interactions with Vascular Endothelial Growth Factor. *Biopolymers,* 91**,** 145-156.

Potty, A., K. Kourentzi, H. Fang, P. Schuck & R. Willson (2011) Biophysical characterization of DNA and RNA aptamer interactions with hen egg lysozyme. *International Journal of Biological Macromolecules,* 48**,** 392-397.

Proske, D., M. Blank, R. Buhmann & A. Resch (2005) Aptamers - basic research, drug development, and clinical applications. *Appl. Microbiol. Biotechnol.,* 69**,** 367-374.

Shi, H., B. E. Hoffman & J. T. Lis (1999) RNA aptamers as effective protein antagonists in a multicellular organism. *Proceedings of the National Academy of Sciences of the United States of America,* 96**,** 10033-10038.

Stojanovic, M. & D. Landry (2002) Aptamer-based colorimetric probe for cocaine. *Journal of the American Chemical Society,* 124**,** 9678-9679.

Stojanovic, M. N. & D. M. Kolpashchikov (2004) Modular aptameric sensors. *Journal of the American Chemical Society,* 126**,** 9266-70.

Stoltenburg, R., C. Reinemann & B. Strehlitz. 2007. SELEX-A (r)evolutionary method to generate high-affinity nucleic acid ligands. *Biomolecular Engineering,* 381-403.

Tuerk, C. & L. Gold (1990) Systematic evolution of ligands by exponential enrichment: RNA ligands to bacteriophage T4 DNA polymerase. *Science,* 249**,** 505-510.

Unruh, J., G. Gokulrangan, G. Wilson & C. Johnson (2005) Fluorescence properties of fluorescein, tetramethylrhodamine and Texas Red linked to a DNA aptamer. *Photochemistry and Photobiology,* 81**,** 682-690.

Vieira, J. & J. Messing (1982) The PUC plasmids, an M13MP7-derived system for insertion mutagenesis and sequencing with synthetic universal primers. *Gene,* 19**,** 259-268.

Walsh, R. & M. DeRosa (2009) Retention of function in the DNA homolog of the RNA dopamine aptamer. *Biochemical and Biophysical Research Communications,* 388**,** 732-735.

Wilson, D. S. & J. W. Szostak (1999) In vitro selection of functional nucleic acids. *Annual Review of Biochemistry,* 68**,** 611-647.

Winkler, W. C., S. Cohen-Chalamish & R. R. Breaker (2002) An mRNA structure that controls gene expression by binding FMN. *Proceedings of the National Academy of Sciences of the United States of America,* 99**,** 15908-15913.

Xu, W. C. & Y. Lu (2010) Label-Free Fluorescent Aptamer Sensor Based on Regulation of Malachite Green Fluorescence. *Analytical Chemistry,* 82**,** 574-578.

5. Chapter 5

Agresti, J. J., B. T. Kelly, A. Jaschke & A. D. Griffiths (2005) Selection of ribozymes that catalyse multiple-turnover Diels-Alder cycloadditions by using in vitro compartmentalization. *Proceedings of the National Academy of Sciences of the United States of America,* 102**,** 16170-16175.

Blight, K. & C. Rice (1997) Secondary structure determination of the conserved 98-base sequence at the 3' terminus of hepatitis C virus genome RNA. *Journal of Virology,* 71**,** 7345-7352.

Brackett, D. M. & T. Dieckmann (2006) Aptamer to ribozyme: the intrinsic catalytic potential of a small RNA. *Chembiochem,* 7**,** 839-43.

Branch, A. & H. Robertson (1984) A Replication Cycle for Viroids and other Small Infectious RNAS. *Science,* 223**,** 450-455.

Breier, A. & A. Ziegelhoffer (2000) "Lysine is the Lord", thought some scientists in regard to the group interacting with fluorescein isothiocyanate in ATP-binding sites of P-type ATPases - But, is it not cysteine? General Physiology and Biophysics, 5, 83334-6.

Chen, J., R. Yajima, D. Chadalavada, E. Chase, P. Bevilacqua & B. Golden (2010) A 1.9 angstrom Crystal Structure of the HDV Ribozyme Precleavage Suggests both Lewis Acid and General Acid Mechanisms Contribute to Phosphodiester Cleavage. *Biochemistry,* 49**,** 6508-6518.

Cho, B., T. Yang, L. Blankenship, J. Moody, M. Churchwell, F. Beland & S. Culp (2003) Synthesis and characterization of N-demethylated metabolites of malachite green and leucomalachite green. *Chemical Research in Toxicology,*16,285-94.

Chowrira, B., P. Pavco & J. Mcswiggen (1994) In-Vitro and In-Vivo Comparison of Hammerhead, Hairpin, and Hepatitis-Delta Virus Self-processing Ribozyme Cassettes. *Journal of Biological Chemistry,* 269**,** 25856-25864.

Dumur, F., C. Mayer, E. Dumas, F. Miomandre, M. Frigoli & F. Secheresse (2008) New chelating stilbazonium-like dyes from Michler's ketone. *Organic Letters,* 10,321-324.

FerreDamare, A. R., K. H. Zhou & J. A. Doudna (1998) Crystal structure of a hepatitis delta virus ribozyme. *Nature,* 395**,** 567-574.

Fusz, S., A. Eisenfuhr, S. G. Srivatsan, A. Heckel & M. Famulok (2005) A ribozyme for the aldol reaction. *Chemistry & Biology,* 12**,** 941-950.

Gilman, H. & L. Heck (1930) The influence of acid chlorides and of pyrrole on the color test for reactive organometallic compounds the constitution of pyrrylmagnesium halides. *Journal of the American Chemical Society,*52,4949-4952.

Golding, P., T. King, L. Maddocks, D. Drucker & A. Blinkhorn (1998) Photosensitization of Staphylococcus aureus with malachite green isothiocyanate: inactivation efficiency and spectroscopic analysis. *Journal of Photochemistry and Photobiology B,*47,202-210.

Gooding, K., R. Higgs, B. Hodge, E. Stauffer, B. Heinz, K. McKnight, K. Phipps, M. Shapiro, M. Winkler, W. Ng & R. Julian (2004) High throughput screening of library compounds against an oligonucleotide substructure of an RNA target. *Journal of the American Society of Mass Spectrometry,*15,884-892.

Greig, M. & J. Robinson (2000) Detection of oligonucleotide-ligand complexes by ESI-MS (DOLCE-MS) as a component of high throughput screening. *Journal of Biomolecular Screening,*5,441-454.

Illangasekare, M., G. Sanchez, T. Nickles & M. Yarus (1995) Aminoacyl-Rna Synthesis Catalyzed By an Rna. *Science,* 267**,** 643-647.

Johnson, D., J. Yguerabide & P. Taylor (1984) Effect of rotational diffusion on fluorescence quenching by iodide - assessment of solute assessability to nepsilon-fluorescein isothiocyanate-lysine-23-cobra alpha-toxin bound to the acetylcholine-receptor. Biophysical Society, 20814-3998.

Kao, C., M. Zheng & S. Rudisser (1999) A simple and efficient method to reduce nontemplated nucleotide addition at the 3 ' terminus of RNAs transcribed by T7 RNA polymerase. *RNA,* 5**,** 1268-1272.

Kawazoe, N., N. Teramoto, H. Ichinari, Y. Imanishi & Y. Ito (2001) In vitro selection of nonnatural ribozyme-catalyzing porphyrin metalation. *Biomacromolecules,* 2**,** 681-686.

Ke, A., K. Zhou, F. Ding, J. H. Cate & J. A. Doudna (2004) A conformational switch controls hepatitis delta virus ribozyme catalysis. *Nature,* 429**,** 201-5.

Kumar, D., I. Chaudhury, P. Kar & R. Das (2009) Site-specific cleavage of HCV genomic RNA and its cloned core and NS5B genes by DNAzyme. *Journal of Gastroenterology and hepatology,* 24**,** 872-878.

Kuo, M. Y., L. Sharmeen, G. Dinter-Gottlieb & J. Taylor (1988) Characterization of self-cleaving RNA sequences on the genome and antigenome of human hepatitis delta virus. *Journal of Virology,* 62**,** 4439-44.

Liu, M., T. Kagahara, H. Abe & Y. Ito (2009) In vitro selection of hemin-binding catalytic RNA. *Bioorganic & Medicinal Chemistry Letters,* 19**,** 1484-1487.

Martick, M., T. S. Lee, D. M. York & W. G. Scott (2008) Solvent structure and hammerhead ribozyme catalysis. *Chemistry & Biology,* 15**,** 332-42.

Martick, M. & W. Scott (2006) Tertiary contacts distant from the active site prime a ribozyme for catalysis. *Cell,* 126**,** 309-320.

Nieuwlandt, D., M. West, X. Cheng, G. Kirshenheuter & B. Eaton (2003) The first example of an RNA urea synthase: Selection through the enzyme active site of human neutrophile elastase. *Chembiochem,* 4**,** 651-654.

Peracchi, A., J. MatulicAdamic, S. L. Wang, L. Beigelman & D. Herschlag (1998) Structure-function relationships in the hammerhead ribozyme probed by base rescue. *RNA,* 4**,** 1332-1346.

Perreault, J., Z. Weinberg, A. Roth, O. Popescu, P. Chartrand, G. Ferbeyre & R. Breaker (2011) Identification of Hammerhead Ribozymes in All Domains of Life Reveals Novel Structural Variations. *Plos Computational Biology,* 7.

Pley, H. W., K. M. Flaherty & D. B. McKay (1994) Three-dimensional structure of a hammerhead ribozyme. *Nature,* 372**,** 68-74.

Prody, G. A., J. T. Bakos, J. M. Buzayan, I. R. Schneider & G. Bruening (1986) Autolytic processing of dimeric plant virus satellite RNA. *Science,* 231**,** 1577-1580.

Rydzanicz, R., Zhao, S. X. & Johnson, P. E. (2005) Assembly PCR oligo maker: a tool for designing oligodeoxynucleotides for constructing long DNA molecules for RNA production. *Nucleic Acids Research,* 33, 521-525.

Santoro, S. & G. Joyce (1997) A general purpose RNA-cleaving DNA enzyme. *Proceedings of the National Academy of Sciences of the United States of America,* 94**,** 4262-4266.

Santoro, S. & G. Joyce (1998) Mechanism and utility of an RNA-cleaving DNA enzyme. *Biochemistry,* 37**,** 13330-13342.

Scott, W. (2007) Morphing the minimal and full-length hammerhead ribozymes: implications for the cleavage mechanism. *Biological Chemistry,* 388**,** 727-735.

Scott, W. G., J. T. Finch & A. Klug (1995) The crystal structure of an all-RNA hammerhead ribozyme - a proposed mechanism for RNA catalytic cleavage. *Cell,* 81**,** 991-1002.

Sengle, G., A. Eisenfuhr, P. S. Arora, J. S. Nowick & M. Famulok (2001) Novel RNA catalysts for the Michael reaction. *Chemistry & Biology,* 8**,** 459-473.

Shields, T. P., E. Mollova, L. S. Marie, M. R. Hansen & A. Pardi (1999) High-performance liquid chromatography purification of homogenous-length RNA produced by trans cleavage with a hammerhead ribozyme. *RNA,* 5**,** 1259-1267.

Shih, I. & M. Been (2002) Catalytic strategies of the hepatitis delta virus ribozymes. *Annual Review of Biochemistry,* 887-917.

Srinivas, K., I. Mahender & B. Das (2003) Silica chloride: A versatile heterogeneous catalyst for esterification and transesterification. *Synthesis,* 16,2479-2482.

Tsukiji, S., S. Pattnaik & H. Suga (2003) An alcohol dehydrogenase ribozyme. *Nature Structural Biology,* 10**,** 713-717.

Wecker, M., D. Smith & L. Gold (1996) In vitro selection of a novel catalytic RNA: Characterization of a sulfur alkylation reaction and interaction with a small peptide. *RNA,* 2**,** 982-994.

Wiegand, T., R. Janssen & B. Eaton (1997) Selection of RNA amide syntheses. *Chemistry & Biology*, 4**,** 675-683.

Appendix

Table A1: RNA sequences for various targets with structural features identified to showcase the difference in sequence and structure

Target	Sequence	Notable Structural Features
Neomycin B	GGACUGGGCGAGAAGUUUAGUCC	three consecutive GU base pairs
Tetracycline	GGGCCUAAAACAUACCAGAGAUCGCCACCCGCGCUUUAAUCUGGA GAGGUGAAGAAUACGACCACCUAGGCUC	three helices
Tobramycin	GGGACUUGGUUUAGGUAAUGAGUCCC	UG,GU,GA,UU base pairs
Streptomycin	GGAUCGCAUUUGGACUUCUGCC/CGGCACCACGGUCGGAUC	S turns
Purine	GCGAGUAUAACCUCAAUAAUAUGGUUUGAGGGUGUCUACCAGGAA CCGUAAAAUCCUGACUACUCGC	Encapsulating ligand, base pairing with Y74
Guanine	GGCACGUGUAUUACCCUAGUGGUCGACGUGCC	structure not available
SAM	GGACGAGGAGCGCUGCAAGCGAGAGCCCGAAGCUCGUCCGUUCA AACGGCGCUCA	Psuedoknot
HIV Rev	GGUGUCUUGGAGUGCUGAUCGGACACC	UAU triple, hydrogen bonding with Arg 35 and Arg 39, elongated form
HIV Rev	GGCUGGACUCGUACUUCGGUACUGGAGAAACAGCC	UAU triple, stacking of Trp45, helical form
HIV TAR	GGCUGGUCCCAGACGACC	kissing complex
HIV DIS	CUUGCUGAAGUGCACACGCAAG	kissing complex
HIV Tat	GGGAGCUUGAUCCCGGAAACGGUCGAUCGCUCCC	two adjacent UAU triples
MS2 coat protein	CCGGAGGUCACCACGGG	A10 makes three hydrogen bonds with target
RNA polymerase II	ACAGCACUGAUUGCGGUCGAGGUAGCUUGAUGG	A-form helix
Bovine prp	GGAGGAGGAGGA	GGGG tetraplane
Human IgG	GGAGGUGCUCCGAAAGGAACUCCA	G7 stacking with Tyr373
NF-kb factor	GAUACUUGAAACUGUAAGGUUGGCGUAUC	resembles B-form DNA
Mammalian factor 4A	GGAGAUCGCACUCCACAUGUGAGUGAGGCCGAAACAUAGAUUCG AGAGGAGGCUCACA	AUCGCA loop

Note A1. First page of "Entropy and MG2+ control ligand affinity and specificity in the malachite green binding RNA aptamer"

Molecular BioSystems

Dynamic Article Links View Online

Cite this: *Mol. BioSyst.*, 2011, 7, 2156–2163

www.rsc.org/molecularbiosystems

PAPER

Entropy and Mg^{2+} control ligand affinity and specificity in the malachite green binding RNA aptamer†

Jason Bernard Da Costa and Thorsten Dieckmann*

Received 24th February 2011, Accepted 30th March 2011
DOI: 10.1039/c1mb05075c

The binding of small molecule targets by RNA aptamers provides an excellent model to study the versatility of RNA function. The malachite green aptamer binds and recognizes its ligand *via* stacking and electrostatic interactions. The binding of the aptamer to its original selection target and three related molecules was determined by isothermal titration calorimetry, equilibrium dialysis, and fluorescence titration. The results reveal that the entropy of complex formation plays a large role in determining binding affinity and ligand specificity. These data combined with previous structural studies show that metal ions are required to stabilize the complexes with non-native ligands whereas the complex with the original selection target is stable at low salt and in the absence of divalent metal ions.

Introduction

The multiple roles of RNA in living cells are today well established. Its functions include the catalysis of protein synthesis in the ribosome, post-transcriptional processing in viruses, and the control of gene expression at multiple levels.[1,2] This multitude of crucial roles makes RNA an increasingly interesting target for drug design and the development of assays for biomarkers of cellular function. Aptamers have been developed for a wide variety of targets and are excellent model systems for RNA–ligand interactions.[3,4] In addition, they have found roles in pharmaceuticals,[5,6] and analytical instrumentation.[7,8] The mode of binding in different aptamers varies greatly depending on their targets and selection procedure. For example, the Neomycin B RNA aptamer binding is driven largely by hydrogen bonding[9] while the malachite green RNA aptamer (MGA) binding is driven by electrostatic and stacking interactions.[10] MGA provides an excellent model system to study the role of electrostatic and stacking interactions. MGA has been utilized as a bioprobe in combination with microtubules,[11] as a fluorescent sensor,[12,13] an assay for malachite green (MG),[14] as part of a diagnostic molecular automata[15] and for the validation of molecular docking software.[16]

MGA was originally engineered for binding specificity to the tri-phenyl dye malachite green[18] (Fig. 1A and B). The structure of the aptamer was initially solved by X-ray crystallography in complex with the MG derivative tetramethylrosamine (TMR)[19] and later by NMR spectroscopy in complex with the original selection target MG[10] (Fig. 1C). The binding pocket of the MGA (Fig. 1A) consists of a base quadruple (C7:G24:A31:G29) and a Watson–Crick base pair (G8:C28) which serve as stacking platforms for malachite green (MG, Fig. 1B). In addition, the nucleotides A9 and A30 are positioned in such a way that they almost completely close the pocket on one side (Fig. 1C).[10,19] The other residues in the internal loop region of the aptamer act as linkers and anchors for the nucleotides that are in contact with the ligand. The major difference between the structures of the MGA–TMR and the MGA–MG complexes is that in order to accommodate the non-planar MG, the aptamer undergoes a small rearrangement that can be best described as a rotation of the upper part of the binding pocket relative to the lower part.[10] This provides enough space to accommodate the rings of MG in the binding pocket, but also leads to a loss of some stacking interactions.

The study of the MGA has shown that ligands can undergo significant changes in their electronic structure and charge distribution when bound inside an RNA binding pocket.[20] The MG molecule responds to the unique electrostatic environment inside the RNA aptamer with a redistribution of its positive charge as well as a conformational change.[21] These observations suggested that the environment inside the RNA binding pocket can have a significant effect on the chemical properties of the bound ligand. Further studies revealed that the malachite green aptamer can indeed act as a ribozyme when presented with a suitable substrate molecule. An acetyl-ester derivative of malachite green undergoes an accelerated hydrolysis reaction when bound to the aptamer.[22]

University of Waterloo, Dept. of Chemistry, 200 University Ave West, Waterloo, ON, Canada. E-mail: tdieckma@uwaterloo.ca; Fax: +1-519-7460435; Tel: +1-519-8884567

† Electronic supplementary information (ESI) available: Representative raw data from equilibrium dialysis studies (S1), binding curves from fluorescence (S2), ITC studies (S3), and the plot of $\log(K_a)$ *versus* $\log(Na^+)$ (S4). See DOI: 10.1039/c1mb05075c

Note A2. Permission to reproduce paper for Chapter 2

Dear Jason

The Royal Society of Chemistry (RSC) hereby grants permission for the use of your paper(s) specified below in the printed and microfilm version of your thesis. You may also make available the PDF version of your paper(s) that the RSC sent to the corresponding author(s) of your paper(s) upon publication of the paper(s) in the following ways: in your thesis via any website that your university may have for the deposition of theses, via your universityâ€™s Intranet or via your own personal website. We are however unable to grant you permission to include the PDF version of the paper(s) on its own in your institutional repository. The Royal Society of Chemistry is a signatory to the STM Guidelines on Permissions (available on request).

Please note that if the material specified below or any part of it appears with credit or acknowledgement to a third party then you must also secure permission from that third party before reproducing that material.

Please ensure that the thesis states the following:

Reproduced by permission of The Royal Society of Chemistry

and include a link to the paper on the Royal Society of Chemistryâ€™s website.

pubs.rsc.org/en/content/article/landing/2011/mb/c1mb05075c

Please ensure that your co-authors are aware that you are including the paper in your thesis.

Regards

Gill Cockhead

Publishing Contracts & Copyright Executive

Gill Cockhead (Mrs), Publishing Contracts & Copyright Executive

Royal Society of Chemistry, Thomas Graham House

Science Park, Milton Road, Cambridge CB4 0WF, UK

Tel +44 (0) 1223 432134, Fax +44 (0) 1223 423623

http://www.rsc.org

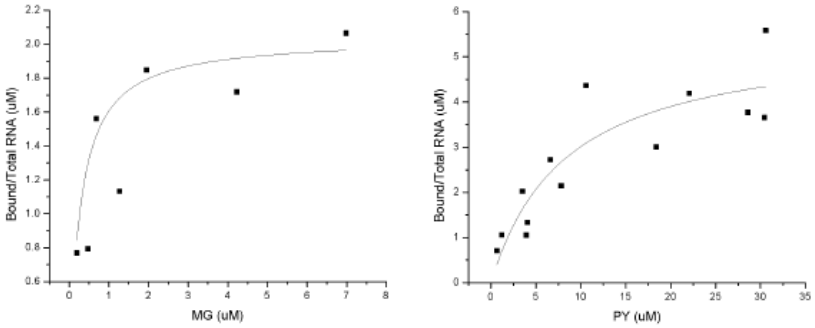

Figure B1. Binding curves from equilibrium dialysis experiments preformed at 100mM phosphate buffer, 50mM NaCl, pH6.0. The binding curves were fit using Origin using the equation $y = (Bmax * x) / (Kd + x)$.

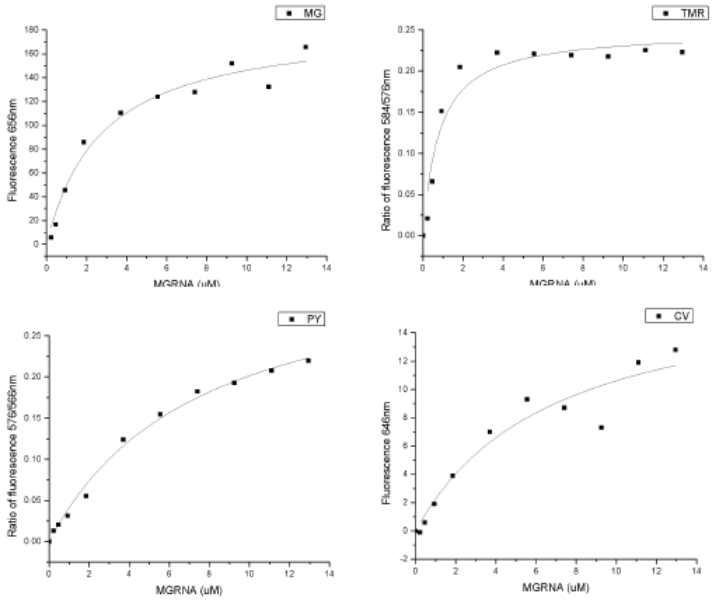

Figure B2. Binding curves from Nanodrop fluorescence experiments preformed at 50mM phosphate buffer, 150mM NaCl, pH6.7. The binding curves were fit using Origin using the equation $y = (Bmax * x) / (Kd + x)$.

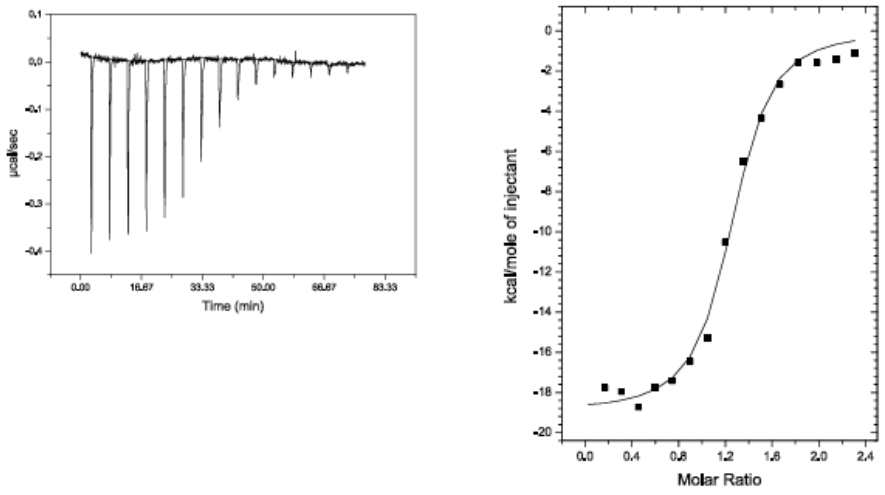

Figure B3. Right: Typical ITC raw data showing heat generated over time as dye is injected into cell containing MGA RNA. Left: Integrated data fitted using Origin to a single binding site model which provides Kd, ΔH, ΔS values. Experiments were preformed at 10mM phosphate buffer with varying salt concentrations (1mM, 150mM, 1M) , pH 6.7.

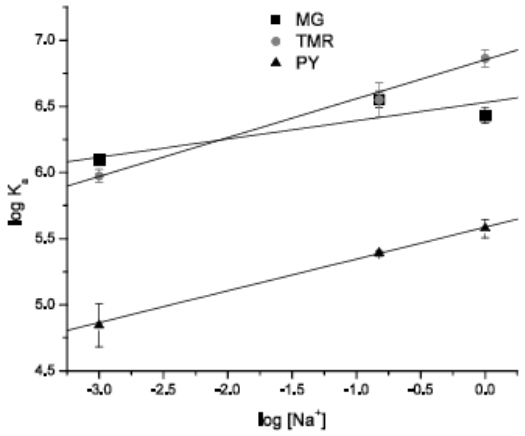

Figure B4. Plot of log Ka versus log [Na+] for MG, TMR and PY binding to MGA. Data points were fit using linear regression (Excel) to generate lines and equations. Linear regression fits of shown as solid lines (_____) MG data (y = 0.1306x + 6.5273, R2 = 0.7426), TMR data (y = 0.29x + 6.8315, R2 = 0.9925), and PY data (y = 0.245x +5.5827, R2 = 0.9996).

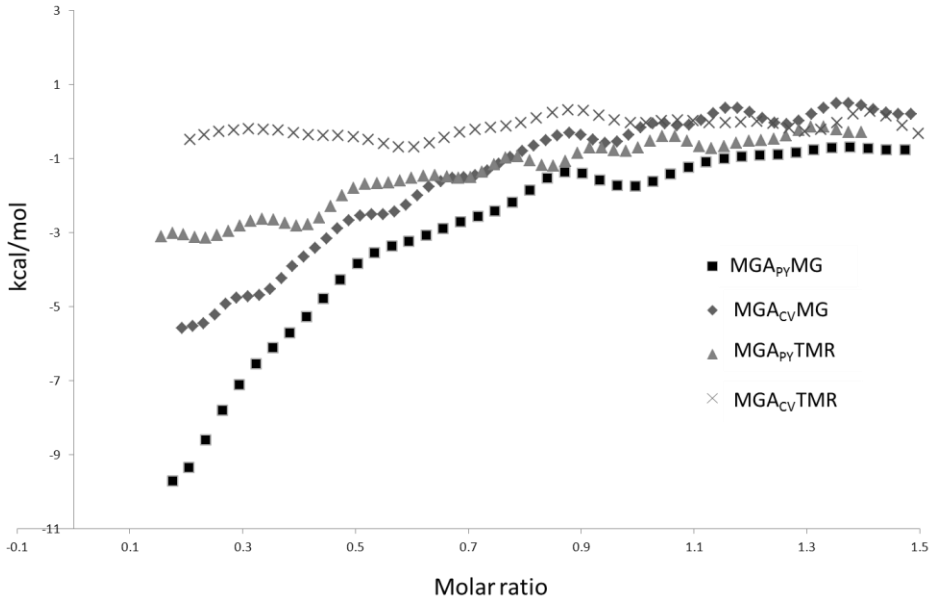

Figure C1 Typical ITC raw data showing heat generated over time. Experiments were performed at 10 mM phosphate buffer with either 150 mM NaCl or 10 mM MgCl2, pH 6.7.

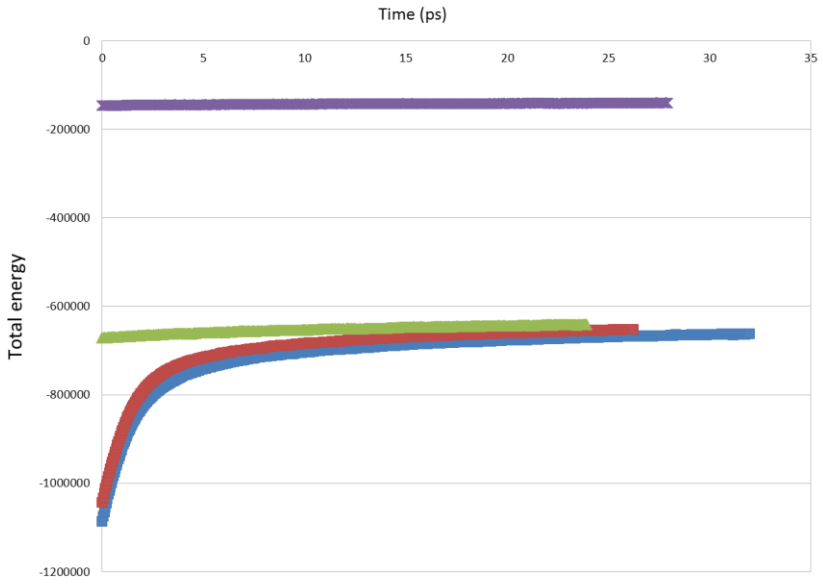

Figure C2 Plot of total energy versus simulation time showing plateauing of rate of change. Purple (MGA$_{TMR}$), Green (MGA$_{MG}$), Red (MGA$_{PY}$) and Blue (MGA$_{CV}$).

Table C1. Comparing multiple injection and single injection values obtained from ITC at 25°C in 10mM phosphate buffer 150mM NaCl, pH 6.7

MG : MGRNA	Multiple Injection	Single Injection
Time for triplicate	~9hrs	~1hr
Kd(μM)	0.28±0.07	0.19±0.08
ΔH (kcal/mol)	-25.92±2.2	-24.80E+1.8
ΔS (kcal/deg/mol)	-56.87±7.97	-52.20±6.32
ΔG (kcal/mol)	8.98±0.14	9.2±0.24

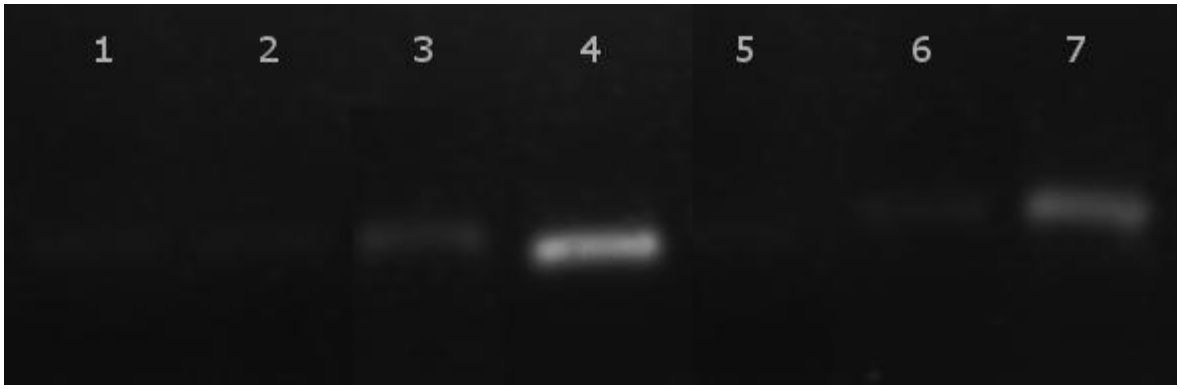

Figure D1. DNA presence after n cycles of PCR after selection Round 1 lane 1: 0 cycles, lane 2: 10 cycles, lane 3: 20 cycles, lane 4: 30 cycles. DNA presence after n cycles of PCR after selection Round 8 lane 5: 0 cycles, lane 6: 10 cycles, lane 7: 20 cycles. Gel stained with ethidium bromide.

> DNA_FDA_3

ACAGAGGTGGATCTAGAAATGGTGTCTGCGGATCGAGAATGCTGACCAGAGAGGCTTAATATTGTACCCCTTGCTGCAAGGCT
T

> DNA_FDA_6

AAATGGCACGACAGGGCGGGAGTTAATAGCTGGTCAAGAATGCTGACCGGATCCTGGATGAATCAACTCGTCCTGCTGAGCTT

> DNA_FDA_8

AGCGGGACTGCCCAATCGAAGCCTGTGGGGCGATCAAGAATGCTGACCGATCAAGGGTGGATAGTATCAAGGATGGATAAGCT
T

Figure D2. Predicted quadruplex forming unit highlight and G involved underlined, identified using QGRS mapper.

Table D1. Fluorescent measurement assay with Cy5 showing RNA interaction with avidin

RNA	RFU	% bound	Wavelength measured	Excitation source	Ligand on beads	Indicator Dye
Before application on beads	880.3	n/a	665	White	FDA	Cy5
After pull down	404.4	54	665	White	FDA	Cy5
Before application on beads	804.1	n/a	665	White	None	Cy5
After pull down	419.1	48	665	White	None	Cy5

Table D2. PCR Protocols

Protocol	
Selection Round	Step 1: 95°C 10 min Step 2: 94°C 45 sec Step 3: 50°C 1 min 25 sec Step 4: 72°C 1 min 25 sec Step 2 to 4 repeated n times, n = #cycles Cooled to 4°C
Elongation PCR	Step 1: 95°C 10 min Step 2: 94°C 45 sec Step 3: 50°C 1 min 25 sec Step 4: 72°C 1 min 25 sec Step 2 to 4 repeated n times, n = #cycles Step 5: 72°C 10 min (elongation) Cooled to 4°C
Colony PCR	Step 1: 94°C 10 min Step 2: 94°C 3 min Step 3: 45°C 1 min Step 4: 72°C 2 min Step 2 to 4 repeated 3 times Step 5: 94°C 45 sec Step 6: 50°C 1 min 25 sec Step 7: 72°C 1 min 55 sec Step 2 to 4 repeated n times, n = 18 cycles Cooled to 4°C

Figure D3. LB plate with blue and white colonies. Blue colonies stand out more in the background of the lb plate. White colonies contain plasmid with insert of interest. Blue colonies lack insert that disrupts β-galactosidase gene.

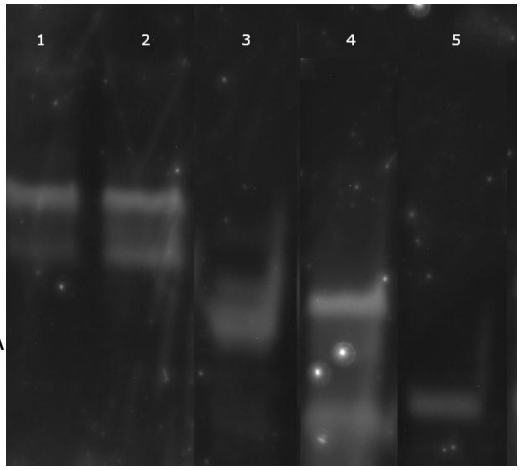

Figure E1. Gel showing Hammerhead MGA lack of cleavage and HDV MGA cleavage. Lane 1 is HH MGA which hasn't been heated. Lane 3 is HDV MGA which hasn't been heated. Lanes 2 and 4 are HH MGA and HDV MGA respectively, in cleavage buffer I (50 mM Tris HCl, pH 7.5, 100 mM NaCl and 10 mM MgCl2). These mixtures (lane 2 and 4) were incubated at 90^{o}C for 5 min then at 4^{o}C for 5 min, this hot and cold cycle was repeated three times. The solution was then allowed to react at 37^{o}C for 12 hrs. Lane 5 is MGA that was transcriped using MGA template. Gel stained with Syber Green II RNA stain.

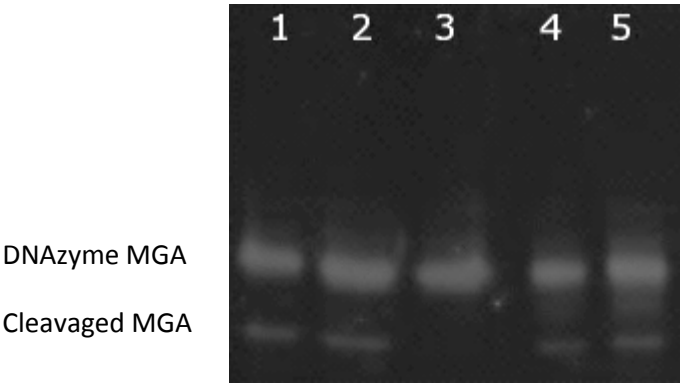

Figure E2. Gel showing DNAzyme cleavage showing increase in temperature and magnesium concentration do not increase cleavage. DNAZyme MGA loaded in lanes were in 50 mM Tris HCl, pH 7.5, 150 mM NaCl buffer. Lane 1,2,3 and 4 had 10 mM $MgCl_2$ buffer

and lane 5 had 50 mM $MgCl_2$. DNAZyme MGA mixture in lanes 2, 4 and 5 incubated at 90^{o}C for 5 min then at 4^{o}C for 5 min. The solution was then allowed to react at 37^{o}C for 4 hrs. DNAzme MGA mixture in lane 1 was incubated at 90^{o}C for 5 min then at 4^{o}C for 5 min, this was repeated three times. Then the solution was allowed to react at 42^{o}C for 8 hrs. DNAzyme MGA mixture in lane 3 was not heated. Gel was stained with Syber Green II RNA stain.

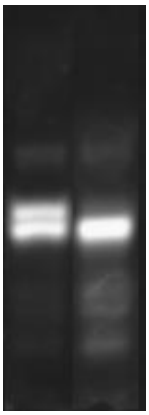

Figure E3. Lane on left is RNA transcribed using 2' O-methyl template; Lane on right is RNA transcribed with regular template. In lane on left clearly observable are two equally bright peaks (brightness is correlated to concentration). Gel was stained with ethidium bromide.

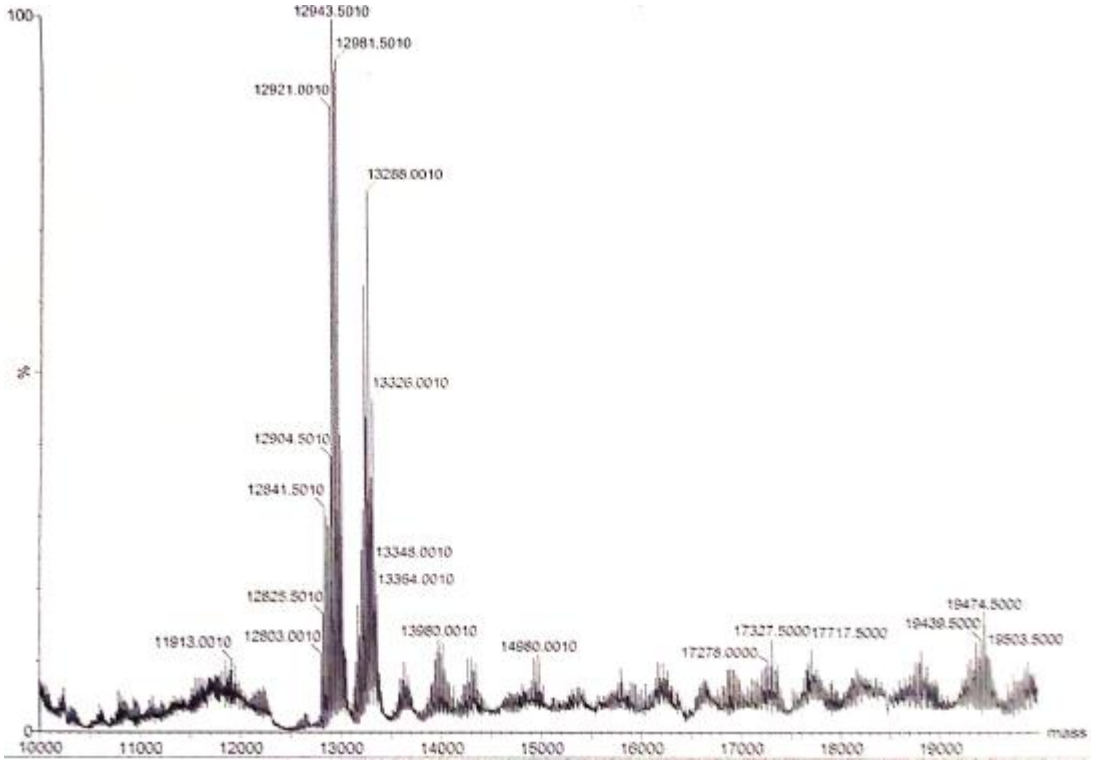

Figure E4. Mass spectra showing dye bound to n (12943 mass) and n+1 (13288 mass) MG bound to MGA.

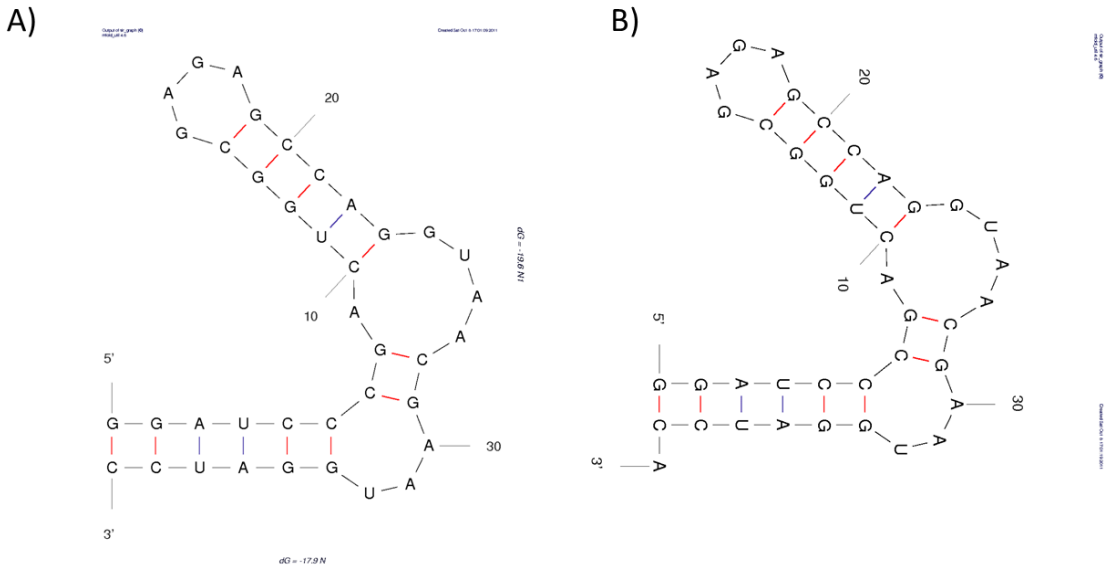

Figure E5. Secondary structure prediction using Mfold A) MGA B) MGA n+1. Showing identical secondary structure for n and n+1.

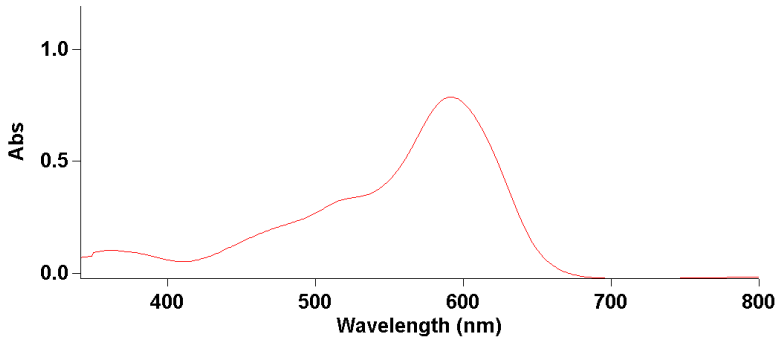

Figure E6. Visible Spectrum of reaction product from MGNCS and lysine reaction after 60 min, showing peak maximum at 590 nm.

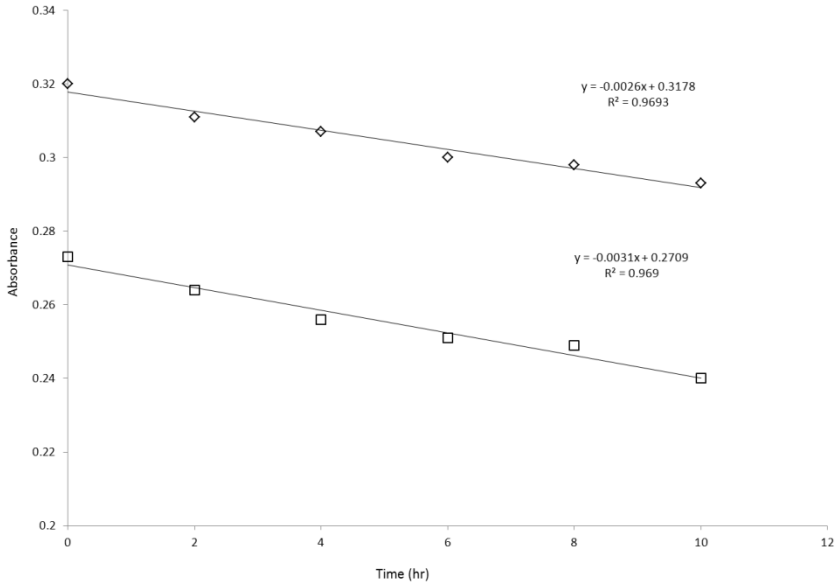

Figure E7. Monitoring reaction of MGNCS and lysine in the presence of MGA (◊) and in the absence of MGA (□). Both reactions are in 50 mM NaCl, 25 mM phosphate buffer, pH 5.0 and room temperature. The appears to be no increase in rate due to presence of MGA seen by the nearly identically slopes.

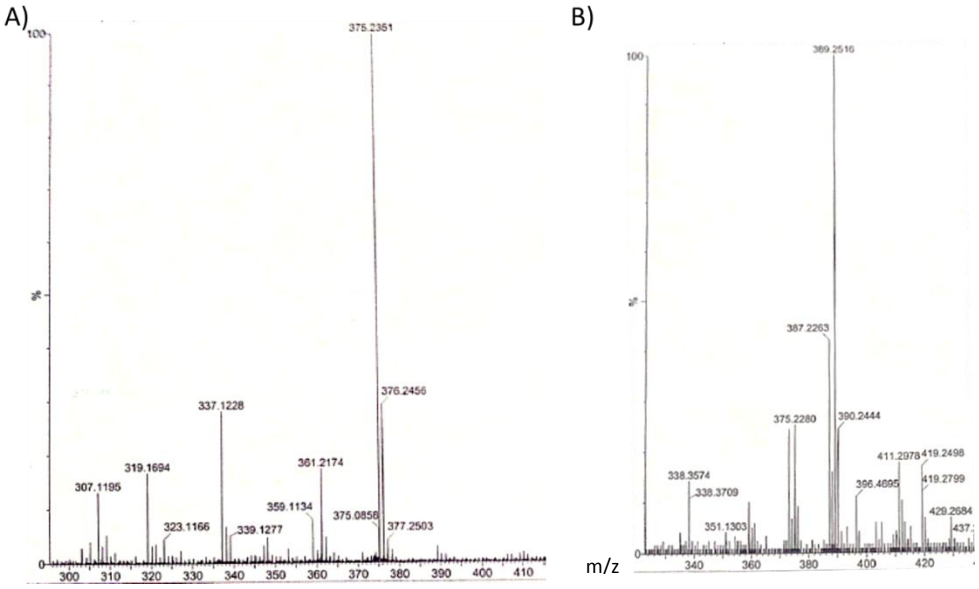

Figure E8. Mass spectra of reaction product of $MGCOOCF_3$ mixed with A) water with peak at 375 m/z suggesting MGCOO B) methanol with peak at 389 m/z suggesting $MGCOOCH_3$.

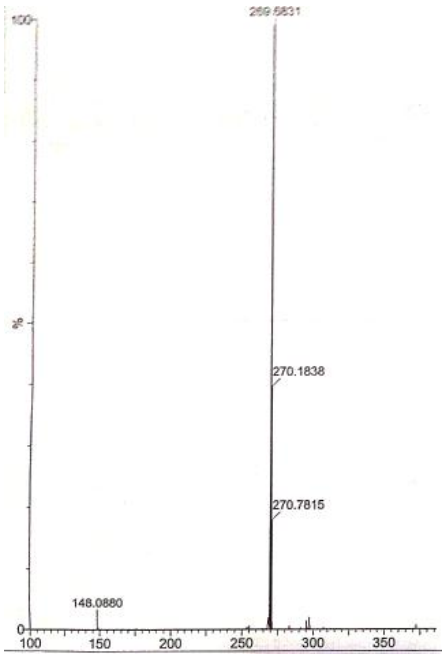

Figure D9. Mass spectra of reaction product of Michlers ketone (268 m/z) and acetyl chloride, expected ester product would have mass of approximately 312 m/z.